UNIVERSITY OF MIAMI

CIRCULATION AND WATER MASS FORMATION IN THE RED SEA, AND THE EXCHANGE WITH THE INDIAN OCEAN

By

Sarantis Sofianos

A DISSERTATION

Submitted to the Faculty
of the University of Miami
in partial fulfillment of the requirements for
the degree of Doctor of Philosophy

Coral Gables, Florida

June 2000

UNIVERSITY OF MIAMI

A dissertation submitted in partial fulfillment of
the requirements for the degree of
Doctor of Philosophy

CIRCULATION AND WATER MASS FORMATION IN THE RED SEA, AND THE EXCHANGE WITH THE INDIAN OCEAN

Sarantis Sofianos

Approved:

....
William E. Johns
Committee Chair and Professor
Meteorology and Physical Oceanography

....
Steven G. Ullmann
Dean of the Graduate School

....
Donald B. Olson
Professor
Meteorology and Physical Oceanography

....
Arthur J. Mariano
Associate Professor
Meteorology and Physical Oceanography

....
Eric P. Chassignet
Associate Professor
Meteorology and Physical Oceanography

....
Steven P. Murray
Professor
Coastal Studies Institute
Louisiana State University

SOFIANOS, SARANTIS (Ph.D., Meteorology and Physical Oceanography)

Circulation and Water Mass Formation in the Red Sea, and the exchange with the Indian Ocean. (June 2000).

Abstract of a doctoral dissertation at the University of Miami. Dissertation supervised by Professor William E. Johns.

No. of pages in text **??**

In this dissertation work, processes involved in the circulation and water mass formation in the Red Sea and the exchange with the Indian Ocean are investigated. The study is carried out with a variety of methods, including analytical models and an Ocean General Circulation Model (the Miami Isopycnic Coordinate Ocean Model - MICOM).

First, the annual mean freshwater and heat budgets of the Red Sea are estimated, using direct observations at the strait of Bab el Mandeb. The advective salt and heat fluxes in the strait are used in the Knudsen formulation and the annual mean freshwater loss to the atmosphere is estimated at $2.06 \pm 0.22\, m/year$ while the annual mean heat flux over the surface of the Red Sea is $11 \pm 5\, Wm^{-2}$.

The mechanisms involved in the seasonal exchange between the Red Sea and the Indian Ocean are then studied using MICOM. By performing experiments with different atmospheric forcing (seasonal winds, seasonal thermohaline air-sea fluxes or both) the seasonal response of the strait is investigated, in order to assess the role of the atmospheric forcing fields in the exchange flow at Bab el Mandeb. It is shown that both the seasonal pattern of the wind-stress and the seasonal thermohaline forcing are important in producing the observed variability at the strait. The effect of the seasonal buoyancy fluxes over the Red Sea is also investigated with an analytical approach, a modified version of Phillips' model (Phillips, 1966). A two-dimensional model driven by a buoyancy flux that changes linearly with latitude is shown to reproduce basic characteristics of the exchange flow, such as the winter inverse estuarine type of exchange and the summer reversal of the exchange pattern.

The three-dimensional circulation in the Red Sea basin is studied analyzing the results of the MICOM simulations. The main findings of this analysis include an intensification toward the coasts, with a transition from western intensified boundary flow in the south to eastern intensified flow in the north, and a series of strong seasonal or permanent eddy-like features. The MICOM experiments which were carried out with different forcing fields (full forcing, wind-stress and buoyancy flux through the surface of the sea) showed that the circulation produced by the thermohaline forcing is overall stronger and dominates the wind-driven part of the circulation. The main circulation pattern is related to the seasonal buoyancy flux (mostly due to the evaporation) which increases the density to the north and produces a northward pressure gradient associated with the sloping of the sea surface. The response of the eastern boundary to a mean cross-basin geostrophic current depends on the stratification and β-effect. In the northern part of the basin this results in an eastward intensification associated with the presence of Kelvin waves while in the south the traditional westward intensification due to Rossby waves takes place.

The rate of Red Sea Water (RSW) formation is also investigated with MICOM and was found to depend on the seasonal buoyancy flux. In experiments not including the seasonal variability of the air-sea thermohaline fluxes the outflow of RSW is reduced almost to half. It is during winter and in the northern part of the basin that the largest amount of this water mass (about 2/3 of the final outflowing layer) is formed. The results of the simulation indicate also that the permanent cyclonic gyre in the northern end of the basin is the most probable location for the RSW formation to take place. Inside this feature the stratification becomes weaker due to doming of the isopycnals. This and the ability of the gyre to trap surface waters and expose them to the winter intense buoyancy loss are characteristics that make the region preferable for water mass formation. This localized type of formation is also indicated in the results from a box model, based on conservation of volume and salt in the Red Sea basin.

Finally, the variability of the exchange flow at Bab el Mandeb at synoptic time scales is examined, and a simple, linear, two-dimensional model is employed to explain the main mechanisms involved. The local wind-stress seems to be the most important forcing mechanism, which, together with changes of the atmospheric pressure inside the Red Sea basin, can explain 70% of the observed variance at synoptic time scales.

Acknowledgements

I wish to express my graditude to Bill Johns, my dissertation advisor, for giving me the opportunity to work on the Red Sea circulation and providing the data on which this work is based, for his continuous support and encouragement and for his invaluable scientific input throughout this study. Our numerous discussions helped me improve my understanding of the ocean dynamics, and his ideas are reflected in all the aspects of this dissertation.

The present study was improved and profited from the interaction with the members of my dissertation committee, Steve Murray, Don Olson, Arthur Mariano and Eric Chassignet. Their ideas and comments helped me define my objectives and clarify the conclusions of my work.

Over the years, I have indebted to a large number of members of the MPO and RSMAS community, who contributed in different aspects of this work and my education. Especially, I want to thank Rainer Zantopp for his help during the time I was processing the data used in this study, and Afonso Paiva and Linda Smith for their guidance and help with MICOM. I want to thank all MPO staff, professors, and students, who provided an excellent environment, at both personal and professional level.

Financial support for this work was provided by the ONR grant N00014-95-1-0025.

Finally, I want to thank my parents, Aliki and Stefanos, and my whole family for their love and support, my son Stefanos, for being an inspiration in my effort, and most of all my wife Maria, to whom this work is dedicated.

Contents

List of Tables

List of Figures

Chapter 1

General Introduction

The Red Sea is a long and narrow channel-like basin separating the African from the Asian continent. For thousands of years it has been the main route connecting Europe with the Indian and eastern Asian subcontinents. Even today, and after the opening of the Suez Canal, it is an important commercial passage. This and a developing oil mining industry put a lot of pressure on a very complicated and fragile ecosystem, consisting of a rich variety of marine fauna and flora, several endemic species and one of the most extensive coral reef formations in the world. Monitoring the dynamics of the basin and the physical and chemical balances involved is an important step in understanding the sensitive balances (physical, chemical and biological) and interactions that are governing the region.

From the point of view of a physical oceanographer the Red Sea is a very advantageous experimental basin combining several interesting characteristics. It has a relatively simple shape and moderate size (about one fifth of the Mediterranean Sea). The connection between the basin and the open ocean, the strait of Bab el Mandeb, is a very narrow and shallow channel (sill depth 160 m and narrowest point 25 km wide) and the dynamics governing a large area are reflected on a very small cross-section of about 2 km^2. The Red Sea experiences strong atmospheric forcing of both wind and thermohaline form with strong seasonal variability. As a result, the Red Sea produces one of the most saline water masses observed in the world ocean, the Red Sea Water, which outflows from the basin and spreads into the Indian Ocean influencing the stratification over an extensive area.

Despite its ecological importance, the Red Sea remains widely unexplored and several processes, such as the basic circulation pattern and the water mass formation, are still obscure and highly debated. This is one of the reasons for the speculative and oversimplistic character of various attempts to describe and explain the circulation patterns and the dynamics governing the exchange between the Red Sea and the Indian Ocean. Recent long-term and comprehensive observations in the strait of Bab el Mandeb (Murray and Johns, 1997), briefly discussed in several points of this dissertation, have improved our picture of several aspects of the regional dynamics and provide a starting point for investigating the circulation and water mass formation in the region and their variability in more detail. Some of these efforts are included in the following chapters, focussing on the formation of the Red Sea Water, the exchange between the Red Sea and the Indian Ocean and the circulation connecting the two regimes. A variety of methods is used here ranging from simple box and analytical models to a general circulation ocean model.

The first question addressed in this dissertation is the estimation of the annual mean heat and freshwater budgets of the Red Sea using the observed exchange and characteristics in Bab el Mandeb. Through these estimates we can constrain the available atmospheric forcing data to produce suitably accurate forcing fields for numerical model simulations. These fields, in turn, are used to investigate the influence of the different forcing mechanisms, wind or thermohaline, and their seasonal variability, on the circulation in the Red Sea and especially on the exchange flow at the strait, where the available observations make this possible. A general circulation ocean model is presented and used in Chapter 3 to answer these kinds of questions. In Chapter 4 the effects of the thermohaline forcing over the Red Sea and its seasonal variability are investigated in a more theoretical framework, a modified version of Phillips' model (Phillips, 1966). The results of the general circulation model are analyzed in Chapter 4 and 5 to address questions about the circulation of the Red Sea and the Red Sea Water mass formation. Finally, in Chapter 6 the exchange at the strait of Bab el Mandeb is revisited but focusing on the synoptic time scale variability (time scales from a few days to a few months).

Chapter 2

Heat and freshwater budgets in the Red Sea from direct observations at Bab el Mandeb

2.1 Introduction

The Red Sea is a concentration basin where extensive evaporation and winter cooling transform the surface waters to form one of the most saline water masses of the world ocean, the Red Sea Water (RSW). These processes are reflected in the strait of Bab el Mandeb, a very shallow and narrow channel, located at the southern end of the basin. This is the only connection of the Red Sea with the Gulf of Aden - Indian Ocean and a typical inverse estuarine exchange is observed for most of the year, with a relatively fresh inflow on top of a deep outflow of RSW. This simple picture is disrupted by a three-layer exchange during summer (June to September) with a shallow surface outflow, an intermediate inflow bringing the fresh and cool Gulf of Aden Water (GAW) inside the basin and a deep RSW outflow which is greatly diminished (Murray and Johns, 1997).

The wind-stress is also strong in the area and, in the southern part of the Red Sea, the wind direction reverses seasonally in association with the Indian monsoon system. Which of the two forcing mechanisms, wind or thermohaline, is controlling the observed circulation in the Red Sea and the exchange with the Indian Ocean is highly debated (Neumann and McGill, 1962; Siedler, 1969; Phillips, 1966; Patzert, 1974a). Although the dynamics governing the region is still an open subject and have been the focal point of several recent studies (Eshel and Naik, 1997; Tragou and Garrett, 1997; Maxworthy, 1997), our knowledge of the forcing fields is very poor. Observations of the air-sea fluxes in the area have been very sparse in space and time and most of the available estimates rely on bulk formula parameterizations which are known to include several uncertainties for parts of the world ocean (da Silva et al., 1994) and in particular for the Red Sea basin (Tragou et al., 1999). The importance of the seasonal or even higher frequency variability of the forcing to the Red Sea dynamics is well known (Patzert, 1974a and b; Chapter 3; Chapter 4). However, the available estimates differ considerably even for the annual mean budgets (Table 2.3 and Table 2.2). Therefore, the present study will focus on the annual mean freshwater and heat budgets of the Red Sea, based on observed oceanic fluxes at the strait of Bab el Mandeb.

The Red Sea is located in a very arid area and the precipitation is very small (from different estimates it ranges from 0.5 to $0.15 m/year$) while no major river discharges into the basin. The evaporation rate is one of the highest in the world ocean but the available estimates differ considerably in the annual mean value as well as its seasonal cycle. The first attempt to measure the evaporation was carried out by Vercelli (1925) using pan measurements aboard a ship and on the coast. The estimated value of 3.5 $m/year$ is extremely high and the results seem doubtful since pan measurements over the land are very different from those on the sea surface (Sverdrup et al., 1942; Morcos, 1970). To convert pan measurements to evaporation rate from the sea surface Wust (1954) recommended an empirical reduction by 45% which gives a revised value of 1.9 $m/year$ for Vercelli's measurements, which is closer to recent estimates. All later estimations use either bulk formulae or conservation of volume and salt inside the Red Sea basin and are summarized in Table 2.3. Yegorov (1950) and Neumann (1952), using bulk aerodynamic formula and meteorological tables, produced values of 2.3 and 2.15 $m/year$, respectively. The same formula applied to data from British ships for the period 1921-1950 was used by Privett (1959) for an estimate of 1.83 $m/year$. Morcos (1970), in his Red Sea review, used an average of the last three estimates to produce a best estimate of 2.1 $m/year$, and assuming an average precipitation of 0.05 $m/year$, he obtained an $E - P$ rate of 2.05 $m/year$ for the Red Sea. Various other formula-based estimates by Hastenrath and Lamb (1979), Bunker et al. (1982), Ahmad and Sultan (1987 and 1989) and the Comprehensive Ocean Atmosphere Data Set (COADS - da Silva et al., 1994) using different climatological data products yield evaporation rates of 1.54, 2.3, 2.07, 2.13 and 1.62 $m/year$, respectively. Osman (1984) following the same method, but using daily values of the atmospheric conditions from a single coastal station in the Port Sudan region, and using the sea surface temperature climatology from Robinson's (1973) Red Sea atlas, estimated an evaporation rate of 2.04 $m/year$.

Since the freshwater deficit of the Red Sea must be compensated by the oceanic flux through the strait of Bab el Mandeb, another method for estimating the $E - P$ rate is to

AUTHOR	METHOD	EVAPORATION (m/year)
Vercelli, 1925	pan measurements	3.5
Yegorov, 1950	bulk formula	2.3
Neumann, 1952	bulk formula	2.15
Wust, 1954	correction on Vercelli, 1925	1.925
Privett, 1959	bulk formula	1.83
Bogdanova, 1966	volume and salt conservation	2.66
Morcos, 1970	average of previous estimations	2.1
Hastenrath and Lamb, 1979	bulk formula	1.54
Bunker et al., 1982	bulk formula	2.3
Ahmad and Sultan, 1987	bulk formula	2.07
Ahmad and Sultan, 1989	bulk formula	2.13
Osman, 1984	bulk formula	2.04
da Silva, 1994	bulk formula	1.5
Tragou et al., 1999	volume and salt conservation	1.75

Table 2.1: Review of evaporation rate estimates.

use the conservation of volume and salt for the basin evaluated at the strait. Although it seems a favorable approach, since fluxes at the 0.45 million square kilometers of the air-sea interface must be reflected on the 2 square kilometers of the cross-sectional area of the strait, it requires long term observations of transport and hydrographic properties. Tragou et al. (1999) followed this method using transport estimations at Bab el Mandeb by Patzert (1974c) derived from ship drift observations and the salinity profile from the Levitus climatology (Levitus, 1982) at the point inside the Red Sea closest to the strait. Assuming a constant evaporation rate and separating the transport in three layers, to include both winter and summer circulation, their estimate for the $E - P$ rate is 1.6 $m/year$. For comparison with the previous estimates they assumed a precipitation of 0.15 $m/year$ so that their final evaporation rate estimate is 1.75 $m/year$.

Both advective and bulk formulae methods have been employed for the evaluation of the heat flux at the air-sea interface of the Red Sea and the results are presented in Table

AUTHOR	METHOD	HEAT FLUX Wm^{-2}
Patzert, 1974	heat advection at Bab el Mandeb	7
Bunker, 1976	bulk formulae	-75
Hastenrath and Lamb, 1979	bulk formulae	-47
Bunker et al., 1982	bulk formulae	-47
	after corrections	-1
Sharaf el-Din and Mohamed, 1984	heat advection at Bab el Mandeb	19
Ahmad and Sultan, 1987	bulk formulae and observations	-1
Ahmad and Sultan, 1989	bulk formulae and observations	22
da Silva, 1994	bulk formulae	-83
	constrained	-42
Tragou et al., 1999	bulk formulae	-15
	best guess	5

Table 2.2: Review of estimates of the annual mean heat flux from the surface of the Red Sea.

2.2. Patzert (1974c) estimated a heat loss from the surface of the Red Sea of 7 Wm^{-2} using monthly ship drift observations and temperature observations at the strait (from the National Oceanographic Data Center). The same approach was followed by Sharaf el-Din and Mohamed (1984) but using the average exchange transport at the strait for each season (December to March for the winter and June to September for the summer) to get an annual average heat loss of 19 Wm^{-2}. With the same bulk formulae method incorporating different coefficient and different meteorological data sets the heat budget of the Red Sea was estimated by Bunker (1976) at $-75\,Wm^{-2}$, Hastenrath and Lamb (1979) $-47\,Wm^{-2}$, and by Bunker et al. (1982) at $-47\,Wm^{-2}$ and $-1\,Wm^{-2}$ after implementing Budyko's (1963) method. The negative heat fluxes indicate heat *gain* by the sea.

Two estimates by Ahmad and Sultan (1987, 1989) use the bulk formula approach but with direct observations of the solar radiation from stations on the coast of the Red Sea. Meteorological and sea surface temperature data for the first estimation are from oceanographic stations between 21^oN and 22^oN and the result is $-1Wm^{-2}$. The second estimation uses data from meteorological stations spanning most of the length of the basin along the eastern coast of the Red Sea. For the basin as a whole the result is $19\,Wm^{-2}$. The air-sea heat fluxes from COADS (da Silva et al., 1994) present the highest heat gain by the Red Sea at $-83\,Wm^{-2}$. The data set includes also net heat fluxes constrained by global balances at 65^oS which produce a neat heat gain of the Red Sea of $-42\,Wm^{-2}$. Tragou et al. (1999), in their thorough investigation of the COADS data set, applied several corrections to the bulk formulae for a better application in the region and estimated a net heat flux of $-15\,Wm^{-2}$. Due to uncertainties introduced by the bulk formulae parameterization and possible systematic errors in the observations they calculated a total uncertainty of $\pm 21\,Wm^{-2}$. From this their best guess for the net heat flux was $5\,Wm^{-2}$.

In the present study long term observations at the strait of Bab el Mandeb (Murray and Johns, 1997) of transport, salinity and temperature will be used to estimate the annual mean freshwater and heat budgets. These are independent from vagaries of the bulk parameterization and forcing terms over the surface of the Red Sea.

2.2 Data and Method

The long-term (18-month) observations at Bab el Mandeb for the period between June 1995 and November 1996 were carried out with current meter, Acoustic Doppler Current Profiler (ADCP) and temperature-salinity chain moorings at the Hanish Sill and the Perim Narrows (described by Murray and Johns, 1997). Additional moorings inside the channel and outside the basin, pressure gauges, an anemometer station and a series of cruises during both seasons were also included for a complete picture of the strait dynamics and the

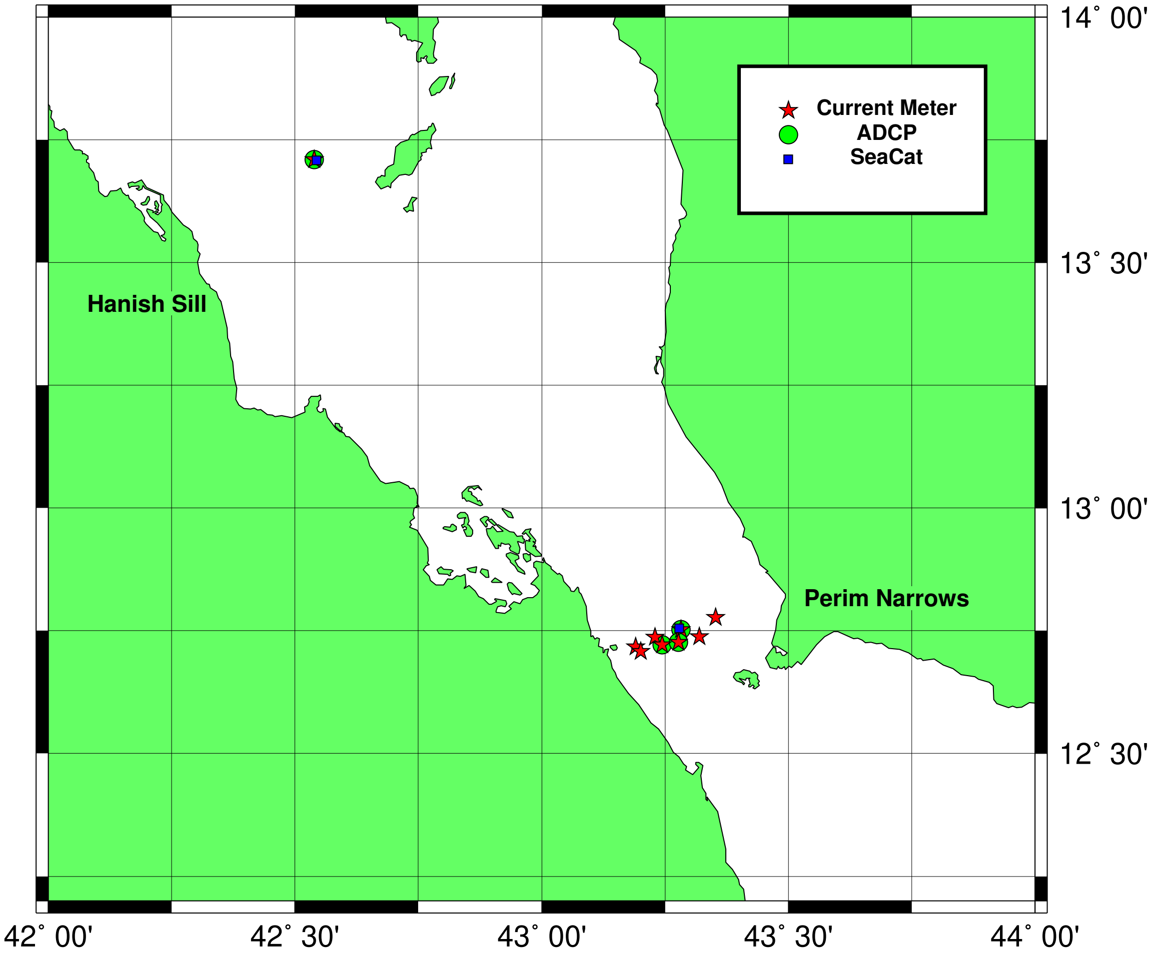

Figure 2.1: The location of the instruments used in the heat and freshwater budgets

exchange between the Red Sea and the Gulf of Aden - Indian Ocean system. Figure 2.1 shows the location of the measurements that will be used here to estimate the heat and freshwater fluxes through the strait.

The two transport-resolving current meter arrays across the strait were located near the Perim Narrows and at the shallowest section, the Hanish Sill. Each of these arrays includes an upward looking ADCP moored near the bottom in the deep central position of the channel and three flanking moorings instrumented with current meters. During the second half of the deployment a second ADCP was deployed in the Perim section for a better coverage in that location. As can be seen in Figure 2.1 the best spatial coverage was achieved in the Perim Narrows. This and limited width of the strait at this location make this section preferable for an accurate estimation of the transport through the strait.

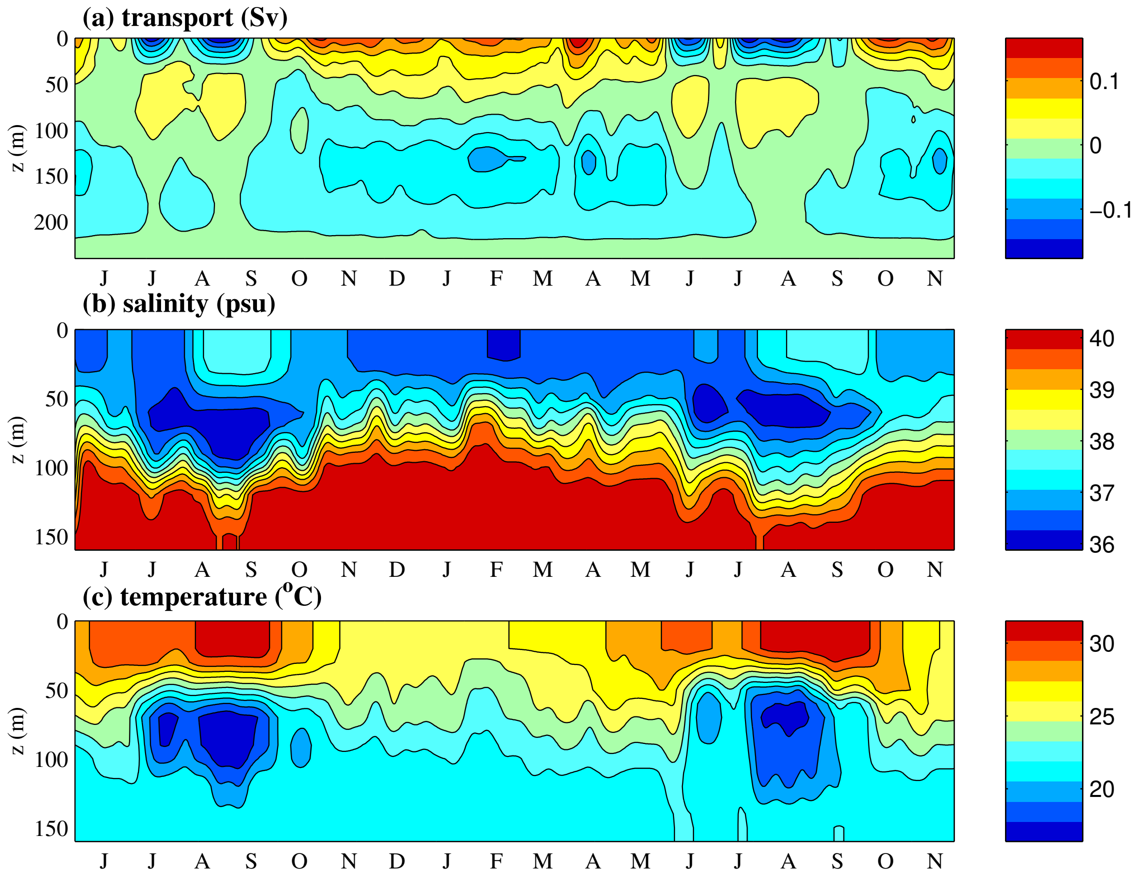

Figure 2.2: Transport from the Perim section (Sv), salinity and temperature from the deepest point of the Hanish Sill (20-day low-passed).

The velocity measurements of this section were interpolated over the cross-section and extrapolated linearly to the surface beyond the reach of the moorings. With this coverage the transport through the section was calculated and the resulting 18-month time series transport profile is plotted in Figure 2.2, where positive values represent inflow into the basin. Two salinity-temperature moorings instrumented with six Sea Cats were deployed within $100m$ of the ADCP moorings at Perim and Hanish. Due to instrument malfunctions data are missing from several of the temperature-salinity recorders at the Perim mooring, while good data were obtained at the Hanish mooring. Assuming a uniform surface layer, the salinity and temperature profiles at the Hanish Sill were extended to the surface, using the $20m$ values for the water column characteristics above this level. The time series profiles of salinity and temperature, filtered with a 20-day low-pass filter, are presented in Figure 2.2 (b and c).

To estimate the advective freshwater and heat fluxes, simultaneous velocity, salinity and temperature data on the same cross-section of the strait should be used. Unfortunately, due to the missing temperature-salinity data from the Perim Narrows, and also the loss of velocity data from some of the current meters at the sides of the Hanish Sill, the observations from both locations must be combined. The transport at the Hanish Sill cannot be resolved with sufficient accuracy for the fluxes. To calculate the best estimates of heat and freshwater fluxes, four time series will be used: (i) the transport profile at Perim, (ii) the velocity profile from the ADCP located at the center of the Hanish Sill, and (iii) temperature and (iv) salinity profiles from the Hanish Sill (Figure 2.2). Assuming that the pattern and magnitude of the transport does not change much between the two points of the channel, the transport from Perim is projected on Hanish taking into account the velocity zero-crossings that are available from the ADCP profile at the Hanish Sill, as illustrated in Figure 2.3. This assumption is supported by the similarity of the velocity profiles at the two points. In this way the winter two-layer and the summer three-layer exchange systems are preserved and the transport of each layer corresponds to the correct temperature and salinity characteristics. Using the salinity and temperature observations at Hanish we can

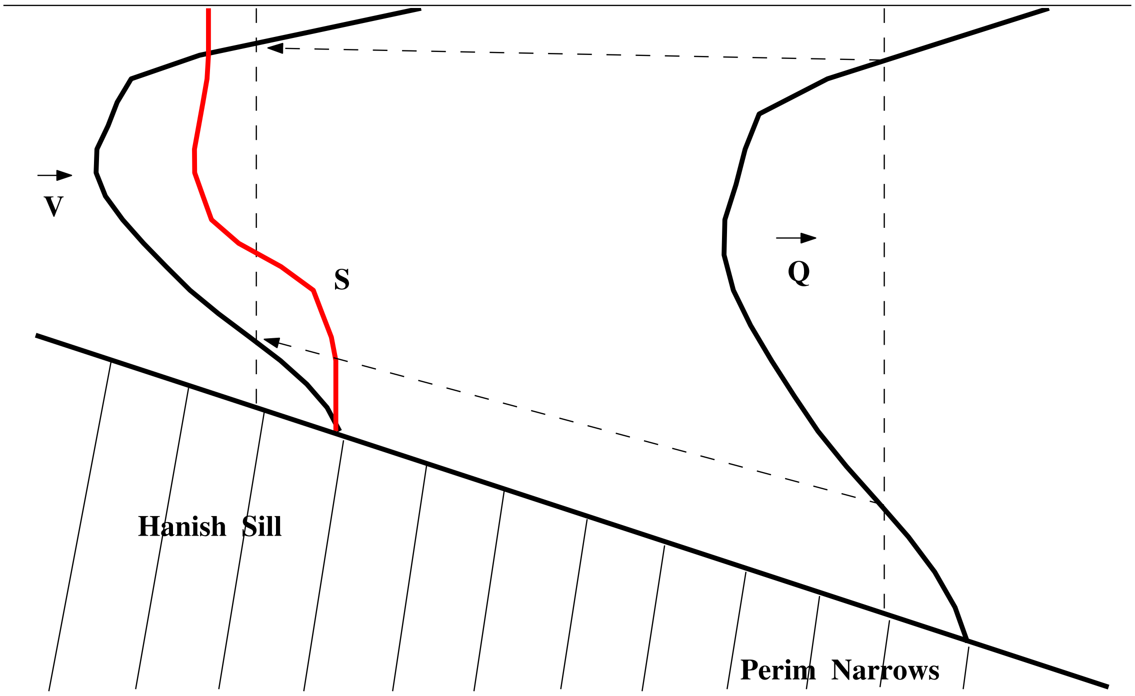

Figure 2.3: Schematic representation of the projection of the the transport from Perim to Hanish. Q is the transport profile at Perim, whose zero-crossings are aligned with the zero-crossings of the ADCP velocity profile at Hanish, and the transport is conserved in layers.

now estimate the average salinity and temperature of the layers weighted by the transport

$$\overline{S_i} = \frac{\int_{z_i}^{z_{i-1}} Q(z) \cdot S(z)\ dz}{\int_{z_i}^{z_{i-1}} Q(z)\ dz} \tag{2.1}$$

$$\overline{T_i} = \frac{\int_{z_i}^{z_{i-1}} Q(z) \cdot T(z)\ dz}{\int_{z_i}^{z_{i-1}} Q(z)\ dz} \tag{2.2}$$

$$Q_i = \int_{z_i}^{z_{i-1}} Q(z)\ dz \tag{2.3}$$

where i ($i = 1, 2, 3$) denote the surface, intermediate GAW intrusion and RSW layer, respectively (only layers 1 and 3 are present in winter), z_i represents the zero crossings of the transport profile (or sea surface and bottom) bounding each layer, and $\overline{S_i}$, $\overline{T_i}$ and Q_i are the layer salinity, temperature and transport, respectively.

2.3 Results

The monthly mean values of the three above quantities (Q_i, $\overline{S_i}$, $\overline{T_i}$)are presented in Figure 2.4 and will be used for the estimation of the freshwater and heat budgets of the Red Sea. The layer transport annual cycle corroborates the seasonality discussed in the beginning of the chapter, with a two-layer exchange from October to May and a three-layer exchange starting during June and ending in September. The strength of the winter exchange achieves its maximum during February when the RSW layer has an outflow rate of more than $0.6\,Sv$. This outflow becomes very weak in summer with a minimum of $0.05\,Sv$ during August. During August the strongest three-layer exchange is present in the strait, when the GAW intrusion reaches a rate of about $0.3Sv$. The temperature and salinity of the RSW layer fluctuates little throughout the year with mean values of 23^oC and $39.7psu$, but during summer and early fall both values slightly decrease due to mixing with the fresher and cooler GAW intruding into the basin. The temperature and salinity of the surface layer show a weak seasonal cycle associated with the annual atmospheric forcing and the circulation pattern of the region. The maximum temperature and salinity values occur in summer when the surface waters from the Red Sea basin, previously exposed to the strong freshwater and heat air-sea fluxes inside the basin, come out as a shallow surface outflow.

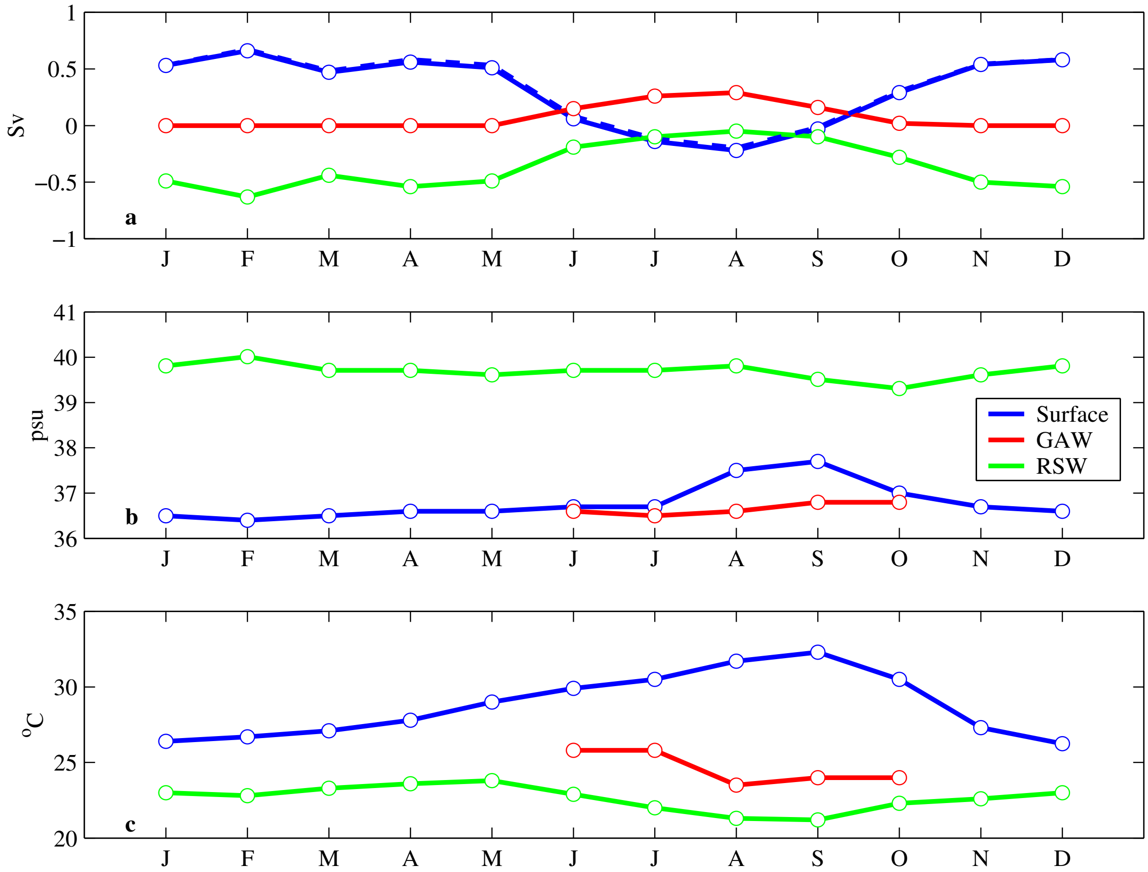

Figure 2.4: Monthly mean values of transport, salinity and temperature of the three layers involved in the exchange at Bab el Mandeb. The dashed line is the surface transport estimated through the E-P calculation.

The GAW summer layer is present in the water column as an intermediate minimum in temperature and salinity. Mixing

with the other water masses in the strait region produces a very thick layer (more than half of the water column), and the weighted average temperature and salinity characteristics are less pronounced in the time series of Figure 2.4.

MONTH	Q_2	Q_3	S_1	S_2	S_3	T_1	T_2	T_3	T_s	Q_1 (der.)
Jan	-	-0.49	36.7	-	39.8	25.9	-	23.1	22.5	0.53
Feb	-	-0.61	36.6	-	39.9	26.2	-	23.0	25.0	0.65
Mar	-	-0.44	36.7	-	39.7	26.6	-	23.4	25.3	0.48
Apr	-	-0.54	36.8	-	39.7	27.3	-	23.8	26.6	0.58
May	-	-0.49	36.8	-	39.6	28.5	-	23.9	28.3	0.53
Jun	0.15	-0.19	36.9	36.6	39.7	29.4	25.6	23.1	29.4	0.08
Jul	0.26	-0.10	36.9	36.5	39.7	30.0	25.6	22.1	30.3	-0.12
Aug	0.29	-0.05	37.7	36.6	39.8	31.2	23.3	21.5	30.8	-0.20
Sep	0.16	-0.10	37.9	36.8	39.5	31.8	23.8	21.3	30.6	-0.02
Oct	0.02	-0.28	37.2	36.8	39.3	30.0	23.8	22.4	30.1	0.30
Nov	-	-0.50	36.9	-	39.6	26.8	-	22.7	28.4	0.54
Dec	-	-0.54	36.8	-	39.8	25.8	-	23.2	26.7	0.58

Table 2.3: Variables used in the estimates and the derived surface transport

2.3.1 Salt Balance

To conserve volume and salt in the basin the transport and salt fluxes must add to zero over the annual cycle and the Knudsen formulae can be used. We therefore seek a constant (annual mean) $E-P$ value that satisfies the following equations

$$\overline{(E-P)}A = \overline{Q_1} + \overline{Q_2} + \overline{Q_3} \tag{2.4}$$

$$\overline{\rho_1 Q_1 S_1} + \overline{\rho_2 Q_2 S_2} + \overline{\rho_3 Q_3 S_3} = 0 \tag{2.5}$$

where A is the surface area of the Red Sea, Q_1, Q_2 and Q_3 are the layer transports, S_1, S_2 and S_3 are the layer salinities at the strait and ρ_1, ρ_2 and ρ_3 are the layer densities at the strait, and the indices correspond to the surface, GAW, and RSW layer, respectively. Because the largest uncertainties are in the surface layer transport since no instrumentation can be deployed very close to the surface, and the ADCP does not perform accurately in the first meters below the sea surface, this value (Q_1) is included as one of the unknowns in the volume and salt budgets. The $E-P$ is estimated at $2.06\, m/year$ and the associated Q_1 values are plotted in Figure 2.4 (dashed line), and are almost identical to the original estimates. Note, that even though the original surface transport is very close to the derived estimate, if we use the original Q_1, the residual in the mass budget will drop by $O(0.014\, Sv)$ which is large enough to throw off the $E-P$ estimate by about $1\, m/year$. Thus this small transport correction, with Q_1 as an unknown, is necessary for an accurate estimation of $E-P$.

The uncertainty in the $E-P$ estimate must take into account uncertainties in the transports and salinities of the layers. The lower RSW layer is well resolved by the instrument arrays and confined by topography, so that only small errors are expected in the estimated values for this layer, related mostly to the interpolation techniques. Linear and more complicated (spline) interpolation methods give very similar results for the lower part of the water column and so the uncertainties assigned to Q_3 and S_3 are $0.02 Sv$ and $0.1 psu$, respectively. The possible errors for the intermediate layer can be larger, since the resolution of the instrument grid is lower at this depths, and the uncertainties assigned for this layer are $0.01\, Sv$ (or more than 10% of Q_2) and $0.15 psu$. Finally, the largest uncertainties are located in the surface layer and this was the reason for leaving $Q-1$ as an "unknown" in the $E-P$ estimation. The uncertainty estimated for the surface layer salinity is $0.2\, psu$. If we propagate these values in our $E-P$ calculations, the final estimate is $\overline{E-P} = 2.06 \pm 0.22\ m/year$. Note that the uncertainty estimated here is much smaller than the possible error when using the original Q_1 directly in the $E-P$ estimation through the mass consrvation in the basin (almost $1\ m/year$). The additional condition of conservation of salt used in the Knudsen formulae contsrains the mass balance and reduces the uncertainty.

2.3.2 Heat Balance

The transport and temperature profiles at the Hanish sill can be used to determine the advective heat flux that is necessary to balance the surface heat flux over the Red Sea. Following the Tragou et al. (1999) formulation, with the same conservation of mass equation as above

$$\overline{Q_1} = \overline{(E-P)}A - \overline{Q_2} - \overline{Q_3} \tag{2.6}$$

$$\overline{F_T} = \frac{1}{A}\rho c_p(\overline{Q_1 T_1} + \overline{Q_2 T_2} + \overline{Q_3 T_3} + A\overline{(E-P)T_s}) \tag{2.7}$$

where T_1, T_2 and T_3 are the layer temperatures, ρ the mean water density (1026 kgm^{-3}), c_p the heat capacity of water (3986 $Jdeg^{-1}kg^{-1}$) and T_s the sea surface temperature. The last term in equation (2.7) represents the heat loss due to the volume that leaves the basin through the surface, evaporated at the sea surface temperature T_s. Using the National Oceanographic Data Center (NODC) data set to get a sea surface temperature climatology for the Red Sea and the $E-P$ rate estimated from the salt balance, the annual mean net heat flux is $11.2\,Wm^{-2}$. Following the same reasoning and error analysis used in the $E-P$ estimate, we can assign uncertainties of 1.5, 1 and 0.5 ^oC for the surface, intermediate and RSW layer temperature, respectively. If we use the error values for the transport measurements from the previous subsection and 2 ^oC fro the sea surface temperature (T_s), the final estimate is $\overline{F_T} = 11.2 \pm 5\,Wm^{-2}$.

Another important source of uncertainty in both freshwater and heat balance estimates is the possible interannual variability of the transport and/or the stratification in the region. Little is known about this kind of variability, but the few direct observations in the strait of Bab el Mandeb corroborate the values used here (Vercelli, 1927; Siedler, 1968; Maillard and Soliman, 1984). Future long term observations at the strait and inside the Red Sea basin will be needed to resolve the variability at time scales larger than the seasonal.

2.4 Summary and Discussion

The present study represents an improvement of our understanding of the freshwater and heat budgets of the Red Sea, since it is the first time that direct observations of high quality have been used. This is the reason that there are relatively big differences with previous estimations using the advective method. Tragou et al. (1999) used a similar method, but since their transport estimates are derived from ship drift observations, only the surface layer transport was assumed known. For the summer subsurface inflow they used measurements by Maillard and Soliman (1986) (July to September) and the values for June were derived by interpolating between the ship drift May values and Maillard and Soliman's July observations. Despite the different choice of unknowns (Q_3 instead of Q_1 used in the present study), the transport values used by Tragou et al. (1999) do not differ much from the transport values used here. However, Tragou et al. (1999) used salinity values from Levitus climatology inside the Red Sea at $15.5^o N, 41.5^o E$, $230 km$ away from the Hanish Sill, to define the water properties inside the strait. Large differences appear in the layer averaged salinity values used by Tragou et al. compared to ours measured directly in the strait. Also, in Tragou et al.'s analysis the summer salinity minimum of the GAW is totally absent at this point in the Levitus climatology. Comparing with previous studies, using the oceanic advection of salt and heat, we can notice that the heat budget is not very sensitive to the new observations (Patzert, 1974c; Sharaf el-Din and Mohamed, 1984) but the freshwater balance is (Tragou et al., 1999). An overall comparison of the present study with previous ones is presented in Figure 2.5. As a result of these new measurements the errors in both heat and salt fluxes at the strait are small enough to provide robust constraints on surface flux climatologies.

Although a budget constraint from the advective fluxes at the strait is very important, this method can not be used with accuracy for the investigation of the seasonal and higher frequency variability and the spatial distribution of the air-sea fluxes. The reason is that volume, salt and heat storage inside the Red Sea basin must be taken into account on time scales shorter than the annual. Several studies (Patzert, 1974a; Bogdanova, 1974; Bethoux, 1987) have shown that these parameters are large and important. The investigation of temporal and spatial variability has to focus on the air-sea fluxes through direct observations or bulk formulae methods.

Studies of parameters involved in the surface fluxes (sea surface temperature, cloudiness, aerosol optical thickness, precipitation, etc.) using satellite observations over the Red Sea are not available, and several problems, such as the shape and size of the basin in association with the resolution and orientation of the satellite tracks, may complicate this approach. Bulk formulae in conjunction with meteorological and ship observations are still the most widely used methods. The extensive discrepancies between the values proposed by different authors and the generally poor agreement with the directly determined heat and freshwater transports through Bab el Mandeb can have several explanations. One problem is the origin of the meteorological observations which in most of the cases come from land stations with poor spatial distribution and from poorly calibrated merchant ship measurements (Privett, 1960; Bunker et al., 1982). Also, Tragou et al. (1999) pointed out that the bulk formula used globally to calculate the insolation does not appear to perform well in the Red Sea. They attributed this to the high aerosol content of the atmosphere in the area, based on evidence from satellite observations detecting the aerosol optical thickness (Husar et al., 1997). Another very important source of possible error is the estimated wind speed included in some of the bulk formulae. Although the basic pattern of the seasonal wind field is well documented and observed, there are major differences between data sets (like the COADS and the older Koninklijk Nederlands Meteorologisch Instituut Atlas of 1949 used by Patzert (1974a)). Furthermore, the averaging processes used to get climatological values of the wind field can lead to errors by the neglect of higher frequency variability and especially the sea and land breezes which are strong and occur almost daily and in all months (Pedgley, 1974).

These effects lead to a bias toward net heat gain over the Red Sea in most available climatologies (Figure 2.5), often by considerable amounts. For example, COADS and Bunker (1976) suggest heat gain of approximately $80\,Wm^{-2}$ compared to our heat loss of about $10\,Wm^{-2}$. While Tragou et al. (1999) show that much of this error can be explained by biases in the radiative fluxes, errors related to the latent heat flux also directly affect the heat budget. The $E-P$ value of $1.5\,m/year$ obtained from COADS is lower than ours by about $0.6\,m/year$, which corresponds to an equivalent latent heat bias of almost $50\,Wm^{-2}$ ($1\,m/year$ of evaporation corresponds to about $100\,Wm^{-2}$ of latent heat loss). This suggests that as much as 60% of the heat flux bias in COADS could be due to underestimated evaporation. Despite an attempt to balance the heat budget, Tragou et al.'s (1999) $E - P$ estimate for the Red Sea of 1.6 $m/year$ is only marginally higher than COADS. Thus, it appears that both radiative fluxes and bulk formulae used for the estimation of the evaporation over the Red Sea will need considerable attention before reliable climatological heat and freshwater surface fluxes are available for the region.

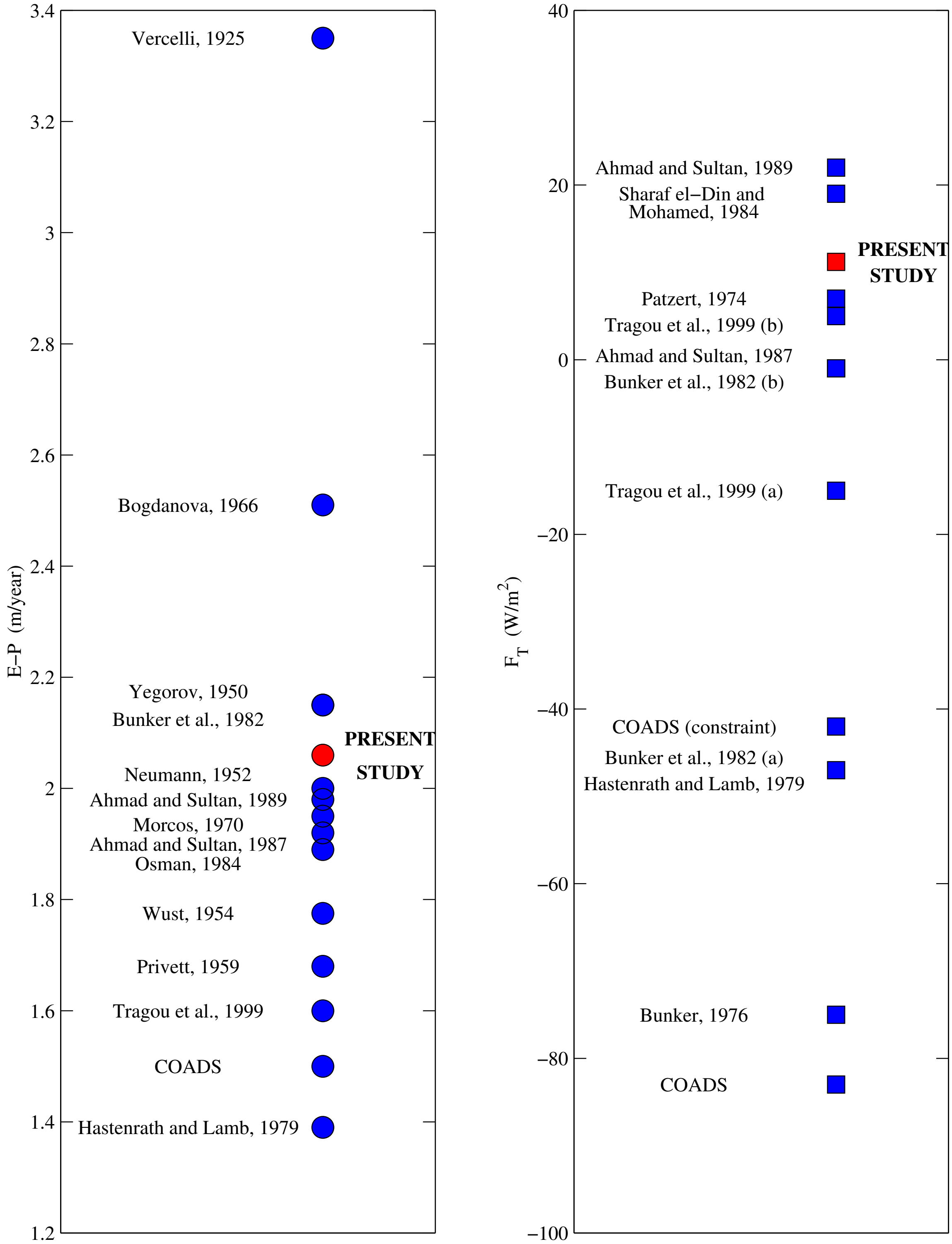

Figure 2.5: Comparison of the results from the present study with previous estimates.

Chapter 3

The seasonal variability of the exchange flow between the Red sea and the Indian Ocean, an OGCM investigation

3.1 Introduction

Due to the excess evaporation, the Red Sea is a typical concentration basin and an inverse estuarine circulation is expected at the strait of Bab el Mandeb, with a relatively fresh surface inflow on the top of a deep outflow of higher salinity water mass. For more than a century the general idea among the scientists investigating the region was that a two layer exchange must persist throughout the year, like the case of the Mediterranean

Sea and the Gibraltar strait (Maury, 1855; Schott, 1929). This idea was supported by several observational attempts, all of them taking place during the winter months (October to May) (Luksch, 1901; Krümmel, 1911; Vercelli, 1927). It was in July 1929 when an Italian expedition on board the AMIRAGLIO MAGNAGHI carried out current measurements along the strait, from which Vercelli (1931) for the first time demonstrated the presence of a three-layer exchange during the summer, with surface and deep outflows and an intermediate inflowing layer. Later observations (Sewell, 1934; Thompson, 1939b; Maillard and Soliman, 1984) supported the existence of this kind of seasonal variability as a permanent feature of the exchange between the Red Sea and the Indian Ocean. So, the overall picture emerging from all available investigations in the area is an eight-month two-layer winter inverse estuarine (fresh inflow on top of a hypersaline outflow) exchange replaced between June and September by a three-layer exchange comprised of a shallow surface outflow, an intermediate intrusion of the relatively fresh and cold Gulf of Aden Water mass (GAW), and a deep hypersaline outflow which is a small fraction of the winter value.

The explanation of the exchange flow and its variability must include consideration of the forcing and dynamics governing the whole region (the system Red Sea - Strait - Gulf of Aden). Although all previous studies agree that the evaporation over the Red Sea far exceeds the precipitation, the actual $E-P$ rate is highly debated, ranging in the available literature from 1.5 to 2.3 $m/year$ (Yegorov, 1950; Neumann, 1952; Privett, 1959; da Silva, 1994; Tragou et al., 1999). The annual mean heat flux from the surface of the Red Sea is very small (Patzert, 1974c) but the seasonal variability is important with an annual cycle of more than $200\,Wm^{-2}$ range (Tragou et al., 1999). Recent observations (Murray and Johns, 1997) have made possible an accurate estimation of the fresh water and heat budgets of the Red Sea (Chapter 2) producing an $E-P$ rate of $2.06 \pm 0.22\, m/year$ and a heat loss of approximately $11.2 \pm 5\, Wm^{-2}$ from the surface of the sea. The wind field is also strong and exhibits considerable seasonality (Patzert, 1974a). In the northern part of the Red Sea the climatological winds are from the northwest around the year but in the southern part of the basin, influenced by the Indian Monsoon, they reverse annually from southeast during winter to northwest during summer (June to September).

Although there is a general agreement that both thermohaline and wind forcing play a role in generating the horizontal and vertical circulation and stratification of the area and the exchange at Bab el Mandeb, the relative importance of each one and the role they play are highly disputed. The different theories that evolved during the last century ignore in general one or the other forcing mechanism and emphasize either the mean exchange or its seasonal variability. The buoyancy loss has been thought by several investigators to be the basic controlling mechanism of the flow (Maury, 1855; Luksch, 1901; Neumann and McGill, 1962; Phillips, 1966). Others believe that the wind-stress field is more important in determining the circulation pattern (Thompson, 1939a; Siedler, 1969; Patzert, 1974a).

The most representative theory of the thermohaline-driven circulation of the Red Sea is by Phillips (1966), involving similarity solutions of a convectively driven model. He assumed a semi-enclosed basin, with a sill and constant width, so that the circulation is on the vertical plane and no rotational effect is present. The model is driven by a uniform buoyancy loss over the surface of the basin and the circulation is in steady state. The circulation produced by the model is a two-layer flow and exchange at the sill in qualitative agreement with the observed winter pattern.

A very different approach was pursued by Patzert (1974a) for explaining the mechanisms behind the basic circulation features observed in the Red Sea and the exchange with the Indian Ocean. Based on the obvious coincidence of the reversal of the the wind field in the southern Red Sea with the reversal of the surface flow, he hypothesized that the variable wind-stress and the associated changes of the sea level in the southern Red Sea and the Gulf of Aden control the circulation in the region throughout the year and the exchange flow at the strait of Bab el Mandeb. To explain the three-layer system, present at the strait during summer, Patzert proposed that the northwest winds and a drop in the sea level at the northwestern Gulf of Aden due to wind-induced upwelling forces a shallow surface layer outflow from the basin. The same mechanism displaces the subsurface isopycnals upward, producing an opposite pressure gradient at intermediate depths that induces the intermediate intrusion of GAW. The relative importance of the direct wind-stress effect and the indirect effect through sea level setup across the strait were not determined, however.

During the past century very few studies were carried out to measure directly the exchange flow at Bab el Mandeb and most of them were very short term lasting for only a few days to a few months (Vercelli, 1927; Siedler, 1968; Maillard and Soliman, 1984). In order to assess the annual mean strength of the exchange and the seasonal variability most investigators have used indirect methods. Patzert (1974c) put together ship's drift observations from the KNMI Atlas and hydrographic data at the strait to estimate the seasonal cycle of the exchange flow. He calculated the monthly mean transports for a two-layer exchange (Table **??**), using a $0.03\,Sv$ adjustment for the lower layer to account for the freshwater loss inside the basin due to $E-P$, and assuming that the summer deep outflow was negligible. Using an evaporation rate of about $2.1\,m/year$ he estimated the annual mean surface transport to be $0.33\,Sv$ and the outflow of the saline Red Sea Water (RSW) to be $0.30\,Sv$. Siedler

(1969) used an $E - P$ value of $2\,m/year$ and average salinities for a two-layer exchange in Knudsen's formula (Knudsen, 1900) to estimate an annual mean RSW outflow of $0.33\,Sv$. Finally, Bethoux (1987) used the same method and salinity values but with $2.4\,m/year$ of $E - P$ and an annual cycle around this annual mean value, estimated by Hasternath and Lamb (1979), to get a mean RSW outflow of $0.38\,Sv$. The annual cycle of the exchange flow from Bethoux (1979) differs greatly from all the previous estimates. The very large difference in the RSW outflow from October to December (Table **??**) can be attributed to his assumption that all the GAW that entered the Red Sea during the summer season must exit as an intermediate outflow in the following months. All of the direct and indirect estimates described here are presented in Table **??** and plotted in Figure **??**.

The most complete in space and time investigation of the exchange flow at the strait of Bab el Mandeb was carried out during 1995-1996 (Murray and Johns, 1997). It lasted 18 months and resolved accurately the velocity, temperature and salinity structure in the strait. It is the first time that the complete seasonal cycle is captured with one set of direct observations. Murray and Johns (1997) confirmed most of the earlier deductions on the seasonal cycle of the exchange flow and showed that the transition between the two-layer winter exchange to the three-layer summer exchange is a robust feature of the seasonal flow pattern. The biggest advantage of this new data is that this pattern can be quantified and several important details, such as the RSW outflow during summer, are clear. The annual mean RSW outflow, which is a good measure of the overall strength of the exchange, was estimated at $0.36Sv$ but showed a large annual cycle ranging from over $0.6Sv$ during the peak of the winter (February) to less than $0.1Sv$ during the peak of the summer season (August). The reversal of the surface flow and the intrusion of GAW lasts four months

AUTHOR	JAN	FEB	MAR	APR	MAY	JUN	JUL	AUG	SEP	OCT	NOV	DEC
Vercelli			0.58									
(1927)			0									
			-0.49									
Siedler											0.58	
(1968)											0	
											-0.42	
Patzert	0.57	0.40	0.57	0.42	0.38	-0.06	-0.20	-0.21	-0.09	0.52	0.57	0.51
(1974c)	0	0	0	0	0	0.09	023	0.24	0.12	0	0	0
	-0.54	-0.37	-0.54	-0.39	-0.35	0	0	0	0	-0.49	-0.54	-0.48
Maillard and Soliman							-0.16	-0.25	-0.14			
(1984)							0.25	0.33	0.20			
							-0.06	-0.05	-0.03			
Bethoux	0.72	0.70	0.69	0.68	0.67	0.67	-0.26	-0.23	-0.20	0.54	0.50	0.49
(1987)	0	0	0	0	0	0	0.35	0.35	0.35	-0.35	-0.35	-0.35
	-0.67	-0.67	-0.67	-0.67	-0.67	-0.67	-0.09	-0.09	-0.09	-0.09	-0.09	-0.09

Table 3.1: Direct and indirect estimates of the layer transport (in Sv) at Bab el Mandeb (the three rows for each author correspond to the three layer, surface, GAW intrusion and RSW outflow, respectively)

(June to September) when an average of $0.22Sv$ of GAW enter the Red Sea basin. The monthly mean values of the layer transport are plotted in Figure **??** and compared with earlier observations and indirect estimates.

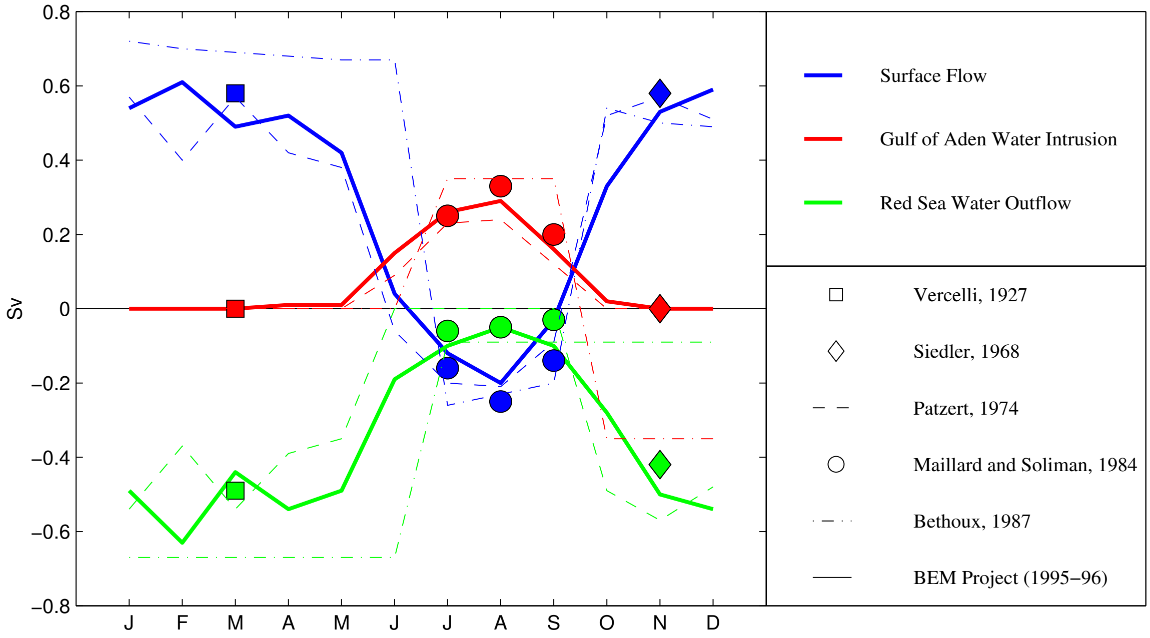

Figure 3.1: Historic and recent estimations of the layer transport at Bab el Mandeb

The basic features of the seasonal exchange cycle between the Red Sea and the Indian Ocean can now be taken as well defined and quantified, yet there is still a poor understanding of what causes this seasonal cycle. Specifically, what are the roles of the seasonal wind and buoyancy forcing fields in the exchange? The present paper focuses on the mechanisms involved in the observed variability using an Oceanic General Circulation Model (OGCM) numerical approach, with the goal to assess the relative importance of the different processes and forcing fields.

3.2 Model Configuration and Experiments

The available data that can be used to investigate the dynamics governing the circulation in the region are very sparse in space and time with the exception of the recent observations in the strait. This is one of the reasons for the numerous simplifications and assumptions used in all the hypotheses and models proposed to explain the Red Sea circulation and exchange with the Indian Ocean and the qualitative nature of their findings. The Red Sea has usually been treated as a two-dimensional basin driven by idealized atmospheric forcing of only the wind-stress or thermohaline type. A more complete and quantitative approach should include a three-dimensional numerical model of the Red Sea. In this chapter, we follow such an approach and perform a series of experiments using different combinations of wind stress and buoyancy forcing to resolve their respective roles in the mean exchange with the Indian Ocean and its seasonal cycle. Since the primary goal is to examine the effect of the different forcing mechanisms, and since detailed data are available only at Bab el Mandeb, it is desirable to include the strait within the model domain as a point of comparison between model results and observations, rather than using it as a boundary. Furthermore, important processes taking place outside the basin that may affect the exchange flow have been proposed, such as the wind-induced upwelling in the northwestern Gulf of Aden (Patzert, 1974a). Therefore, the domain chosen for numerical experiments includes a part of the Gulf of Aden.

The numerical experiments were carried out with the Miami Isopycnic Coordinate Ocean Model (MICOM) (Bleck et al., 1992; Bleck and Chassignet, 1994). The most important difference of MICOM compared with other models is that it has a vertical discretization in layers of constant potential density. On the top of the isopycnic layers there is a thermodynamically active mixed layer of the Kraus-Turner type (Kraus and Turner, 1967; Gaspar, 1988), which is vertically homogeneous but of varying density in the horizontal. The isopycnic layers are allowed to outcrop into the mixed layer by becoming massless. The horizontal grid is defined on a Mercator projection with the grid size fixed in the longtitudinal direc-

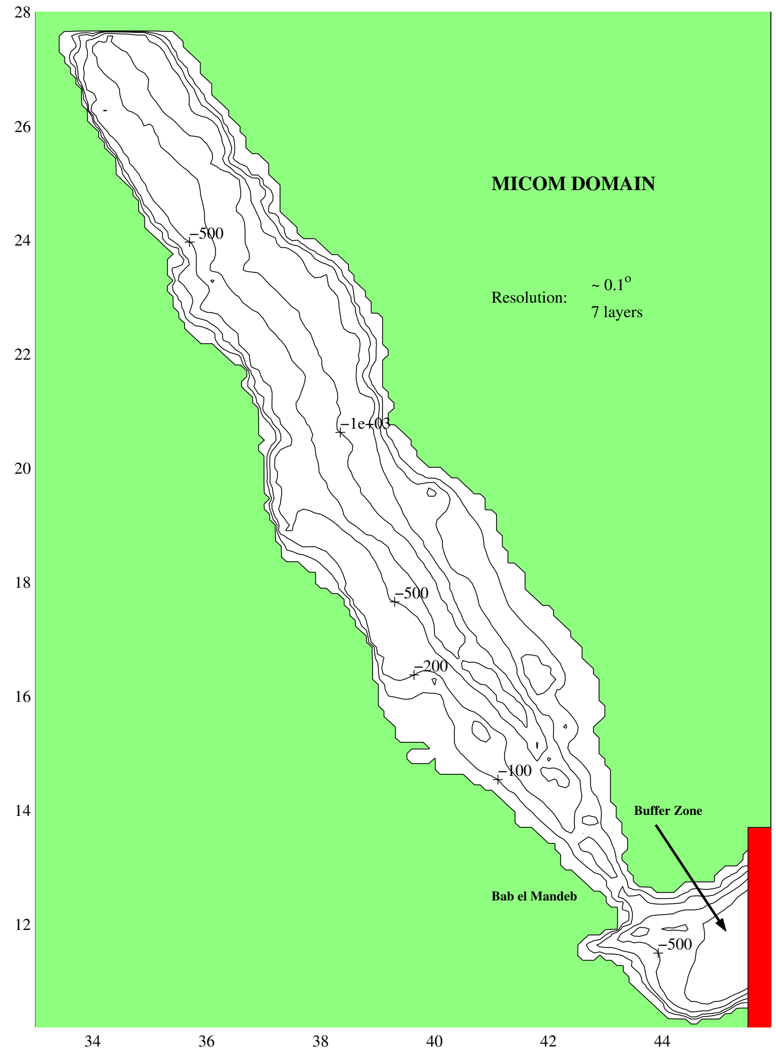

Figure 3.2: The geographical domain included in the OGCM experiments.

tion but varying with the cosine of latitude. In the experiments presented here a horizontal grid interval of 0.1^o (or about $10km$) was chosen in order to resolve the very narrow channel at Bab el Mandeb. The two gulfs in northern end of the Red Sea (Suez and Aqaba) are very small with very complicated topography and were not explicitly included in the present experiments. The domain is extended outside the Red Sea to incorporate part of the Gulf of Aden reaching the 45^oE (Figure **??**). The vertical density structure is defined by 6 isopycnic layers and a mixed layer, shown in Table **??**. The number and densities chosen for the layers used in these experiments take into account the need to represent all the basic water masses and the strong pycnocline located at the base of the mixed-layer, so that the model can reproduce the basic density structure observed and involved in the Red Sea circulation. The distinction between water masses must take into account the temperature salinity characteristics, since the density stratification does not always reflect the presence of a certain water type. Bottom topography and coastlines were obtained from a digital data set with $5'$ resolution (ETOPO5) by averaging the topographic data located in each grid box. A correction was applied in the area of the strait where ETOPO5 data had a maximum sill depth of about 100 m which is 60 m shallower than the 160 m sill depth at the Hanish Sill. At the open end of the domain, in the Gulf of Aden, a 0.5^o buffer zone was fitted in which hydrography is relaxed towards monthly values derived from the Levitus (1982) climatology, with a relaxation time of 60 days.

Both mechanical and thermodynamic forcing are used to drive the model. The momentum flux is given by the components of the wind stress. The thermodynamic forcing consists of the heat flux and the freshwater flux (which is imposed as a virtual salt flux, Bleck et al., 1992) and the mixed layer is stirred by turbulence generated by the oceanic friction velocity and the buoyancy flux. The atmospheric forcing functions applied to the model are derived from COADS (da Silva et al., 1994) but with several adjustments. In Chapter 2, we derived constraints on the annual mean heat and freshwater budgets of the Red Sea, using the observed heat and salt fluxes at the strait, which give $11\,Wm^{-2}$ heat loss and $2.06myear^{-1}\,E-P$, respectively. COADS presents a heat gain of $90\,Wm^{-2}$ and about $1.5myear^{-1}\,E-P$ for the Red Sea basin. These values are considerably different from the observed values and cannot be expected to yield reasonable results for the exchange flow if used as is. The heat gain of $90\,Wm^{-2}$ from COADS, in particular, is approximately $100\,Wm^{-2}$ greater than the heat loss of about $10\,Wm^{-2}$ obtained from observations. The first correction applied is an addition of $0.5myear^{-1}E-P$ uniformly in space and time throughout the year. While in reality it is unlikely that this correction is uniform in space or time, it is not clear what its spatial or seasonal variations should be, and therefore the simplest approach is taken. After adding the latent heat produced by this correction term in the heat flux (each $0.5\,m/year$ of evaporation corresponds to approximately $40\,Wm^{-2}$ of heat loss) we need another $60Wm^{-2}$ of heat loss to the atmosphere, which is added again uniformly in space and time since the spatial distribution and the seasonal cycle of the air-sea fluxes over the Red Sea involve great uncertainties. Thus, we are effectively assume that the spatial and temporal (monthly) patterns in the air-sea fluxes over the region from COADS are valid but with a constant bias. The seasonal cycles of $E-P$ and heat flux from COADS, after applying the corrections, are plotted in Figure **??**. The model experiments were initialized using the National Oceanic Data Center (NODC) hydrographic data for the winter state (Figure **??**).

Six experiments were carried out using the same configuration but differing in the application of the forcing fields or in the buffer zone implementation, as summarized in Table **??**.

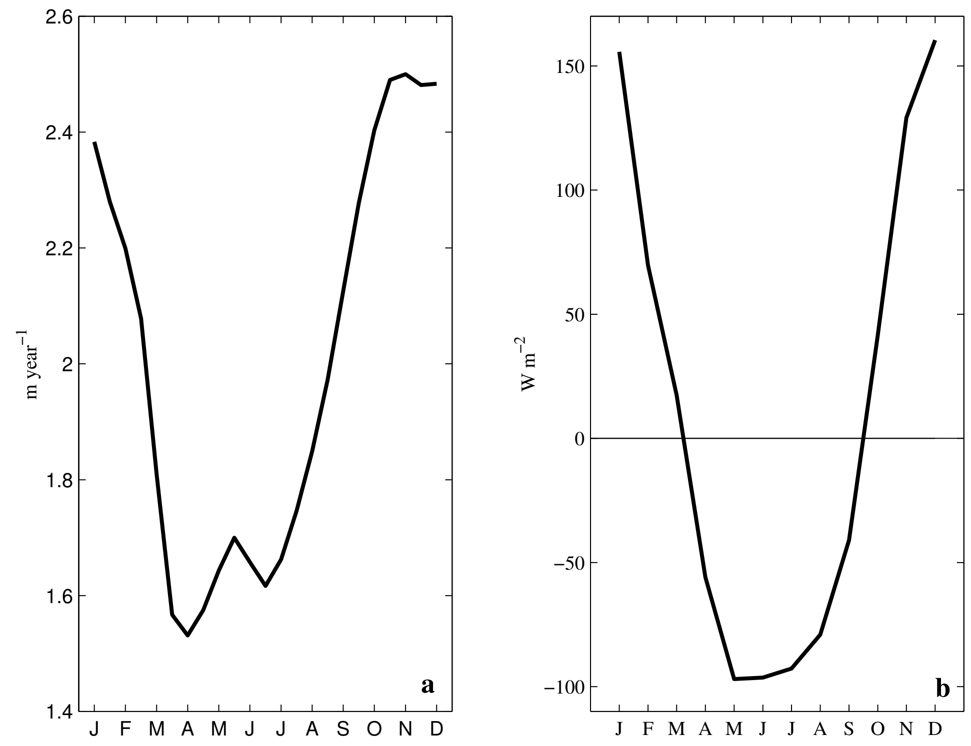

Figure 3.3: Seasonal cycles of (a) freshwater and (b) heat fluxes over the model domain from COADS, after corrections.

The first one (E1) is the most "realistically" forced experiment and includes seasonal wind and buoyancy forcing and a seasonally varying hydrographic profile at the Gulf of Aden buffer zone. The goal of this experiment is to capture as much variability of the exchange flow as possible, to serve as a reference experiment for all the other experiments. The next two (E2 and E3) include only one driving field, either wind or thermohaline forcing, to investigate the different role and importance of each one on the exchange flow. Without any buoyancy loss in E2, the basin is no longer a concentration basin and the exchange is not of the inverse estuarine type and cannot be compared with observations and other experiment results. To avoid this, another experiment (E4) is carried out where the seasonal wind forcing is combined with steady (annual mean) thermohaline forcing. In the fifth experiment (E5) the opposite combination was chosen (annual mean wind forcing and

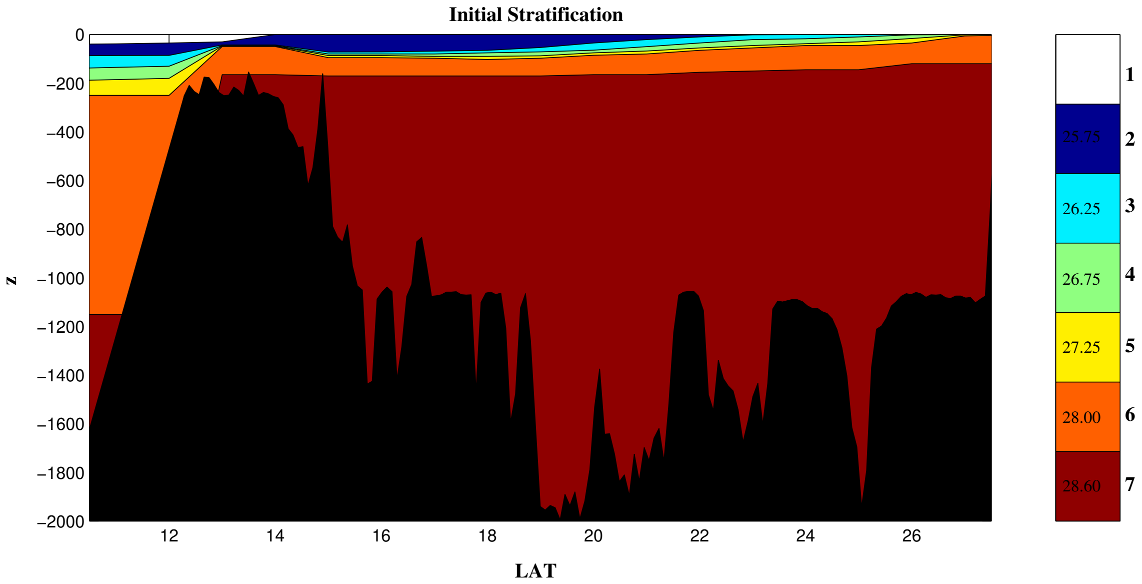

Figure 3.4: Initial stratification.

LAYER DENSITY (kgm^{-3})	EXPERIMENTS
mixed layer	full forcing (E1)
1025.75	wind forcing only (E2)
1026.25	thermohaline forcing only (E3)
1026.75	wind forcing and annual mean thermohaline forcing (E4)
1027.25	thermohaline forcing and annual mean wind forcing (E5)
1028.00	annual mean hydrography in the buffer zone (E6)
1028.60	

Table 3.2: Vertical resolution (layer density) and experiments performed

seasonally varying thermohaline forcing). Finally, a diagnostic experiment was performed (E6), where hydrography in the buffer zone is relaxed towards the annual mean (no seasonal variability present in the buffer zone), to investigate the influence of the buffer zone on the variability of the exchange flow.

The wind- and/or thermohaline-driven circulations develop rapidly, and the flow acquires its basic characteristics after the first few months of adjustment. Fully equilibrated solutions have not been obtained and long term adjustments, different for each simulation, are still taking place at the end of the simulations, associated with the heat and fresh water fluxes into the model interior driven by transformations occurring within the buffer zone. Nevertheless, after the first few months of simulation the pattern and strength of the flow through the strait of Bab el Mandeb changes little. All the experiments were carried out for 10 years and the results presented in the next section are an average of the last 9 years of the model integrations.

3.3 Model Results

The exchange flow produced in the experiments E1, E3 and E4 will be presented and compared with the recent observations at the Bab el Mandeb (Murray and Johns, 1997). The model data are taken from the location in the model equivalent to the Perim Narrows, which is where the Murray and Johns observations were conducted. In all the numerical simulations the most active layers in the area of the strait, in which most of the volume transport of inflow and outflow is taking place, are the surface layer (the mixed layer), the second layer representing the GAW, and the sixth layer which comprises the core of the RSW outflow. Although the other 4 layers produce much smaller transport, they are also included in the transport estimation according to their temperature and salinity characteristics and the direction of the flow in them. In order to compare the model results with the layer transports available from observations, the mixed layer is taken to represent the surface layer (the inflow layer in winter and shallow outflow layer in summer), layers 2 and 3 represent the GAW water intrusion (these layers disappear during winter inside the basin when the mixed layer deepens due to atmospheric forcing), and the layers below this (layers 4, 5, 6, and 7) comprise the RSW outflow.

The three-layer transports from the first experiment are plotted in Figure ??. Although some differences with the observations do exist, as described below, the basic conclusion

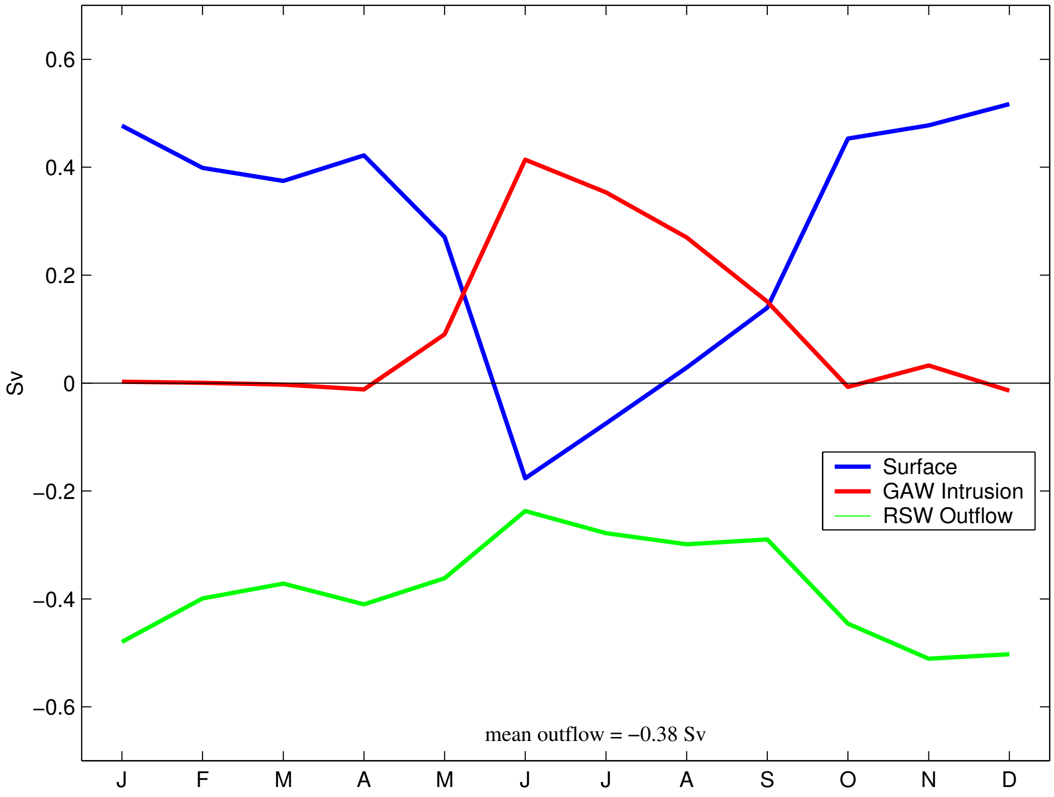

Figure 3.5: Layer transport from the full-forcing experiment (E1).

is that the model is able to capture the seasonal pattern of the exchange flow. There is a reversal of the surface flow during summer, accompanied by weaker RSW outflow. At the same time a strong intermediate inflow is present with an average transport of $0.23Sv$. Furthermore, the strength of the exchange is of the correct order of magnitude, with an annual mean RSW outflow of $0.38Sv$ (compared with the $0.36Sv$ obtained from observations).

The most important differences between the model and the observations are in the phase and range of the seasonal cycle. The peak of the summer season (represented by the reversal of the surface flow, the maximum of the intermediate intrusion and the minimum of the RSW outflow) takes place during June in the model instead of August as suggested by observations (Figure **??**). The amplitude of the seasonal cycle, for both surface and RSW outflow layer (and particularly the latter), is smaller than the observations. These discrepancies can arise for several reasons such as the model configuration and the problems in the atmospheric forcing data set. Also, we do not know if the period of the observations is a typical one, in the sense that it can be represented by the climatological data sets used for driving the model simulations and relaxing the buffer zone (COADS and Levitus). Overall, this experiment is quite successful, reproducing the the main features and the strength of the exchange flow. Therefore, we can proceed with the other two (thermohaline- and wind-driven) experiments to investigate the role of the forcing mechanisms.

Experiment E3 includes thermohaline forcing but no wind forcing. Although no wind forcing is applied, the strength of the exchange does not change perceptibly. The annual mean RSW outflow is now $0.39Sv$, almost identical to the previous result and the observations. The seasonal cycle is now changed with the RSW outflow showing very little variation throughout the year. But the surface and subsurface layers still show a strong seasonal cycle with a much weaker surface inflow during summer and most of the fall accompanied by a strong intermediate intrusion (Figure **??**). The GAW intrusion in summer and fall is similar in magnitude to that found in experiment E1 while the surface inflow reduces by about half its winter value.

The exchange flow from the next experiment (E4) forced by the wind-stress and the annual mean thermohaline fluxes is presented in Figure **??**. The first and perhaps most

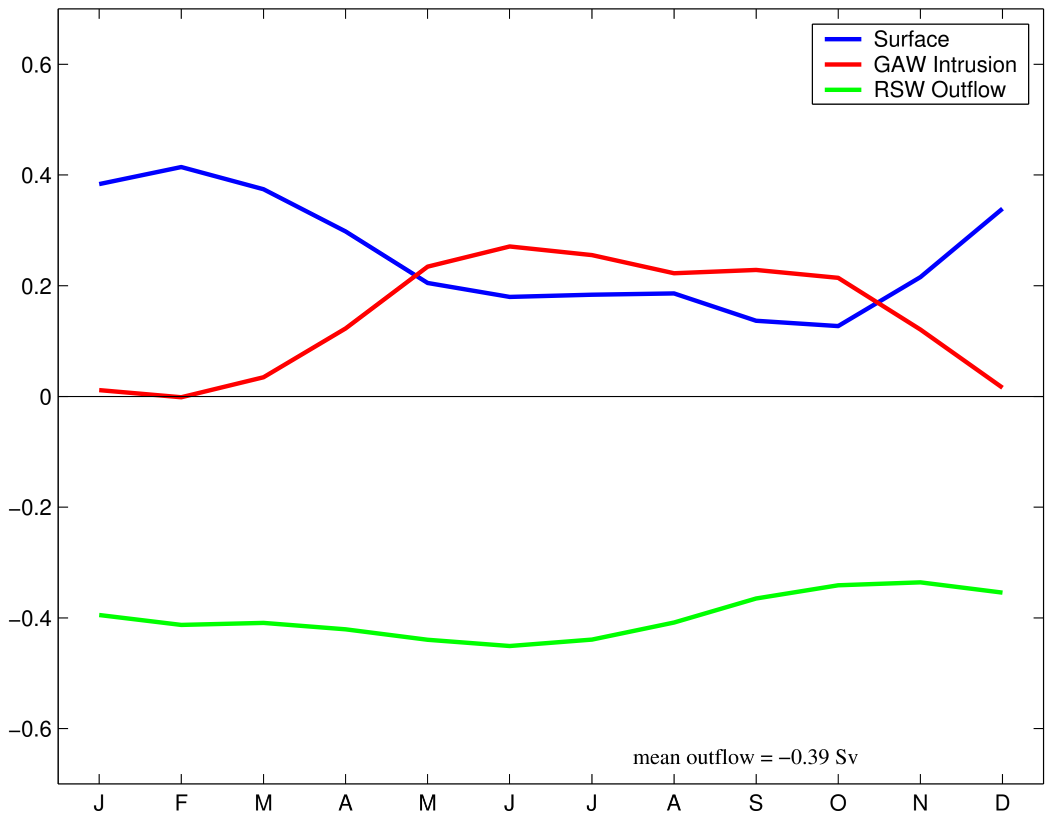

Figure 3.6: Layer transport from the thermohaline-driven (E3) experiment.

striking result is the reduction in the overall strength of the exchange. The annual mean RSW outflow is now $0.23Sv$, 40% weaker than in the case of the full forcing experiment (E1) which can be used as a reference value. In general, the flow at the strait is much weaker than the previous two experiments and more irregular. Nevertheless, some of the characteristics of the seasonal exchange cycle are present in this model. The summer reversal of the surface flow, although very weak, does exist during July and at the same time the intermediate inflow acquires its maximum. The RSW outflow also seems to respond at this time, becoming weaker, but it remains weak during the fall when the flow pattern becomes more irregular.

The combination of the thermohaline and mechanical forcing is not expected to be simple

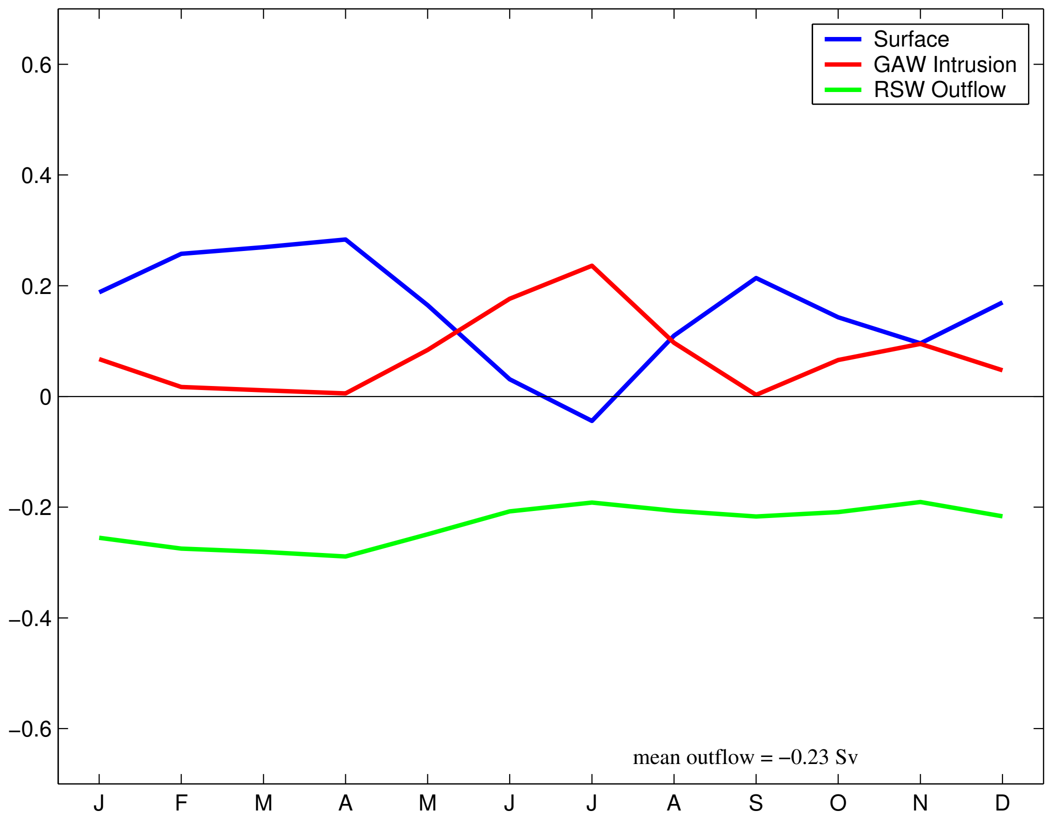

Figure 3.7: Layer transport from the wind-driven (E4) experiment.

one. One way to investigate this is to compare the results of the experiment forced by both the seasonal wind and thermohaline fields (E1) with the sum of the exchange flow produced by the experiments involving the seasonal winds only (E2) and the seasonal thermohaline forcing only (E3). The comparison is presented in Figure **??**. The obvious differences of the two result suggest that the final outcome is not a simple linear addition of the two effects. While the summer intrusion of GAW is reproduced, the surface flow does not reverse in the summer nor does the deep outflow show a significant reduction in summer. The wind and thermohaline forcing are connected and interact, and their combination produces an exchange flow similar to the observed one.

Since the general circulation of the whole domain ends at the buffer zone which also

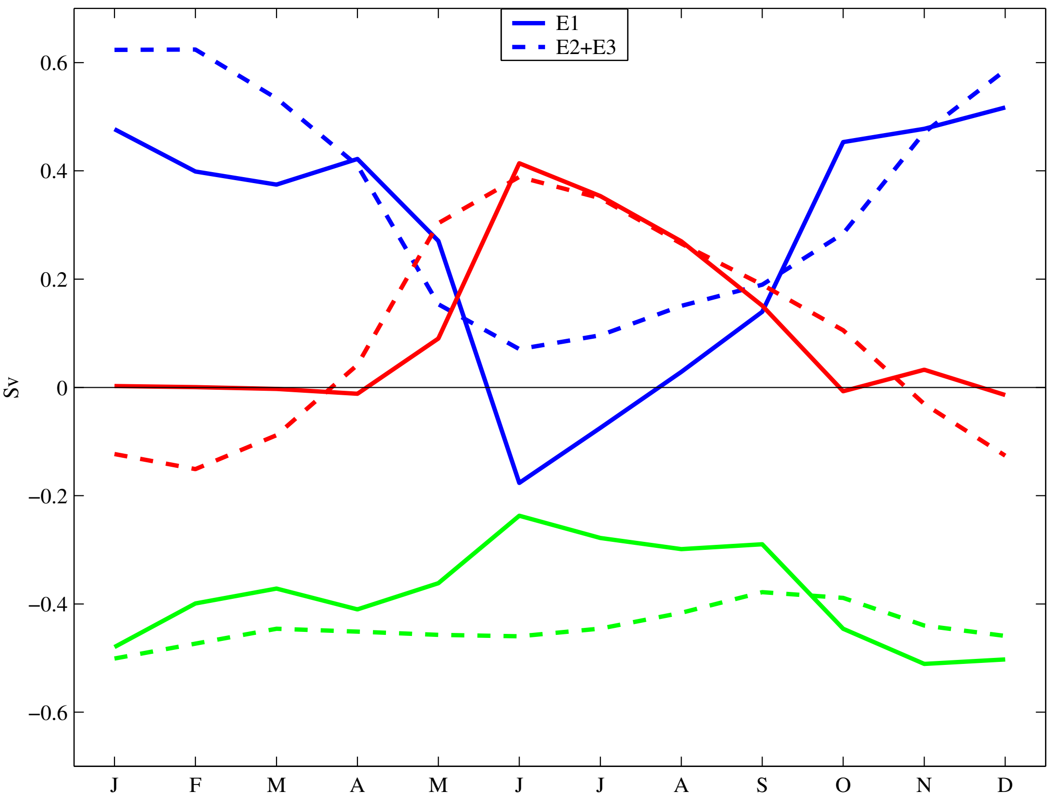

Figure 3.8: Comparison between the results of the full forcing experiment (E1) and the sum of the experiments E1 (seasonal winds only) and E3 (seasonal cycle of the thermohaline forcing only).

provides the necessary supply of fresh water to compensate the huge evaporation rate, special attention must be given to the influence of the variability in the buffer zone on the variability of the flow at the strait. With this in mind the last experiment (E6) was carried out, where the hydrography is held constant with the annual mean values at the outer edge of the buffer zone. Apart from some minor differences in the temperature and salinity characteristics of the water masses taking part in the exchange flow, which arise from the constant values of temperature and salinity used in the buffer zone, the result is the same as for the full forcing experiment (E1). Thus, although the water masses present in the Gulf of Aden play an important role in the circulation and the heat and fresh water budgets of the Red Sea, the variability in seasonal stratification far away from the strait does not seem to influence the dynamics of the Red Sea.

3.4 Summary and Discussion

As expected, the answer to the question of what is driving the exchange flow at Bab el Mandeb is not simple and straightforward. Both wind and thermohaline forcing are important and contribute to the seasonal variability observed. Their combination is not a simple linear addition but they interact to produce the final pattern. For example, the peak of the winter two-layer exchange in the thermohaline-driven experiment takes place during February, in the wind-driven experiment during April, and when combined during December. It is the combination of the two that generates the circulation and sets up the proper pressure gradients capable of driving the seasonal cycle of the flow at the strait. The wind forcing seems to be most influential in controlling the seasonal changes, such as the reversal of the surface flow and the abrupt commencement of the GAW intrusion. However, a strong reduction of the surface inflow during summer appears to be related to buoyancy forcing. Without this effect the wind driven reversal in summer would be either very weak or perhaps not occur at all. Some of the irregularities present in the wind-driven result, especially during the fall, can be attributed to the very weak wind field of COADS in the end of the summer and beginning of fall (August to October). Nevertheless, it is the combination with the thermohaline forcing that produces the pattern similar to the observed. Although the annual mean heat and freshwater budgets are known with accuracy, the seasonal variability of the different terms involved in the buoyancy flux include large uncertainties and some of them are highly disputed. The weaker seasonal cycle in the thermohaline-driven experiment (E3) and the prolonged summer type of exchange might be explained by the uncertainty in the seasonal range of this forcing mechanism. Recall that the corrections in the heat flux and $E-P$ were added uniformly around the year, although it is possible that they can contribute to a stronger seasonal variability.

There are some special issues that can be addressed using the model results. One of the most interesting is the mechanism through which the summer wind field contributes to or controls the surface outflow. Namely, what is the relative importance of the direct wind-stress and indirect wind-stress effect (through the wind-induced upwelling in the northwestern Gulf of Aden proposed by Patzert (1974a), which lowers the sea surface outside the basin to produce a surface pressure gradient driving surface waters outside the Red Sea)? To investigate this question the sea surface elevation difference between the the two ends of the strait and the wind-stress influence on the surface layer were computed and compared in the momentum equation

$$\frac{\partial u}{\partial t} = -g\frac{\partial \eta}{\partial x} + \frac{\tau^x}{\rho H} \tag{3.1}$$

where H and ρ are the thickness and density of the surface layer. The two terms on the right hand side were computed at the time of the summer reversal and the acceleration that can be produced from each one was estimated. The ratio of the two terms is $O(1)$, so that we can conclude that direct and indirect influence of the wind are of equal importance. Furthermore, the upward displacement of the subsurface isopycnals at the same time in the northwestern Gulf of Aden can produce a pressure gradient to drive the intermediate layers (representing the GAW) inside the basin as shown in Figure **??**.

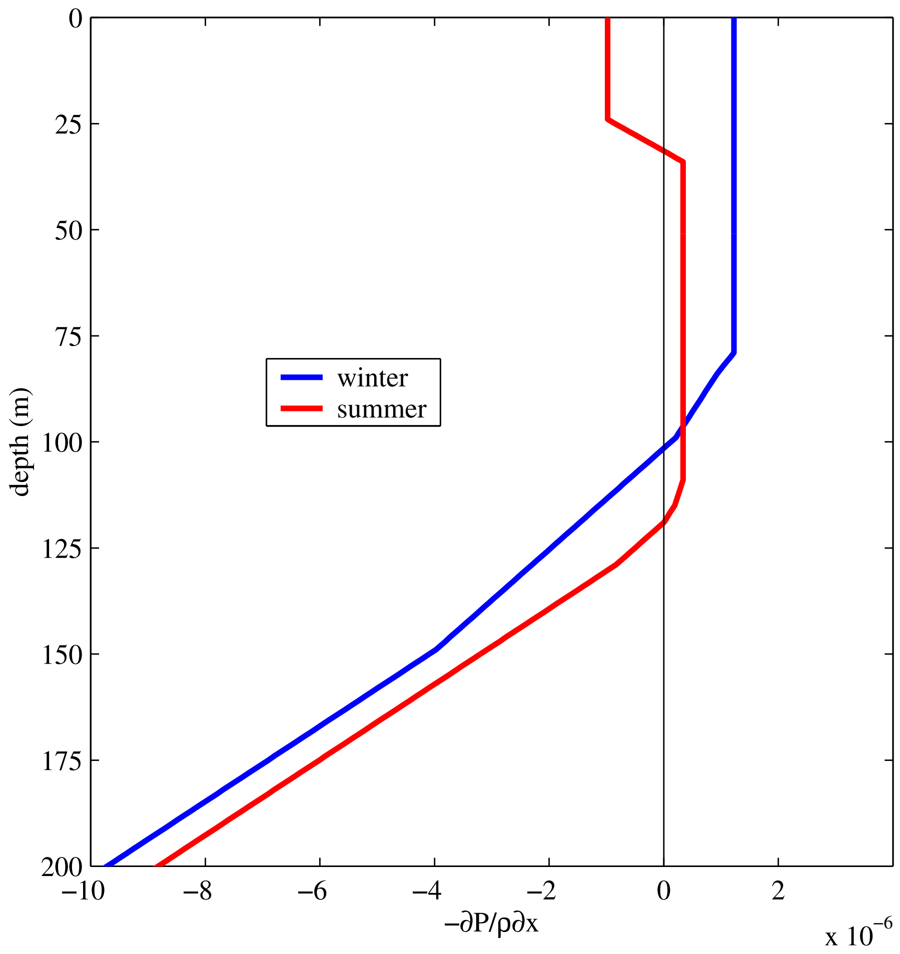

Figure 3.9: The pressure gradient between the two ends of the strait from the experiment E1, for winter (January) and summer (June). Positive values correspond to higher pressure in the Gulf of Aden, forcing inflow to the Red Sea.

A very striking result of the experiments is the influence of each forcing mechanism on the mean flow and especially the large reduction in the strength of the exchange for experiment E3 which has seasonal wind forcing but only steady (annual mean) thermohaline forcing. The RSW outflow is almost half in the annual mean although the average buoyancy loss was used in driving the model. The seasonal variability of the thermohaline forcing seems very important in creating the observed magnitude of the annual mean exchange. This must be closely related to the maximum buoyancy loss during the peak of the winter when the layers of RSW are formed. Without this extensive buoyancy flux to the atmosphere, especially in the northern part of the Red Sea, the amount of RSW formed is not enough to account for the observed values. Futhermore, the circulation produced in the simulations including the seasonal cycle of the buoyancy flux (E3 and E5) present a more vigorous basinwide circulation (Chapter 5) than the one produced by the respective experiment including the seasonal cycle of the wind-stress forcing (E2 and E4).

Although there is no intention here to discuss details of the circulation inside the basin (for a detail description of the results of the model, the reader is referred to Chapter 5), it is important to give an idea of the basic circulation pattern on the vertical plane, the overturning circulation, which produces the exchange flow at the strait. Since MICOM is a layer model overturning circulation is ploted on the σ_θ-latitude plane, and is presented in Figure **??** for (a) the peak of the winter (December), when the strongest two-layer exchange is taking place and (b) the peak of the summer (June) when the strongest surface outflow is present in the model results. The seven layers (six isopycnic and a mixed layer with variable density in the horizontal) are also included in the figure. Although during December the production of RSW does not achieve its maximum, which takes place one to two months later, the two-layer cellular circulation is well established.

A single broad recirculation cell is present in winter centered at about 17^oN. Most of the fluid (about 2/3) sinks in the northern Red Sea north of 22^oN. A small amount of upwelling from the 2nd and 3rd layer into the mixed layer occurs south of 17^oN within the Red Sea. The summer overturning circulation presents two cells, a shallow one in the southern part and a deeper one centered in the middle of the basin (about 20^oN). The shallow cell is associated with the reversal of the surface flow and the GAW intrusion, while the second one

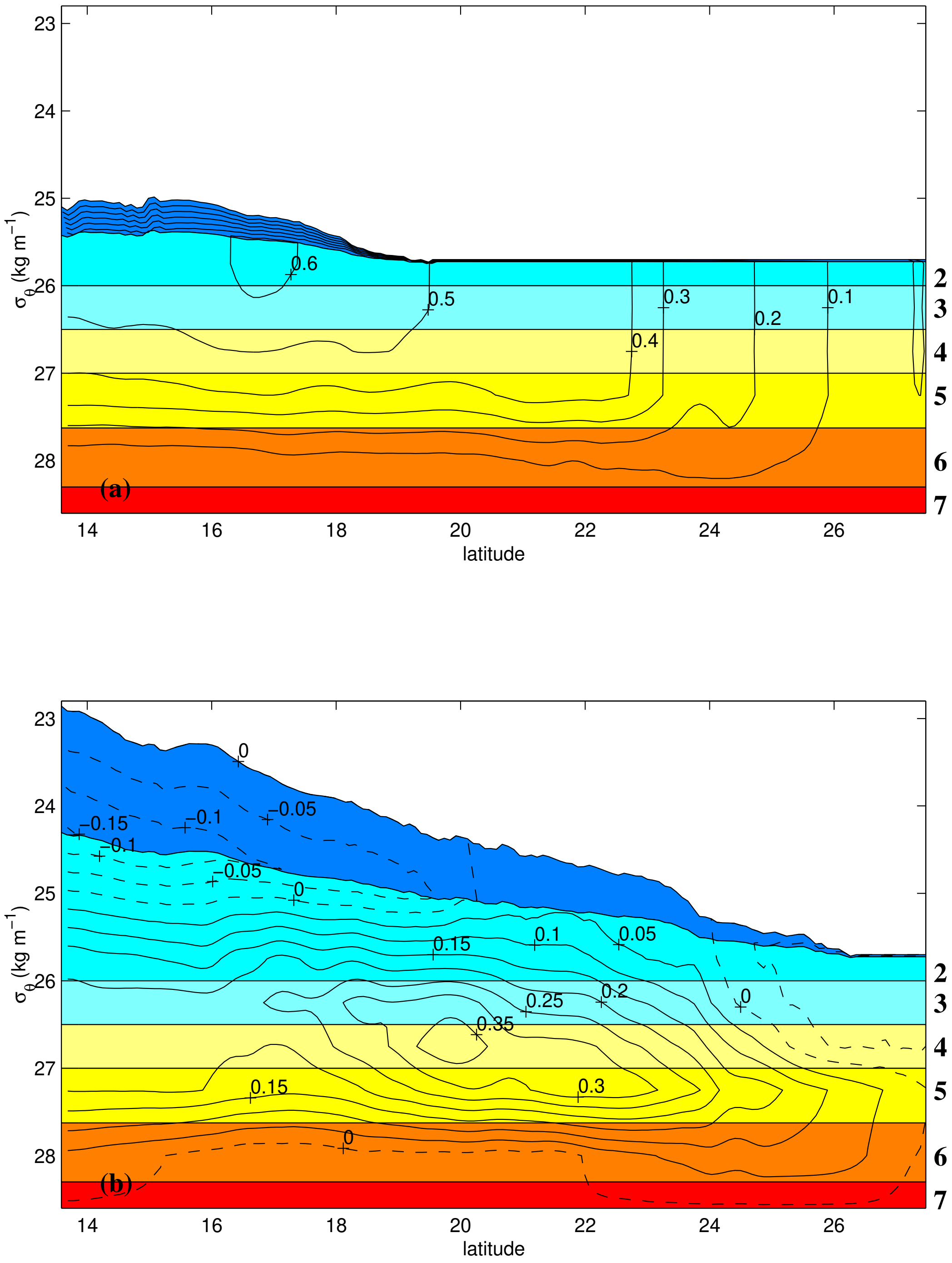

Figure 3.10: Meridional overturning volume fluxes for (a) December and (b) June, from MICOM simulation.

connects the intermediate inflow with the weaker RSW outflow. Some recirculation within the basin also occurs in the deeper cell. We have to emphasize here that the numerical model result for RSW outflow, although very close to the observations on the annual mean, presents a weaker annual cycle and the summer RSW outflow is overestimated.

To construct a numerical model for the Red Sea circulation is not an easy task. As shown here there are several uncertainties in the atmospheric fields to drive such a model and very few data to compare against the model results away from the strait. The development of reliable data sets is one of the most important needs to further improve our understanding of the Red Sea circulation and exchange with the Indian Ocean. Future modelling attempts could also investigate the higher frequency variability which may play an important role in the dynamics not considered here.

Chapter 4

A modified Phillips' Model for the Red Sea

4.1 Introduction

Semi-enclosed seas, like the Red Sea, although accounting for a very small fraction of the world ocean can play an important role in the general circulation. The formation of water masses with exceptional properties inside their basins which outflow and spread in the major oceans can affect the thermohaline characteristics of vast areas. The very saline (about $39.7 psu$) outflow from the Red Sea, usually referred to as the Red Sea Water (RSW), can be traced far away from its source as an intermediate salinity maximum in the Indian Ocean (Rochford, 1964; Hamon, 1967; Grundlingh, 1985; Shapiro and Meschanov, 1991; Mantyla and Reid, 1995). Recent long-term observations at the strait of Bab el Mandeb, which connects the Red Sea with the Gulf of Aden and the Indian Ocean, (Murray and

Johns, 1997) have provided an accurate estimate of the annual mean outflow of 0.36 Sv and given a more complete picture of the variability. During winter the exchange flow has the typical two layer inverse estuarine form, but during summer (June to September) it is replaced by a three-layer exchange with a surface outflow, an intermediate intrusion of the relatively fresh and cold Gulf of Aden Water (GAW) and a much weaker RSW outflow.

What dynamical mechanisms are controlling this outflow? The Red Sea is well known as a place where one of the highest $E - P$ (around 2 $m/year$) (Chapter 2) rates in the world ocean occurs. As a consequence, extremely high surface and subsurface salinities are observed, reaching values over the 40psu at the northern part of the basin and in the deep and intermediate layers. Because of this strong salinity gradient along the axis of the Red Sea and the formation of the very saline outflowing water mass inside the basin, the buoyancy loss (mostly due to the extensive evaporation rate) has been thought by several investigators as the basic controlling mechanism of the flow (Maury, 1855; Luksch, 1878; Neumann and McGill, 1962; Phillips, 1966; Tragou and Garrett, 1997). But the air-sea fluxes alone can not determine uniquely the final product reflected in the exchange flow at the strait. As shown by Bryden and Stommel (1984), it is possible to have a vigorous circulation with small temperature and salinity differences, or a sluggish flow with large differences. Thus, at the strait of Bab el Mandeb, one could have two extreme cases, either an outflow with salinities close to saturation that just trickles over the sill of the strait, or very large outflow but with salinity close to that of the ambient waters in the Indian Ocean that flow into the Red Sea. The additional constraints needed to describe the state of the Red Sea (or other concentration basins like the Mediterranean) are the dynamical balances controlling the circulation and especially the mixing processes.

The effects of the wind forcing on the Red Sea circulation also cannot be ignored. The wind field is strong and exhibits large seasonal variability, especially in the southern part of the Red Sea, where it reverses from SSE during winter (October to May) to NNW during summer, influenced by the Indian Monsoon. This seasonal pattern and its coincidence with the seasonal variability of the exchange flow was the basis for the development of theories proclaiming that the wind field controls the seasonal circulation and exchange flow at Bab el Mandeb (Thompson, 1939a and 1939b; Siedler, 1969; Patzert, 1974a).

The most energetic part of the circulation in the Red Sea is located in the upper $200\,m$ of the water column (Chapter 5). Below this a very uniform water mass, the Red Sea Deep Water (RSDW), fills the basin to maximum depths of about $3000\,m$. Although some contribution of the RSDW in the general circulation and exchange flow at the strait is expected, observations, tracer analysis and numerical modelling techniques (Neumann and McGill, 1962; Cember, 1988; Quadfasel and Baunder, 1997; Chapter 5; Chapter 6) indicate that the core of the outflowing water mass is derived from intermediate depths in the Red Sea. Another fact that supports this idea is the relatively small rate of RSDW formation (about 0.04 to 0.06 Sv) (Maillard, 1974; Wyrtki, 1974), which is much smaller by about an order of magnitude than the total outflow from the basin. In this chapter, we therefore focus on the surface and intermediate circulation in the basin.

Phillips (1966) first provided a theoretical context for the steady, two-dimensional circulation in the basin. As it will be shown in the next section, Phillips' model is able to reproduce, at least qualitatively, the winter circulation in the Red Sea. However, it cannot be used to understand the seasonal variability of the Red Sea circulation and exchange with the Indian Ocean. Partly because of this, the Phillips' approach was neglected by several investigators who sought to understand the strong seasonal variability observed in the circulation and exchange flow at Bab el Mandeb, and particularly the reversal of the surface and subsurface flow that occurs there for four months of the year in summer (Patzert, 1974a; Murray and Johns, 1997). Patzert (1974a and b) argued that since the wind seems to change the exchange pattern so drastically in summer, its influence on the Red Sea circulation must be more important than the that of the buoyancy forcing. The debate about the relative importance of the different forcing mechanisms (wind or thermohaline) in the Red Sea circulation is not closed. But today, although not explicitly mentioned, there seems to be an agreement that the buoyancy loss over the Red Sea drives the mean Red Sea circulation, while the seasonal variability around the mean state is controlled by the wind. One of the reasons for this idea is that the thermohaline forcing is often treated as a uniform field in time and space. The question of how temporal variability and/or gradients in the thermohaline fluxes can affect the circulationhas not been adequately addressed. In Section 3 a modified version of Phillips' model will be presented, where we consider the effects of the temporal and spatial variability of the thermohaline forcing on the circulation in the Red Sea and the exchange with the Indian Ocean. Finally, the results of the modified model are discussed and compared to available observations in the last section.

4.2 Background: Phillips' model

Because of its very elongated shape (about $2000km$ long and $220km$ wide on the average) and because most of the observations exist along the main axis of the basin, the Red Sea has most often been treated by treated by investigators as a two-dimensional basin. Although today we know that the circulation probably has a strong cross-basin component (Maillard, 1974; Quadfasel and Baunder, 1997; Chapter 5), it is convenient to simplify our approach when dealing with the basic balances involved in the Red Sea dynamics. Phillips (1966), using this approach, constructed a model for the Red Sea circulation forced by a constant and spatially uniform buoyancy loss (B_0). The circulation takes place in the vertical plane ($0 \leq x \leq L$, $0 \leq z \leq h$), where L is the length of the basin and h is the depth of the sill separating the Sea from the open ocean. Below this depth there is an inactive layer, of density ρ_0, that does not play any role in the circulation. Since the circulation is in the vertical plane, rotational effects are neglected. Assuming the Boussinesq approximation, hydrostatic balance in the vertical and mixing only in the z-direction, the set of equations describing Phillips' model (here the notation followed by Garrett et al., 1995 is used) is

$$\mathbf{u} \cdot \nabla b = \frac{\partial}{\partial z}\left(\kappa \frac{\partial b}{\partial z}\right) \tag{4.1}$$

$$\mathbf{u} \cdot \nabla u + \frac{1}{\rho_0}\frac{\partial p'}{\partial x} = \frac{\partial}{\partial z}\left(\nu \frac{\partial u}{\partial z}\right) \tag{4.2}$$

$$\frac{1}{\rho_0}\frac{\partial p'}{\partial z} = b \tag{4.3}$$

$$\frac{\partial u}{\partial x} + \frac{\partial w}{\partial z} = 0 \tag{4.4}$$

where b is the buoyancy ($b = -g(\rho - \rho_0)/\rho_0$), u and w are the longtitudinal and vertical velocities, respectively, p' is the perturbation pressure referenced to the pressure in a fluid at rest with density ρ_0, and κ and ν are the eddy diffusivity and eddy viscosity coefficients.

Phillips pursued similarity solutions based on dimensional considerations. He proposed that the most general forms (which also provide separation of variables) for the horizontal velocity and buoyancy that preserve the correct units for the variables are

$$u = (B_0 x)^{\frac{1}{3}} (x/h)^{\beta} f(z/h) \tag{4.5}$$

$$b = B_0^{\frac{2}{3}} x^{-\frac{1}{3}} (x/h)^{\gamma} g(z/h) \tag{4.6}$$

where f and g are dimensionless functions and β and γ are power coefficients to be determined. In order to find β and γ, he used the buoyancy conservation integral which requires that the gradient of buoyancy advection is equal to the buoyancy flux across the sea surface

$$\frac{\partial}{\partial x} \int_{-h}^{0} u\, b\ dz = -B_0 \tag{4.7}$$

and assumed that the advective and buoyancy torque terms in the vorticity equation

$$\frac{\partial}{\partial z}\left(u\frac{\partial u}{\partial x} + w\frac{\partial u}{\partial z}\right) = \frac{\partial^2}{\partial z^2}\left(\nu\frac{\partial u}{\partial z}\right) - \frac{\partial b}{\partial x} \tag{4.8}$$

have the same x-dependence. With these constraints the final similarity solutions for the velocity and buoyancy have the form

$$b = (B_0 x)^{2/3} h^{-1} g(\eta) \tag{4.9}$$

$$u = (B_0 x)^{1/3} \frac{d\psi(\eta)}{d\eta} \tag{4.10}$$

$$w = -\frac{1}{3}(B_0 x^{-2})^{1/3} h\psi(\eta) \tag{4.11}$$

where η is z/h, and $g(\eta)$ and $\psi(\eta)$ ($f = d\psi/d\eta$) are the similarity functions (what Phillips calls universal functions) of the buoyancy and streamfunction, respectively, that have to be specified using observations. Phillips applied these solution to available hydrographic observations along the central axis of the Red Sea and found good agreement between the observed stratification and the predicted buoyancy distribution from the model.

Garrett et al. (1995) and Tragou and Garrett (1997) pursued particular solutions of the same form that matched observations of the stratification in the Red Sea and were described in the vertical by a strongly mixed surface layer overlying a much less viscous and diffusive lower layer. Under these specifications, the similarity functions (g and ψ) as well as the eddy diffusivity and eddy viscosity can be estimated (Tragou and Garrett (1997), Figure 3a-d) and the associated circulation and stratification is plotted in Figure **??** (their Figure 3e). The circulation is a two layer system with lighter water entering the basin at the surface, which becomes denser as it flows towards the "north" and sinks gradually to form a dense lower layer that outflows from the basin. Although this picture is in qualitative agreement with the winter circulation in the Red Sea, there are some quantitative implications with these solutions. Tragou and Garrett (1997) estimated that in order for the solutions to match the observed stratification the lower layer must be very viscous. At half the distance from the head of the basin ($x = 1 \times 10^6\, m$), and for $B_0 = 2 \times 10^{-8}\, m^2 s^{-3}$ and $h = 140\, m$ Tragou and Garrett (1997) calculated the eddy viscosity of the lower layer (about mid depth of the lower layer) at $\nu \approx 4.4 \times 10^{-2}\, m^2 s^{-1}$. This means that the lower layer is very viscous

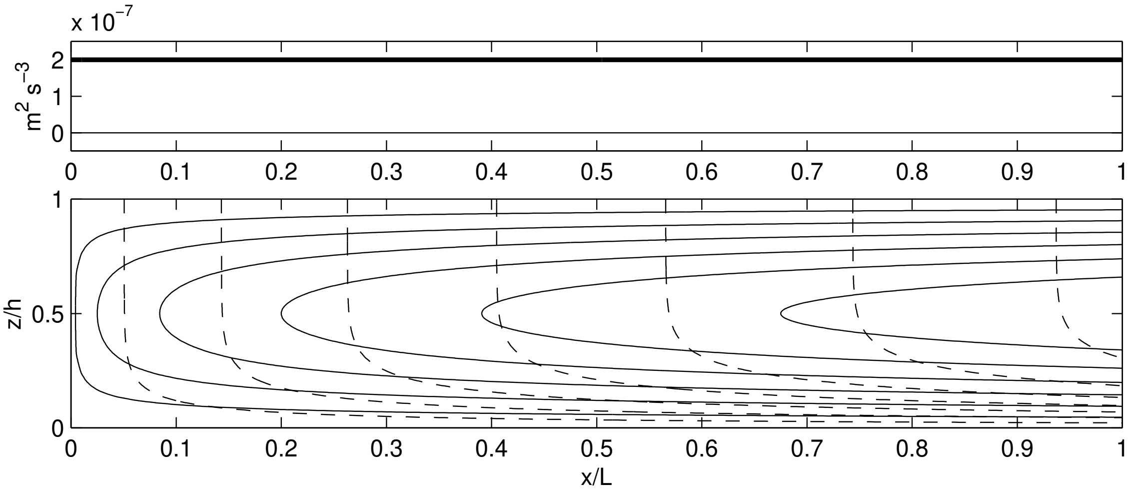

Figure 4.1: Streamfunction and buoyancy distribution using Phillips' similarity solution.

and at the same time weakly mixed. The introduction of bottom friction and simple wind-stress patterns did not explain this peoblem, and the high eddy viscosity value in Phillips' model remains an open issue.

4.3 The modified Phillips' model: Solutions for a variable buoyancy flux

Although the Red Sea is a relatively small basin (its surface area is about one fifth of that of the Mediterranean Sea), it spans about 20^o of latitude and experiences strong atmospheric forcing with large seasonal and spatial variability. The annual cycle and the mean latitudinal distribution of the buoyancy flux derived from the Comprehensive Ocean Atmosphere Data Set (COADS) (da Silva et al., 1994), after being adjusted to match advective constraints derived from the recent observations mentioned in the introduction of the present chapter (see also Chapter 2), are plotted in Figure **??**. They show a large

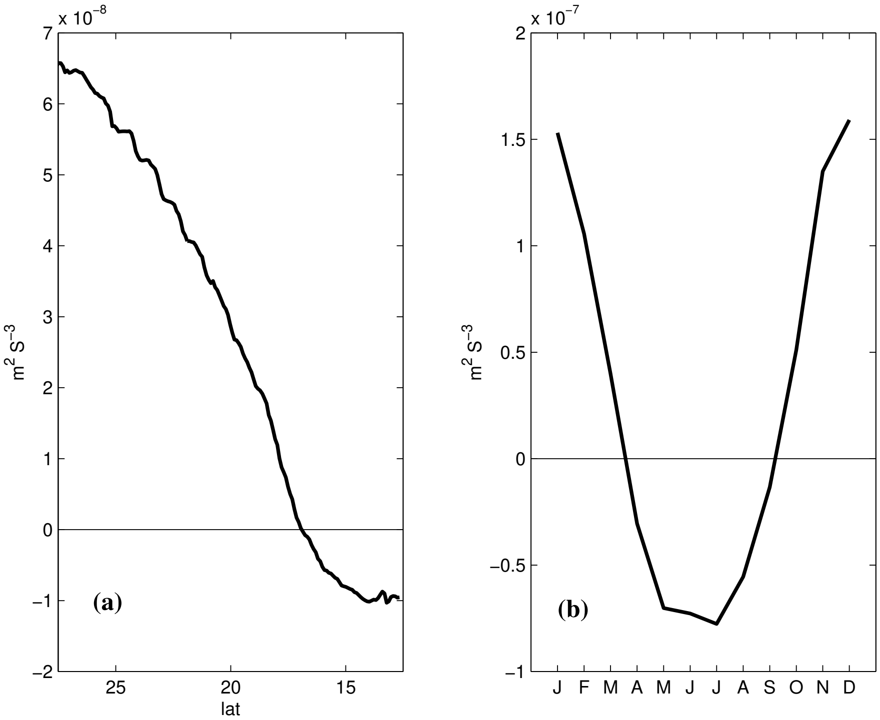

Figure 4.2: Buoyancy fluxes over the Red Sea, (a) annual mean meridional gradient and (b) annual cycle.

seasonal variability with a range of $2.4 \times 10^{-7}\ m^2s^{-3}$ and a strong meridional gradient with a range of $7.5 \times 10^{-8}\ m^2s^{-3}$. In this section, we revisit Phillips' approach, aiming to incorporate the spatial and seasonal variability in the buoyancy flux (B_0) driving the circulation.

In the form Phillips' similarity solutions are written the buoyancy flux must be constant. If it is to include a meridional dependence, the x-dependence in the velocity and buoyancy functions must be redefined. Here, we adopt the similarity functions for the buoyancy ($g(\eta)$) and the streamfunction ($\psi(\eta)$) proposed by Tragou and Garrett (1997), since they present a reasonable pattern of the vertical distribution of properties and because this provides a continuation of ideas. Furthermore, the parts of the similarity solutions that involve the horizontal and vertical dependence can be treated separately. Since the maximum buoyancy loss takes place at the northern end of the basin which is approximately the origin of the horizontal dimension ($x \approx 0$), a form to define a buoyancy flux that decreases linearly toward the mouth of the basin ($x = L$), which approximates the meridional distribution of the buoyancy flux from COADS (Figure **??**), is

$$B_0 = B_m \left(1 - \frac{x}{\alpha\, L}\right) \tag{4.12}$$

where B_m is the maximum buoyancy loss at the origin and α is the a constant that represents the meridional dependence of the forcing, so that $x = \alpha\, L$ is the location where the buoyancy flux becomes zero.

The Phillips' horizontal velocity and buoyancy forms (1.5) and (1.6) are still valid, but since B_0 is a function of x the two constraints described in the previous section should be applied again. Using (1.7)

$$u\, b\, h \propto B_m\, x \left(1 - \frac{x}{2\,\alpha\, l}\right) \tag{4.13}$$

and assuming that the advective and buoyancy terms in the vorticity equation (1.8) have the same x-dependence.

$$u^2 \propto b\, h \tag{4.14}$$

Applying (1.13) and (1.14), the new form of the similarity solutions is

$$b = (B_m\, x)^{2/3} \left(1 - \frac{x}{2\,\alpha\, L}\right)^{2/3} h^{-1} g(\eta) \tag{4.15}$$

$$u = (B_m\, x)^{1/3} \left(1 - \frac{x}{2\,\alpha\, L}\right)^{1/3} \frac{d\psi(\eta)}{d\eta} \tag{4.16}$$

$$w = -\frac{1}{3} (B_m\, x^{-2})^{1/3} \left(1 - \frac{x}{2\,\alpha\, L}\right)^{-2/3} \left(1 - \frac{x}{\alpha\, L}\right) h\psi(\eta) \tag{4.17}$$

where the continuity equation (1.4) is used to derive the vertical velocity function. According to these solutions there is another singularity at $x = 2\,\alpha\, L$, but this is inevitable, since the circulation cells should be closed at a distance where the integral of the buoyancy flux becomes zero. For large values of α, the solutions converge to the original forms derived by Phillips.

The above solutions can be applied for several cases. The most interesting are those that represent winter conditions in the Red Sea, where there is buoyancy loss all over the basin, and summer conditions, with buoyancy loss in the northern part of the Sea and buoyancy gain in the southern part of the basin. Although these two conditions are rather simplistic, as the air-sea fluxes fields are more complicated and variable than this, they can give us some insight to the basic patterns of the thermohaline circulation. For the winter case the buoyancy flux is described by $B_m = 2.5 \times 10^{-7}\, m^2 s^{-3}$ and $\alpha = 1.5$ and for the summer case by $B_m = 1 \times 10^{-7}\, m^2 s^{-3}$ and $\alpha = 0.3$. The buoyancy flux distribution and the resulting circulation and density stratification for the two cases are plotted in Figure **??**. The rate of change of forcing between the two states is comparable with the advective time scale ($\frac{L}{U} = O(\frac{1}{2} year)$ with $L = 1000\, km$ and $U = 0.07\, m/sec$), so that the system can adjust to the two different forcing fields.

The winter solution is almost identical to that of the Phillips' solution except that now much higher velocities (twice those of Tragou and Garrett, 1997) are produced by the stronger buoyancy loss. However, the summer case is very different and presents some interesting characteristics. The northern part of the basin has a circulation cell of the same sense as in winter, but closed in mid basin ($x/L \approx 0.6$) where the integral of the surface buoyancy flux from the northern end of the basin vanishes. At the southern part of the basin the circulation cell is reversed and consists of a surface outflow and a subsurface inflow. From observations we know that a very weak RSW outflow continues to exist during summer, but we do not expect this simple model to resolve this complicated pattern. Neglecting this small deep outflow, the summer conditions at the strait resemble the observed conditions of surface outflow and intermediate GAW inflow (see next section). Another interesting result to notice is that the subsurface summer inflow is confined to the southern part of the basin and does not extend far to the north. From the available observations, the GAW intrusion appears at the strait in June and propagates slowly to the north with an average speed of $5.5 km\ day^{-1}$ (Smeed, 1997) reaching its northernmost point in mid October. The maximum penetration of the water mass never reaches the central latitudes of the Red Sea, and typically reaches about one third of the way up the basin (Jones and Browning, 1971; Smeed, 1997). This is consistent with the penetration of the summer pattern in the model. Although time dependence is not explicitly included in the model, it is reasonable to view the summer season as a slow northward propagation of the point of zero buoyancy flux inside the basin, and thus a northward propagation of the reversed cell inside the Red Sea. The effects of the wind field and its seasonal variability, especially in the south where the

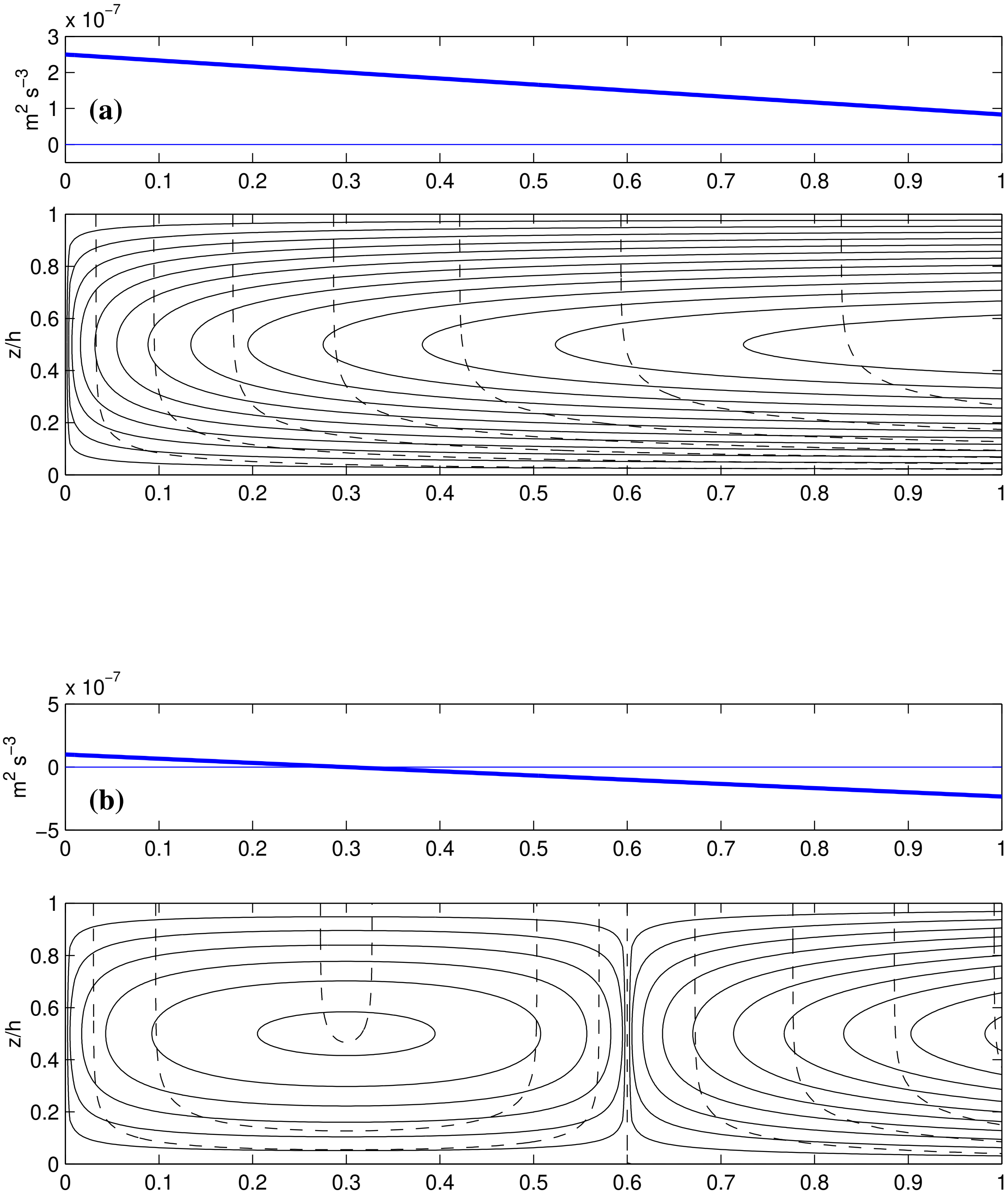

Figure 4.3: Streamfunction and buoyancy distribution for (a) winter buoyancy flux and (b) summer buoyancy flux.

reversal of the direction takes place in summer, cannot be neglected and the final picture is more complicated than the simple ideas presented here.

4.4 Summary and Discussion

Very few observations are available in the Red Sea, and especially in the subsurface layers, an accurate reconstruction of the large scale circulation patterns is currently impossible. The only place that an adequate number of observations exist, to compare with the analytical results presented here is in the strait of Bab el Mandeb. Recent long-term (18-month) and comprehensive observations (Murray and Johns, 1997), have provided an accurate determination of the annual cycle of the exchange flow at the strait. From this data set the monthly mean volume transport exchange at the strait is plotted in Figure **??**, split in three layers, the surface, the intermediate summer inflow (or GAW intrusion) and the RSW outflow. During winter (October to May) a two-layer exchange takes place reaching its maximum strength during February with over 0.6 Sv of surface inflow and RSW outflow. From June to September the exchange exhibits a three-layer pattern, with a reversed surface layer flow, a strong intrusion of GAW and an extremely weak RSW outflow (about 0.05 Sv during July and August). Since the model presented here is two-dimensional, its results can be compared with these observations in a strictly qualitative way. Nevertheless, the agreement between the observations and the analytical results is good. Apart from the very weak RSW, the summer result of the modified Phillips' model reproduces the main exchange pattern, with a surface outflow and a subsurface inflow, and the winter result reproduces the two-layer winter exchange, with the surface inflow and subsurface outflow

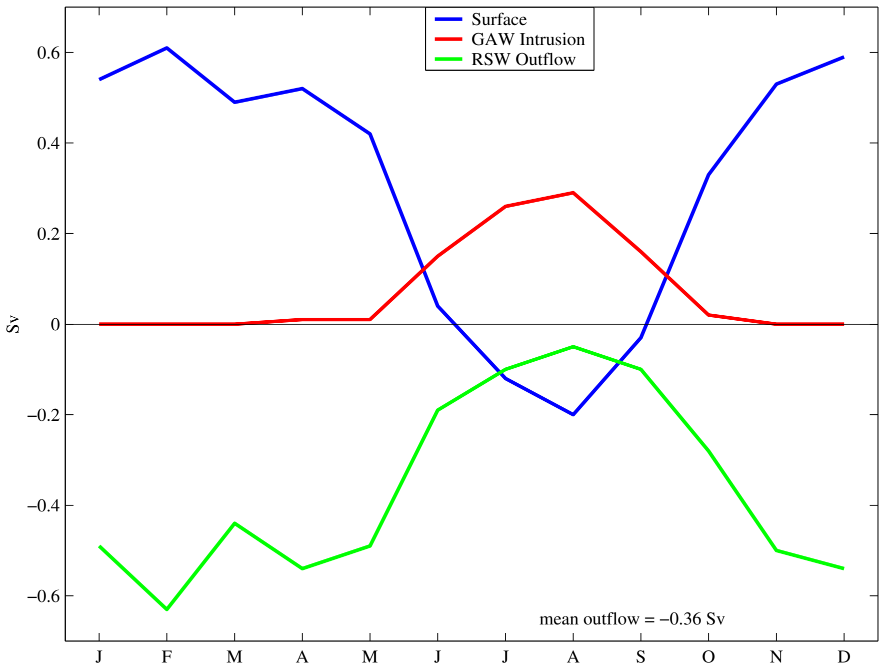

Figure 4.4: Monthly mean transport in Bab el Mandeb from direct observations (Murray and Johns, 1997), separated in three layers, surface (blue line), intermediate summer inflow (red line) and RSW outflow (green line).

from the basin. As more observations and numerical simulations of the general circulation of the Red Sea become available, other aspects of the analytical model presented can be evaluated.

The introduction of a meridional gradient in the buoyancy flux over the Red Sea gives interesting results, and although time is not explicitly included in the solutions, some of the characteristics of the annual cycle of the circulation pattern can be reproduced. The advective time scale ($\frac{L}{U} = O(\frac{1}{2}year)$) is comparable to the rate of change of the forcing and the circulation can adjust to the different patterns of the buoyancy flux. Future time dependent solutions may improve our understanding of the role of the variable thermohaline forcing in the Red Sea circulation.

The presence of the wind can affect the circulation in the Red Sea, although the thermohaline driven part of the circulation is more energetic and dominates the circulation pattern (Chapter 5). This true especially in summer when the reversal of the winds is not only opposing the surface flow, but can affect the surface and subsurface circulation through a wind-induced upwelling outside the basin, in the northwestern Gulf of Aden (Patzert, 1974a; Chapter 3). Another important effect of the wind field is the generation of eddies which do not affect the long-term axial flow but can generate strong velocities and influence the dynamical balances in the Red Sea. The introduction of the wind-stress as well as the the influence of other parameters such as the bottom topography and the meridional change of the width can explain aspects of the dynamical balances in the basin but need a three-dimensional framework and more elaborate methods to be resolved.

Chapter 5

The 3-D circulation of the Red Sea: Results from an OGCM

5.1 Introduction

The Red Sea is one of the most unexplored areas of the northern hemisphere oceans. Most of the available observations are sporadic and sparse in space making any attempt to construct a picture of the three-dimensional circulation in the Red Sea very difficult. The only exception is the area of the strait of Bab el Mandeb which has attracted the interest of several observational efforts during the past century (Vercelli, 1927; Siedler, 1968; Maillard and Soliman, 1984; Murray and Johns, 1997). The latter study one was long-term (18 months) and very comprehensive, monitoring velocity and hydrography profiles at several locations in the channel. The circulation that emerges from these observations is a two-layer exchange flow of the inverse estuarine type that lasts from October to May, with a relatively fresh surface inflow and deep outflow of the very saline (39.7 psu) Red Sea Water (RSW). This simple pattern is interrupted for four months, during the summer season (June to September), when a shallow surface outflow, an intermediate intrusion of Gulf of Aden Water (GAW) and a weaker RSW outflow are taking place.

North of the strait, inside the Red Sea basin, most of our knowledge of the circulation and distribution of oceanographic properties comes from a handful of expeditions that performed mostly hydrographic stations, and data sets from ships of opportunity which usually follow the central axis of the Red Sea. Based on this kind of data and the elongated shape of the basin most of the descriptive and theoretical investigations of the Red Sea circulation follow a two-dimensional approach (on the latitude-depth plane). Between them, the most debated aspect is the relative importance of the thermohaline and wind forcing and their role in the circulation and stratification of the Red Sea. Because of the strong salinity gradient along the axis of the Red Sea and the formation of the very saline outflowing water mass inside the basin, the buoyancy loss (mostly due to the large evaporation rate) has been thought by several investigators as the basic controlling mechanism of the flow (Maury, 1855; Luksch, 1901; Neumann and McGill, 1962; Phillips, 1966; Tragou and Garrett, 1997). Others believe that the wind-stress field is more important in determining the circulation pattern while the thermohaline forcing plays a secondary role (Thompson, 1939a and 1939b; Siedler, 1969; Patzert, 1974a).

Very few clear circulation features can be identified from the observations performed in the Red Sea. Vercelli (1927) during a winter expedition in the southern part of the basin measured significant currents close to the coasts, and especially the African one. During a later cruise (winter 1929, Vercelli, 1931) in the central Red Sea, close to Port

Sudan, he observed a southward counter current at depths greater than $250m$ in the open sea but less than $150m$ near the coast. The area where the most consistent observations were undertaken is the northern part of the basin, north of 23^o latitude. Two winter cruises (1935 on board the R/V MABAHISS and 1963 on board the R/V CDT ROBERT GIRAUD) performed several hydrographic sections in the area (Morcos, 1970; Morcos and Soliman, 1974; Maillard, 1974). The patterns of the estimated geostrophic currents agree in general showing a cyclonic gyre at the extreme north which penetrates up to $300m$ depth and an anticyclonic gyre about 2 degrees to the south. The presence of the cyclonic eddy is verified by a series of five drifter tracks launched during 1993-94 which show a cyclonic circulation north of 26^oN (Clifford et al., 1997). The temperature observations also support the presence of these features with colder waters at the center of the cyclonic flow and much warmer in the center of the anticyclonic flow. These characteristics can also be seen in later cruises (Quadfasel and Baunder, 1993) and can be attributed to vertical displacement of the isopycnals inside cyclonic and anticyclonic vortices. Thus the Red Sea appears to contain several quasipermanent gyres and intensified boundary currents and subsurface counter-currents that are only peripherally understood.

In this study a general circulation ocean model, the Miami Isopycnic Coordinate Ocean Model (MICOM) (Bleck et al., 1992; Bleck and Chassignet, 1994), is used to investigate the three-dimensional circulation in the Red Sea. In the next section we provide background and review some existing theories on the Red Sea circulation. Next, the model configuration and the forcing fields used will be discussed. Section 4 presents the results of the numerical simulation. In Section 5 results from two additional experiments will be presented, investigating the different effects of the thermohaline and wind forcing. Finally, the last section includes a summary and discussion of the overall picture of the Red Sea circulation emerging from this study.

5.2 Background

The Red Sea is an elongated basin separating the African from the Asian continent, extending from $12.5^o N$ to $30^o N$ (a distance of about 2000 km) with an average width of 220 km (Patzert,1974a). The surface area of the Red Sea is $4.5 \times 10^{11} m^2$ and the mean depth $524 m$ (Patzert, 1974a), but with maximum depths recorded at almost $3000 m$. At the northern end it bifurcates into two gulfs, the Gulf of Suez with average depth of 40 m and the Gulf of Aqaba with depths exceeding $1800 m$ and a sill at the entrance of approximately 175 m (Neumann and Gill, 1962). The transport through the Suez Cannal, which connects the Mediterranean Sea with the Gulf of Suez and the Red Sea is extremely small. So, the only signifficant connection between the Red Sea and the open ocean, the Indian Ocean through the Gulf of Aden, is the strait of Bab el Mandeb located at the southern end of the basin. It is a shallow and narrow channel with sill depth of $160 m$ at the Hanish sill and minimum width of about 25 km at the Perim Narrows.

The fresh water deficit of the Red Sea is one of the largest encountered in the world ocean, due to strong evaporation, very small precipitation and negligible river runoff. But the actual $E - P$ rate is highly debated and the values proposed by different investigators range from 1.5 to 2.3 $m/year$ (Yegorov, 1950; Neumann, 1952; Privett, 1959; da Siva, et al., 1994; Tragou et al., 1999). Recent long term observations at the strait of Bab el Mandeb (Murray and Johns, 1997) of the flow and the temperature/salinity characteristcs of the

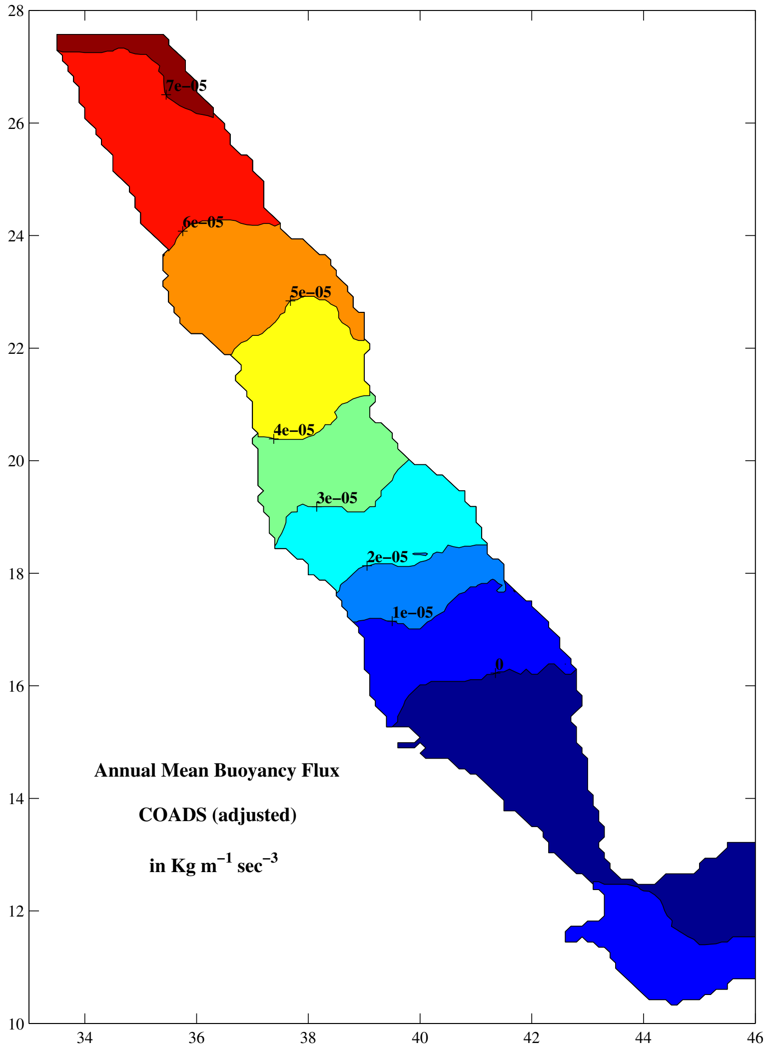

Figure 5.1: Annual mean distribution of the buoyancy loss over the Red Sea.

water masses involved can be used to constrain the average fresh water budget of the whole basin. Using this data, the annual mean $E-P$ rate is estimated at $2.06 \pm 0.22\ m/year$ (Chapter 2). Little is known about the temporal and spatial variability of the freshwater flux and there are large discrepancies between available estimates (Yegorov, 1950; Neumann, 1952; Privett, 1959; da Siva, et al., 1994). The latent heat flux associated with the $E-P$ is very large (about 160 W/m^2). But the sum of the other terms of the heat budget almost compensate this loss, so that the annual mean heat loss from the surface of the Red Sea is small, $O(10\,Wm^{-2})$, (Patzert, 1974; Tragou et al., 1999). Using the same data mentioned before (Murray and Johns, 1997) for the heat flux through the strait of Bab el Mandeb, we estimate a 11 Wm^{-2} loss, for an average over a year and the whole air-sea interface of the Sea (Chapter 2). The combined effects of freshwater and heat flux add up to an annual mean buoyancy loss of approximately $27\times10^{-6}kgm^{-1}s^{-3}$. According to the Comprehensive Ocean-Atmosphere Data Set (COADS) (da Silva, 1994) there is a significant seasonal cycle around this mean value with a large loss during winter and a weak gain during summer, with a total range of the buoyancy flux cycle for the Red Sea basin of $25\times10^{-5}kgm^{-1}s^{-3}$. A strong south to north mean gradient in the buoyancy forcing is also present in the basin (Figure **??**).

The Red Sea experiences strong and complicated wind forcing with surface winds that can reach speeds of more than $10m/sec$, intense land and sea breezes, and synoptic time scale variability. Since the subject of this paper is the seasonal patterns of the circulation, the high frequency variability will be neglected and the monthly mean wind fields will be used. Due to the existence of high mountain ranges along the African and Asian coasts, the direction of the surface winds is orographically steered along the axis of the Sea. The January and July mean fields of the wind-stress from COADS (da Silva, 1994) are plotted in Figure **??** representing the winter and summer extremes. We can identify two different regimes, one in the northern part of the Red Sea and one in the southern part. The former is influenced by the eastern Mediterranean weather systems (Pedgley, 1974) and the wind is from the northwest all around the year. In the south the wind is basically controlled by the Indian Monsoon system and reverses from southeast during winter (October to May) to northwest during summer (June to September). Although this general pattern has been well known for thousands of years and verified by many investigators, some differences in the strength of the wind field can be identified between the different data sets, especially in the northern part of the Red Sea. The Koninklijk Nederlands Meteorologisch Instituut (KNMI) atlas (1949), utilized by Patzert (1974a), presents the strongest winds in the north during summer while in COADS the maximum appears during winter. Nevertheless, the basic seasonal cycle of the wind-stress is a very robust feature and combined with the intensity of the winds it makes the wind forcing an important mechanism for the dynamics of the region.

Phillips (1966) produced a model of the circulation of the Red Sea driven by a uniform buoyancy loss from the surface of the Sea. He assumed a semi-enclosed basin with a sill at the exit and constant width. The circulation is in steady state and on the vertical plane, so that the rotational effect is neglected. Based on dimensional considerations he found that the similarity solutions that can satisfy this kind of model produce a two-layer convective circulation and density pattern, in good qualitative agreement with several characteristics of the winter regime in the Red Sea, such as the density gradient in the south-north direction and the two-layer flow present in the strait of Bab el Mandeb. Although several problems have been identified in Phillips' model, such as the very high viscocity of the lower layer required for the solutions to match the observed exchange flow in the Red Sea (Tragou and Garrett, 1997), this approach provides a useful tool for understanding the dynamics governing semi-enclosed concentration basins. The most important disadvantage of this model is that it can represent only the winter state and gives no explanation for the intense seasonal variability observed in the region and particularly at the strait of Bab el Mandeb. (This may, in fact, be one of the reasons that investigators concerned with this kind of variability neglected the thermohaline forcing and attributed it to the seasonal reversal of the wind-stress.) To address this problem, in Chapter 4 Phillips' general concepts were followed but seeking similarity solutions which included a space dependent buoyancy forcing and could be applied for conditions present in different seasons. Two cases were chosen, one representing winter (buoyancy loss all over the domain but stronger in the north) and the second one representing summer (buoyancy loss in the extreme north and weak buoyancy gain in the south). The winter result is almost identical to that of Phillips (see Figure **??**; Chapter 4), but the summer result is very different and exhibits a reversed surface flow in the southern part of the Red Sea with a subsurface inflow at the bottom of the strait. It is interesting to note that the summer result includes several features that are similar to those observed, such as the surface current reversal, and the subsurface inflow which is confined in the southernmost part of the basin. However, the absence of deep outflow disagrees with observations that suggest that the deep saline outflow from the Red Sea does not dissappear completely during summer. Although Phillips' approach and the subsequent modifications include several simplifications and assumptions, which are reflected in the results (i.e. absence of deep outflow during summer), they give us strong indication of an important role of the thermohaline forcing and its variability in the general circulation of the Red Sea.

Another two-dimensional approach was pursued by Patzert (1974a) for explaining the mechanisms behind the basic circulation pattern observed in the Red Sea and the exchange with the Indian Ocean. Based on the obvious coincidence of the reversal of the the wind field in the south with the reversal of the surface flow, he hypothesized that the variable wind-stress and the associated changes of the sea level in the southern Red Sea and the

Gulf of Aden control the circulation in the region throughout the year. From October to May the southeasterly winds present in the southern Red Sea cause a large surface inflow which "piles-up" surface water in the central part of the Red Sea, between $16^o - 21^o N$, where the winds are convergent. North of these latitudes the winds are from the NNW and the surface flow is against the wind-stress. To explain this discrepancy Patzert proposed that the a surface pressure gradient is created at the northern part of the Red Sea opposite to the wind-stress either by the large evaporation and the winter cooling in the northern end of the Sea or by the water that piles-up in the zone of convergent winds. This pressure gradient overpowers the regional wind-stress, which according to the wind data he used (KNMI) achieves its minimum during winter. To maintain continuity of mass, he assumes that the subsurface pressure gradient and the consequent flow is to the south and outside the basin toward the Gulf of Aden. This winter circulation is closed by sinking of water in the north, but without specifying the mechanisms involved in this process.

During summer, when the three-layer system is present at Bab el Mandeb, the winds are from the northwest all over the Red Sea. This is expected to induce a general surface southward flow in the Red Sea. Since the winds are rather weak in the south, Patzert assumed that another mechanism besides the direct wind-stress forcing must be involved in generating the strong surface outflow from the Red Sea observed in summer. He proposed that outside the basin in the northwestern Gulf of Aden, wind -induced upwelling due to the favorable summer wind field takes place which lowers the sea surface elevation, producing a pressure gradient over the sill that forces a shallow outflow from the basin. The same mechanism displaces the subsurface isopycnals upwards in the Gulf of Aden producing an opposite pressure gradient at intermediate depths capable of inducing the intermediate intrusion of GAW. Patzert's hypothesis was the first one to describe the seasonal reversal of the surface flow and the presence of the GAW intrusion during summer. However, it is a purely qualitative explanation and can give us no idea of the magnitude and the relative importance of the different mechanisms involved. Furthermore, the seasonal thermohaline forcing is neglected in this hypothesis even though the Red Sea is a strong concentration basin.

Although these simple two-dimensional approaches are valuable concepts of the Red Sea circulation and remain useful avenues of further research, their limitations and their inability to describe the whole picture of the basinwide circulation and stratification is obvious. For example, both theories described above predict currents of a few cm/s, but all available direct observations inside the Red Sea show that much larger velocities (up to $0.5m/s$) are possible (Vercelli, 1927; Morcos, 1970; Morcos and Soliman, 1974; Maillard, 1974). Furthermore, the cross-basin currents can be strong and appear to be related to a series gyres and meanders all along the basin. Although the weak average transport, estimated at the central axis of the Red Sea, can give us a fairly accurate picture of the mass fluxes across sections of the basin, it cannot explain the dynamical balances of the circulation and water mass formation. The mixing and dissipation processes that are key factors of the ocean circulation, especially in areas of water mass conversion like the semi-enclosed concentration basins (Bryden and Stommel, 1961; Phillips, 1966; Tragou and Garrett, 1997; Chapter 1), depend on the velocity and velocity shear magnitudes. In order to improve our understanding of the mechanisms controlling the Red Sea circulation, we must extend the invrstigational approach to a the three-dimensional framework.

5.3 Model Configuration

MICOM is primitive equation ocean model that has its vertical discretization in layers of constant potential density. An advantage of isopycnic coordinates is that the vertical resolution of the model can be intensified in regions of higher gradients and the presence of different water masses can be identified clearly all over the domain used in the simulation. This is very important in the case of the Red Sea presenting a high complexity in the exchange flow at the strait of Bab el Mandeb and a variety of water masses involved in the general circulation of the area. On the top of the isopycnic layers there is a thermodynamically active mixed layer of the Krauss and Turner (1967) type, vertically homogeneous but with density varying in the horizontal. This layer provides the connection between the atmospheric forcing and the interior domain. The annual cycle of the atmospheric forcing causes the mixed layer to expand and shrink and thus to exchange properties with the interior layers which can outcrop in the mixed layer by becoming massless.

The horizontal mesh is defined on Mercator projection where the grid size is fixed in the longtitudinal direction and varies in the meridional direction with the cosine of latitude. In the present simulations the grid interval was chosen at 0.1^o (or about 10 km) in order to resolve the exchange flow at the narrow strait. Nevertheless, the two gulfs at the northern end of the Red Sea (Suez and Aqaba) are very small and with very complicated topography and were not included in the experiments performed. The vertical density structure is defined by 6 isopycnic layers and a mixed layer which are presented in Table **??**. The choice of the number of layers and the σ_θ of each one was made in order to incorporate all the major water masses while keeping the model simple and computationally efficient. It has

LAYER NUMBER	LAYER DENSITY (kgm^{-3})	DESCRIPTION
1	mixed layer	surface layer
2	1025.75	core of the GAW
3	1026.25	
4	1026.75	
5	1027.25	
6	1028.00	core of the RSW
7	1028.60	RSDW

Table 5.1: Vertical resolution (layer density) used in the model.

been hypothesized that the core of the outflowing RSW originates from intermediate depths in the Red Sea (Neumann and McGill, 1962; Cember, 1988; Chapter 5) and so special attention was given to distinguish between deep and intermediate waters which possess similar temperature and salinity characteristics and differ only slightly in their density. The bottom layer which represents the Red Sea Deep Water (RSDW) fills the basin from about 200 m to the bottom. The layers above represent the intermediate layers involved in the Red Sea circulation and the first isopycnic layer, just below the mixed layer, the core of the GAW. However, the distinction between water masses must take into account the temperature and salinity characteristics, since the density stratification does not always reflect the presence of a certain water type.

The domain includes the whole Red Sea basin and a part of the Gulf of Aden reaching to 45^{o}E (Figure **??**). There are several reasons for including the western part of the Gulf of Aden and the Bab el Mandeb in the domain. The strait of Bab el Mandeb is the only open boundary of the basin where advective freshwater and heat fluxes can occur to balance the air-sea fluxes over the basin. The dynamics of the region including the formation processes are reflected in the exchange flow at the strait. Furthermore, since the most comprehensive available data set comes from the area of the strait, it is the best point for validation of the results of the numerical simulation. Another reason for including the western Gulf of Aden in the domain is that important water masses and dynamics involved in the seasonal circulation can be located in the area outside the Red Sea basin (e.g., Patzert, 1974a). At the open end of the domain at 45^oE, a 0.5^o wide buffer zone was fitted (Figure **??**) where hydrography is relaxed towards monthly mean values derived from the Levitus (1982) climatology, with a relaxation time of 60 days. Bottom topography and coastlines are from a digital data set with $5'$ resolution (ETOPO5) by averaging the topographic data located in each grid box. A correction was applied in the area of the strait where ETOPO5 data had a maximum sill depth of about $100\,m$ which is $60\,m$ shallower than the $160\,m$ sill depth at the Hanish Sill.

Three different model simulations are presented and discussed, which differ only in how they are forced. Both seasonal wind and seasonal thermohaline forcing are used for driving the model for the main experiment (E1). Two more experiments using only one of the two forcing mechanisms (thermohaline and wind) were carried out (E2 and E3, respectively). The momentum flux is given by the components of the wind stress. The thermodynamic forcing consists of the heat flux and the freshwater flux (which is imposed as a “virtual salt flux”, (Bleck et al., 1992)) and the mixed layer is stirred by turbulence generated by the oceanic friction velocity and the buoyancy flux. The atmospheric forcing functions applied to the model are derived from COADS (da Silva et al., 1994) but with two adjustments. An additional $0.5\,myear^{-1}\ E-P$ and $60\ Wm^{-2}$ of heat loss to the atmosphere were added so that the annual mean of the air-sea fluxes matches the observed advective fluxes at the strait. These corrections were added uniformly in space and time, since the spatial distribution and the seasonal cycle of the atmospheric conditions involve great uncertainties.

The model experiments were initialized using the National Oceanographic Data Center (NODC) hydrographic data for the winter state, and the initial density stratification is presented in Figure **??**. All the simulations were integrated for 10 years. Although the simulations did not reach absolute equilibrium after this time, the circulation develops very fast (within a few months) and does not change perceptively after that either in its mean or seasonal cycle. For all of the experiments the results mentioned here are the average of the last 9 years of integration.

5.4 Results from the simulation

The performance of the model was tested at the strait of Bab el Mandeb where the resulting seasonal cycle of the exchange flow was compared with the available direct observations (Chapter 3). Although some differences in the phase and range of the two cycles exist the main result is that the simulation is able to reproduce the basic characteristics of observed variability (reversal of the surface flow and intermediate intrusion during summer, and seasonal variability of the RSW outflow with a minimum during the summer season) while the strength of the exchange is almost identical to the observed one. This increases our confidence in the results presented here, although comparison with future observations of the general circulation in the area will be a more definite test.

5.4.1 Surface circulation

The 9-year average surface circulation for the winter (September to May) and summer (June to August) seasons are plotted in Figure **??** and **??**, respectively. The choice of the months representing each season takes into account the seasonal patterns of the forcing fields as well as the exchange flow at the strait. Both wind and thermohaline forcing are highly variable at the seasonal time scales and thus the circulation patterns are expected to show a strong seasonality. All the fields show a high degree of complexity with series of eddies and jet-like currents. Although the surface layer transport averaged at central axis of the basin is relatively weak (about 0.4 Sv and decreasing slowly to the north) in agreement with the order of magnitude predicted from the two-dimensional approaches, the cross-basin transport is very strong in accord with previous observations.

South of 18^oN the seasonal variability is strongest as expected by the reversal of the wind field as well as the high variability of the exchange flow at Bab el Mandeb. The dominant feature in the south is a mesoscale gyre with its center located between 15^o and 16^oN which reverses from an anticyclonic rotation during winter to a cyclonic rotation during the summer and achieves velocities of more than 0.5 m/s during the peak of the winter. Other features present in the area are weaker and smaller and most of them have a transient character. During winter, an inflow in the surface layer is observed at the strait. After entering the basin this NNW flow intensifies along the western boundary as a strong boundary current with maximum velocities that vary with the strength of the inflow but are greater than $20cm/s$ throughout the season. After flowing only about 400 km into the Red Sea, near 16^oN, this current ceases and an eastward intensified boundary current is observed for most of the remaining length of the basin. Although this boundary current is a little weaker and more variable than its southern counterpart, interacting with other features of the circulation pattern (mesoscale cyclonic and anticyclonic eddies), it accounts for most of the surface northward flow in the basin.

During summer the northward western boundary current disappears in the southern part of the Red Sea. It is the season when the surface flow reverses and a strong intermediate inflow of the fresher and colder GAW takes place. The model circulation now is relatively weaker and more irregular than in winter, since both wind and thermohaline forcing are weaker in summer. As we saw in the previous sections the atmospheric functions used to drive the circulation present several problems (Tragou et al., 1999) and there is high uncertainty in the seasonal cycles. This can also be the explanation for the brief summer season and the weaker reversal of the surface flow compared with the available direct observations.

In the northern part of the Red Sea, two permanent eddies dominate the circulation field, an anticyclonic gyre centered around 23.5^oN and a cyclonic gyre centered around 25^oN. Both coincide surprisingly well with available observations in the region (Morcos, 1970; Morcos and Soliman, 1974; Maillard, 1974; Clifford et al., 1997). Although their strength, shape and extent show some seasonal variability, they are present throughout the year. The stronger one is the cyclonic gyre in the north reaching maximum velocities of more than 40 cm/s. Due to the doming of the isopycnals inside the cyclonic eddies, which produces a weaker stratification, and the ability of the feature to trap waters and expose them to the extremely strong atmospheric forcing during winter, this is the most favorable place for the formation of the RSW (Chapter 5).

The annual mean surface salinity and temperature fields are plotted in Figures **??** and **??**. There is a distinct salinity gradient toward the north where it reaches its maximum, in agreement with the observations and simple theoretical models. The temperature pattern is more complicated, presenting its maximum at the center of the basin and decreasing towards the two ends of the Red Sea. This is related to the very weak wind speed observed in the central region of the Red Sea where the wind field is convergent for most of the year. These simple pictures are altered by the circulation complexity, and areas of minima and maxima are associated with the dominant features of the circulation pattern. Figure **??** presents the 9-year average of the annual mean sea surface elevation anomaly. Apart from the highs and lows related to the circulation pattern, there is a downward tilt of the sea level to the north. Since the freshwater flux is imposed as a "virtual salinity flux" at the mixed layer, it can not affect the volume of the basin. Thus the tilt is associated with the steric effect caused by the strong north-south density gradient through the basin.

5.4.2 Intermediate circulation

The most active subsurface layer is the second one from the bottom, lying over the RSDW layer which contains a very weak circulation. Layer 6 is the core of the RSW where most of the hypersaline outflow (39.8 psu from the model results compared to 39.7 psu from observations (Murray and Johns, 1997)) takes place at the bottom of the strait of Bab el Mandeb. The winter and summer circulation in this layer are plotted in Figure **??** and **??**. The velocity field is weaker than the surface but involves several interesting features. It is also much more consistent between winter and summer. The magnitude of the flow increases to the south near the Bab el Mandeb due to topographic constrictions and because of mixing with the adjacent layers. It is obvious that the surface circulation features directly affect the flow at this intermediate level, such as the the strong gyres in the nort which extend to the depth of layer 6. Boundary intensification is also observed in this layer, especially south of 20^oN. The general pattern of this intensification has the characteristics of an undercurrent (i.e., opposite to the surface boundary currents) but the transition point is shifted to the north and the currents are affected by topography. Reaching the strait, the velocities in this layer become very large, achieving values of over $0.5\,m/s$.

The annual mean surface circulation and surface density are plotted in Figure **??** and will be compared with the results from two additional experiments described in the next section. Although this is an average of the 9 years of simulation, including both seasons, some of the most important features are present, such as the boundary currents, the anticyclonic eddy in the south and the double gyre system in the northern part of the basin. This happens because some of the features are permanent and also because the winter season lasts about three fourths of the year and presents a more vigorous circulation than the summer one.

5.5 Thermohaline- and wind-driven experiments

Although the effects of the wind stress and the thermohaline forcing do not add linearly to drive the general circulation, since they are connected at least through the wind speed affecting the air-sea fluxes and stirring the mixed layer and thus interact to produce the final circulation and stratification patterns, it is sometimes convenient to separate them and investigate the circulation produced by each one (what is usually called wind- and thermohaline-driven parts of the circulation). With the above caveats in mind, two experiments with the same configuration, described in Section 5.3, were carried out (E2 and E3) but with one forcing field "turned off", wind and thermohaline respectively. The main goals of these additional experiments are twofold: to estimate the relative strength and importance of each mechanism in the general circulation and, if possible, to determine the role each one plays in driving the key features of the circulation pattern presented in the previous section.

The annual mean surface velocity fields for the thermohaline- and the wind-driven cases are plotted in Figures **??** and **??**, respectively. It is obvious from a comparison between the two results that the purely wind-driven circulation is much weaker than the thermohaline-driven one. This is not a result of the averaging, but persists throughout the year. Another indication that the thermohaline forcing is the dominant mechanism in the region, is that in the areas where these two mechanisms compete with each other the patterns generated by the thermohaline forcing dominate. This is the case in the northern end of the Red Sea, where the wind-driven result produces an anticyclonic rotation while the thermohaline-driven presents the cyclonic eddy, which is a permanent feature of the circulation in the area as shown in the previous section and verified by observations. In areas where the two results have similar features (as in the case of of the winter anticyclonic eddy around 16^oN), they reinforce each other producing stronger circulation patterns. Of course, in several cases the final result is the product of the nonlinear interaction of the forcing fields (Chapter 3).

5.5.1 Boundary current structure and intensification

It is very interesting to notice that the thermohaline-driven result presents a similar type of intensification towards the coasts, with boundary currents shifting from the west to east coasts at midbasin, though shifted to the north by a few degrees form the combined forcing experiment (E1). This vigorous and complicated pattern of the thermohaline circulation contradicts previous studies (Phillips, 1966; Tragou and Garrett, 1997) which predict a slaggish and two-dimensional type of circulation. Theoretical investigation can help us get some insight on the kind of mechanisms involved in these patterns. McCreary et al. (1986) investigated the effect of thermohaline forcing on eastern boundary currents. If the surface density increases poleward, the resulting pressure field slopes downward in the same direction creating an eastward geostrophic current in the basin. This will affect the eastern boundary where downwelling must take place. McCreary et al. (1986) incorporated this idea to a three-dimensional, linear, continuous stratified theoretical model and solved for both steady forcing and forcing that oscillates in time with frequency σ. For the inviscid case, the solution at the eastern boundary will involve waves that are described by the dispersion relation

$$k = -\frac{\beta}{2\sigma}\left[1 - \left(1 - 4\frac{\sigma^2\alpha^2}{\beta^2}\right)^{1/2}\right] \tag{5.1}$$

where k is the zonal wavenumber, σ is the forcing frequency, $\alpha_\eta^{-1} = 2\,\Omega\,sin(\theta)/c_\eta$ is the Rossby radius of deformation of the η^{th} normal mode (with speed c_η) and $\beta = 2\,\Omega\,cos(\theta)/R$ is the meridional change of the Coriolis parameter, where R is the earth's radius. The radicand vanishes at a latitude, the critical latitude θ_{cr}, given by

$$\theta_{cr} = tan^{-1}(c_\eta/2R\sigma) \tag{5.2}$$

North of θ_{cr}, k is complex representing Kelvin waves that decay offshore rapidly with an e-folding scale of the order of α^{-1}. South of the critical latitude, k is real and the waves that are generated are Rossby waves that propagate offshore (westward). So, we expect a westward intensification south of θ_{cr} as Rossby waves propagate the pressure gradient to the western boundary, and eastward intensification north of θ_{cr}, as indicated in the schematic of Figure **??**.

Direct application of the above formulas to the model results is difficult, since the stratification and the thermohaline forcing vary in space and time and cannot be compared with the idealized functions used in the theoretical model. Nevertheless, using the annual frequency and the basinwide mean stratification from the thermohaline-driven experiment results, the critical latitude is estimated at about 17^oN (for the second baroclinic mode which is dominant in the Red Sea circulation, presenting a two-layer flow on the top of a mostly inactive layer). The addition of the wind does not significantly change the circulation pattern but is able to change the stratification enough to shift the critical latitude to the south. Using the mean stratification from the main experiment (with both forcing fields) the new critical latitude is estimated at about 14.5^oN, which is consistent with the southward shift of the boundary current transition in the experiment E1 compared to the thermohaline-only experiment (E2) discussed here.

5.6 Summary and Discussion

The numerical simulation study of the Red Sea, presented here, reveals several interesting features of the circulation in the area. The most important findings include the intensification of the flow toward the coasts, the presence of the permanent double gyre system in the northern part of the basin, and the stronger seasonality of the flow in the southern Red Sea. A particularly interesting finding is the transition from western to eastern intensified boundary current regions between the southern and northern parts of the basin predicted by the model. As more observations become available and the modelling efforts more detailed, ideas about the dynamics involved in the Red Sea circulation are changing rapidly. The picture of a sluggish circulation proposed by the simplified two-dimensional approaches seems inadequate to describe the Red Sea dynamics. The patterns of the circulation are vigorous and complicated. These differences can have an important effect on the mixing processes and may answer some puzzling questions concerning the main dynamical balances in the basin (Tragou and Garrett, 1997; Chapter 1).

Overall the thermohaline forcing seems to be the most important mechanism driving this highly complex circulation. The main circulation pattern is related to the buoyancy loss (mostly due to the fresh water fluxes) which increases the density to the north and produces a northward pressure gradient associated with the sloping of the sea surface. An eastward mean cross-basin geostrophic current is established in the upper layer. The response of the eastern boundary depends on the stratification and β-effect and two different regimes were identified. North of a critical latitude an eastward intensification is expected and south of it the disturbance at the eastern boundary leaks offshore by Rossby waves to generate a more traditional westward intensification. Undercurrents are evident in the model results, but show a northward shift and phase differences with respect to the surface currents which can be associated with the interaction of these intermediate currents with the bottom topography.

Although less important, the effects of the wind field are also evident in the results, especially at the southern part of the Red Sea where the winds have their greatest variability and become very strong during winter. The winds in the southern Red Sea affect strongly the exchange flow at the strait of Bab el Mandeb and through this the dynamical balances of the whole basin.

Future observations and numerical simulations can hopefully produce a more accurate and complete picture of the Red Sea circulation. The weakest point of all the attempts is our understanding of the air-sea fluxes in the area. Although recent observations enable us to put some constraints on the fluxes, our knowledge of the spatial and temporal variability of the forcing fields is very poor. The use of real fresh water fluxes rather than a virtual salt flux is another important improvement for future modelling attempts. The addition or subtraction of fresh water from the surface of the sea may play a role in the general dynamics of the area, and give rise to what is known as Goldsbrough-Stommel circulation (Goldsbrough, 1933; Stommel, 1957 and 1984). This circulation although weaker compared with other mechanisms may be important in the Red Sea where one of the highest evaporation rates of the world ocean is observed.

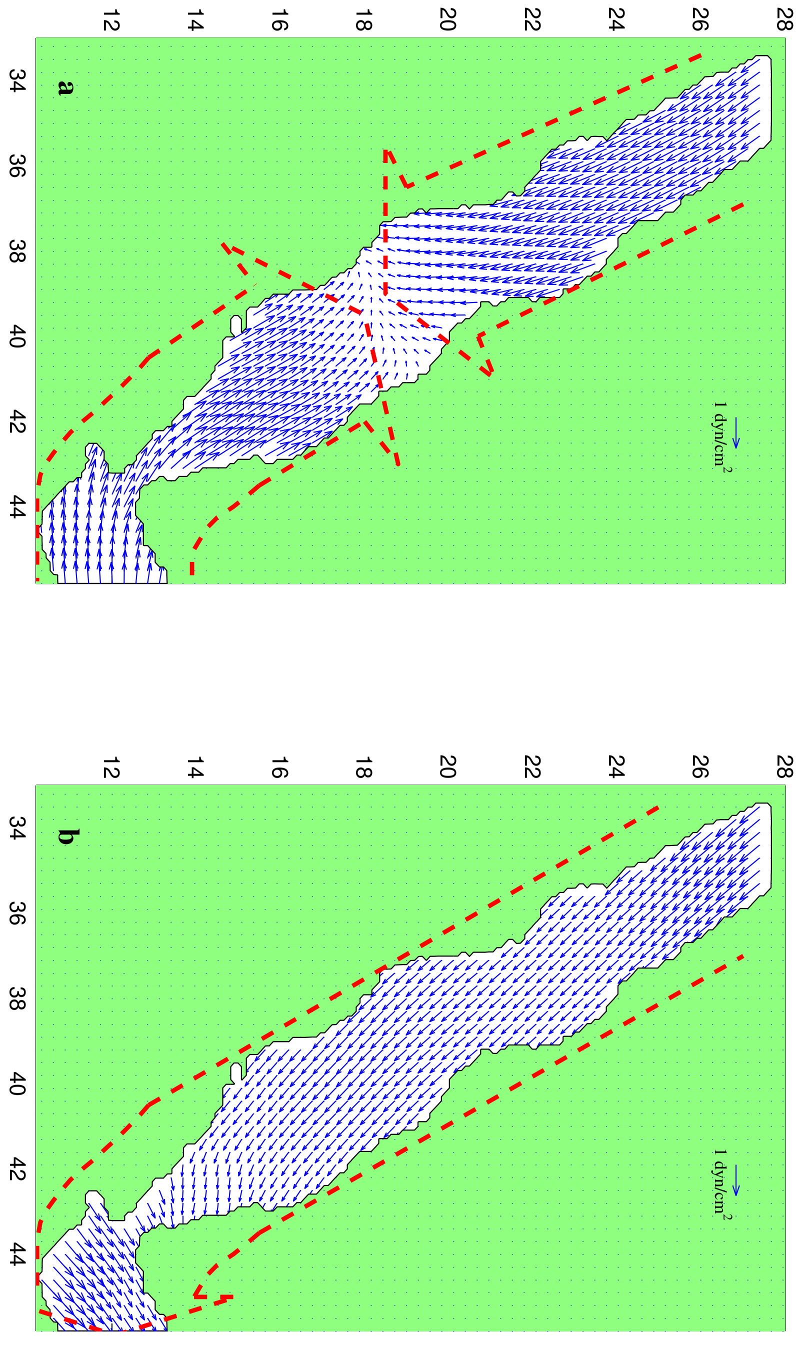

Figure 5.2: Wind-stress fields for (a) January and (b) July from COADS.

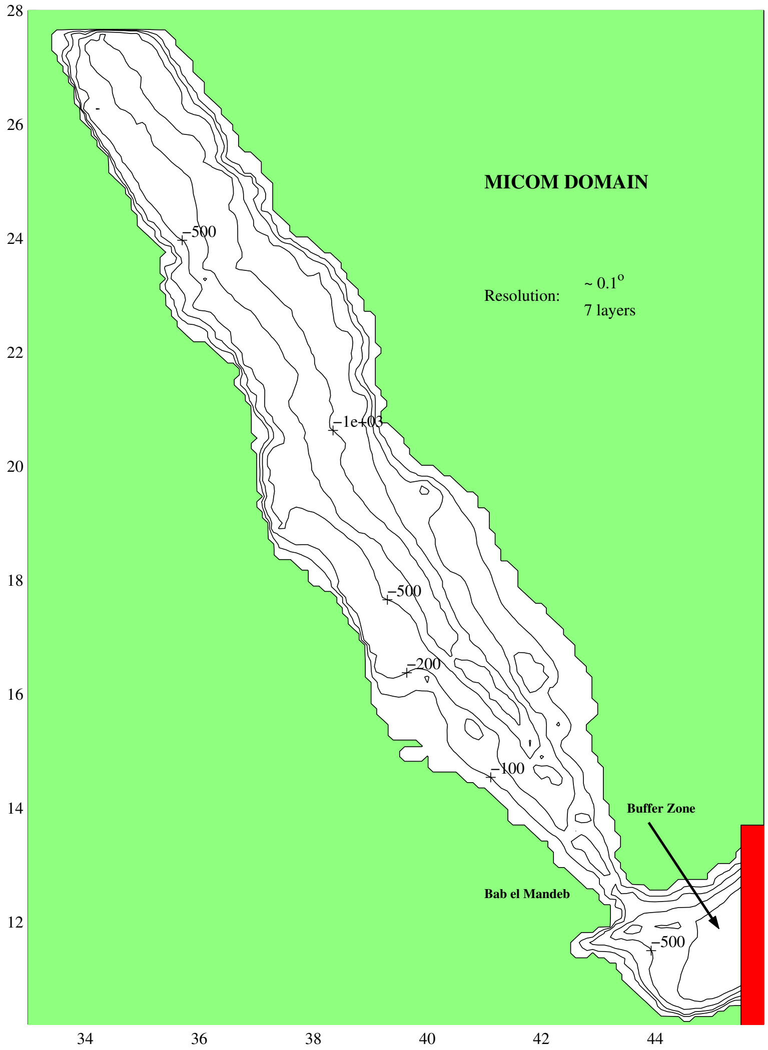

Figure 5.3: The geographical domain included in the OGCM experiments.

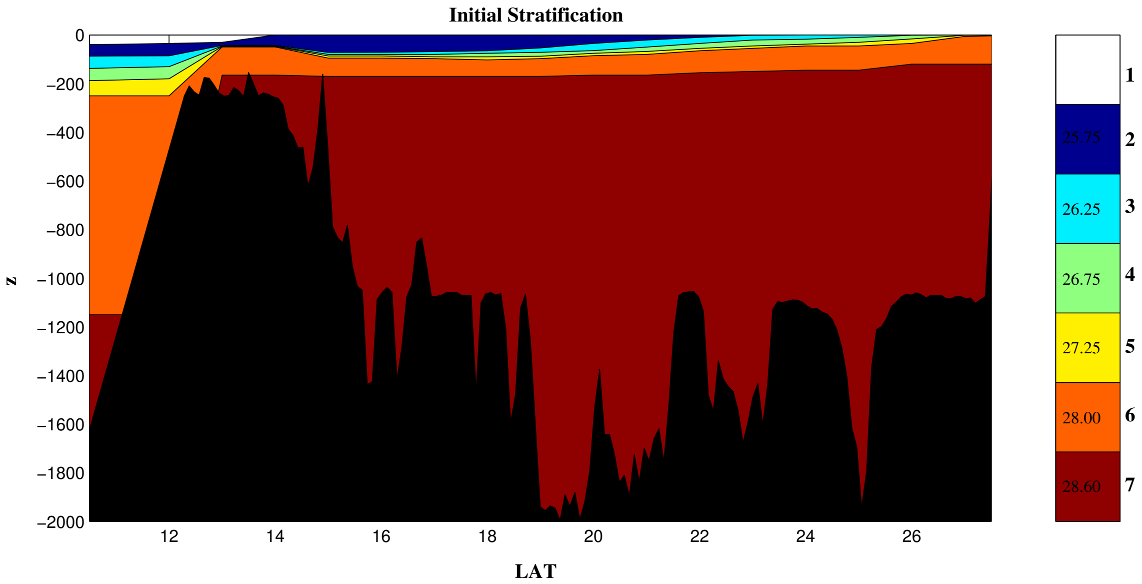

Figure 5.4: Initial stratification used in the simulation.

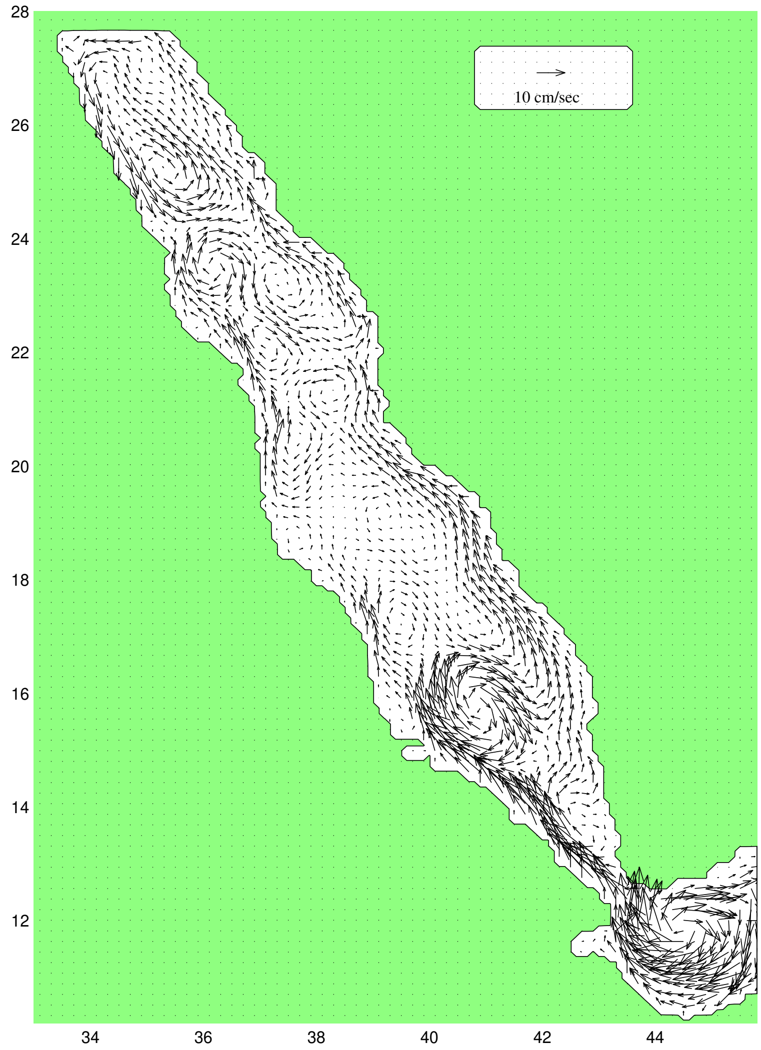

Figure 5.5: Surface circulation from MICOM simulation, experiment E1, 9-year winter average.

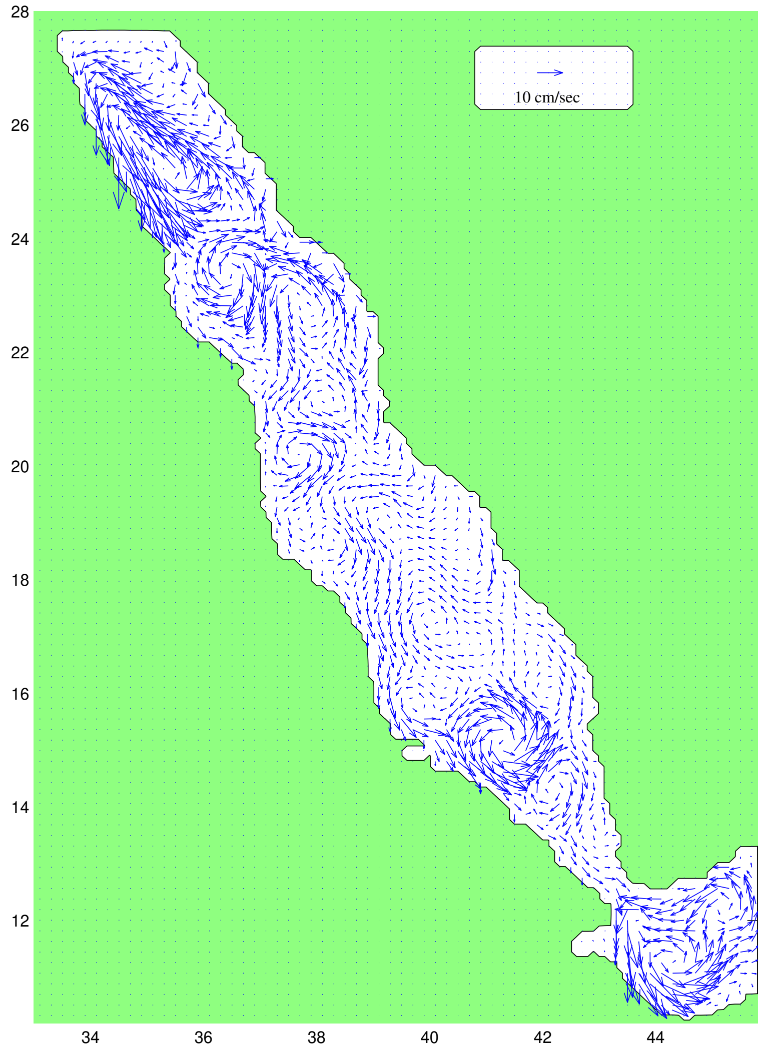

Figure 5.6: Surface circulation from MICOM simulation, experiment E1, 9-year summer average.

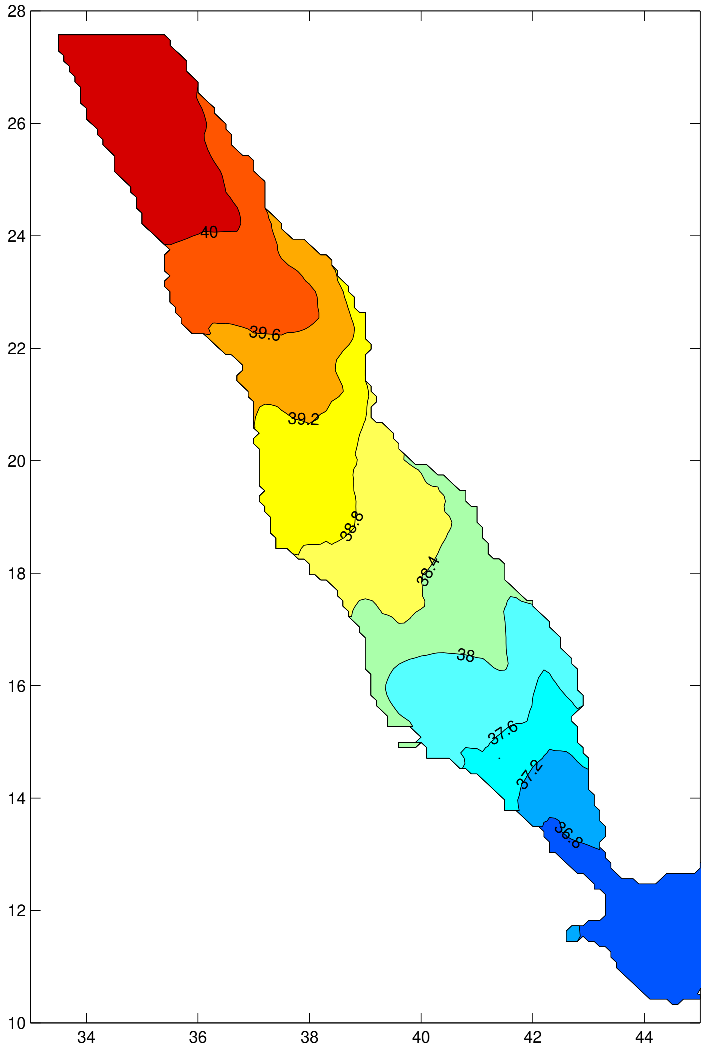

Figure 5.7: Annual mean sea surface salinity from MICOM simulation (9-year average).

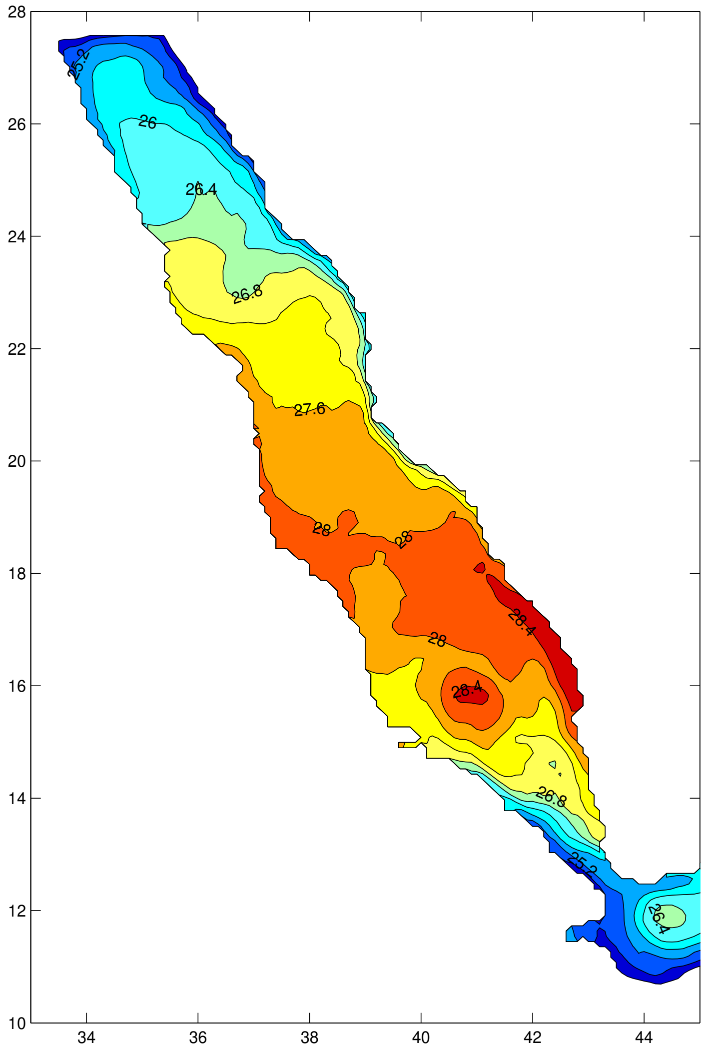

Figure 5.8: Annual mean sea surface temperature from MICOM simulation (9-year average).

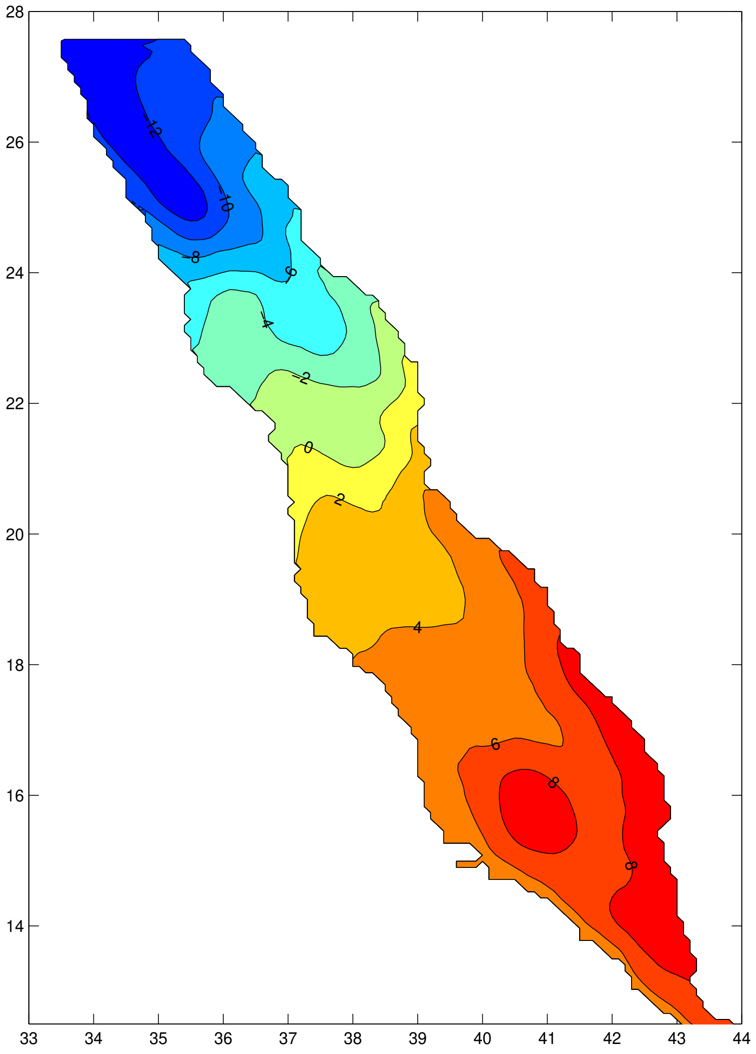

Figure 5.9: Annual mean sea surface elevation anomaly from MICOM simulation (9-year average).

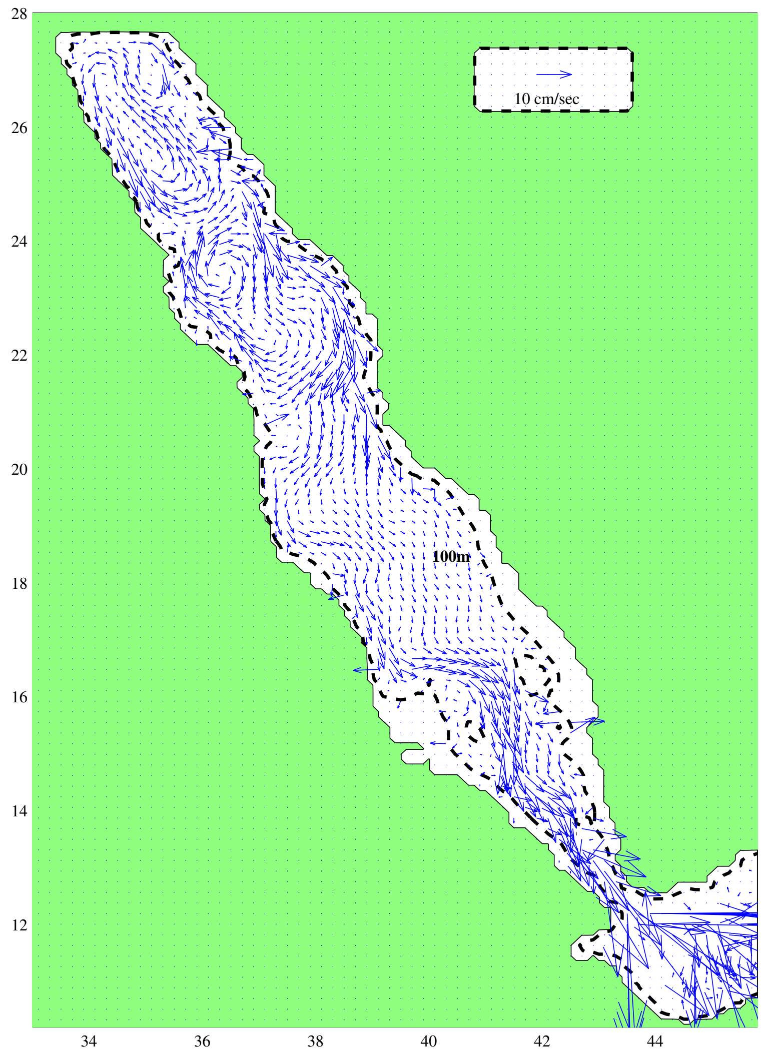

Figure 5.10: Winter layer 6 circulation from MICOM simulation (9-year average).

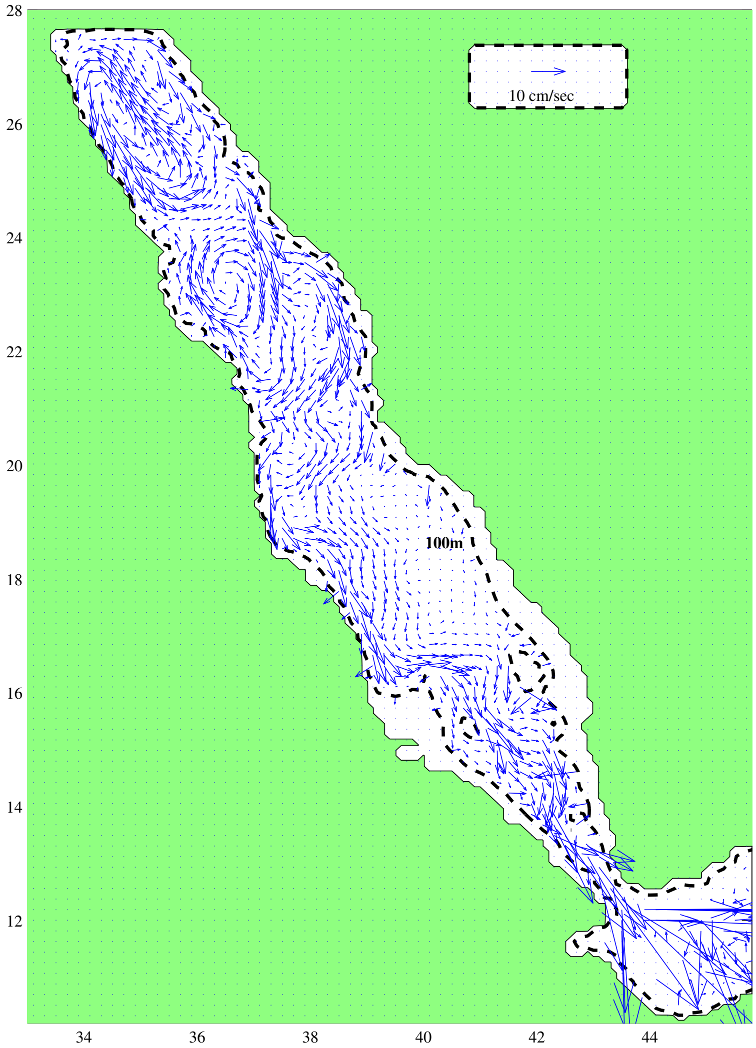

Figure 5.11: Summer layer 6 circulation from MICOM simulation (9-year average).

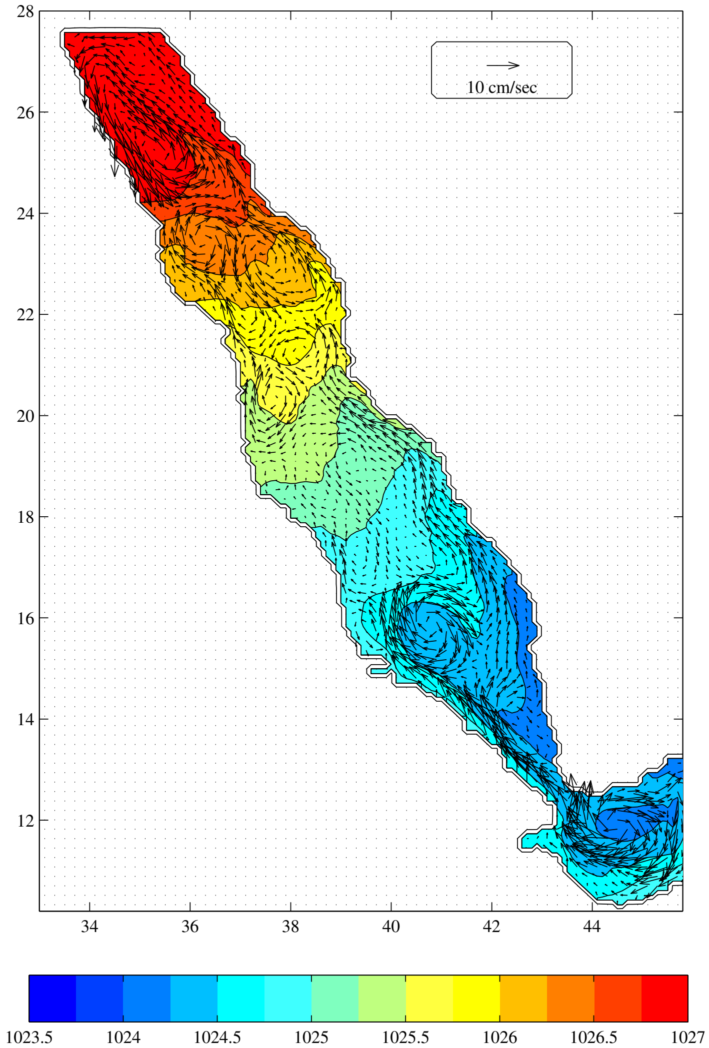

Figure 5.12: Mean surface circulation and mixed layer density from MICOM simulation (9-year average).

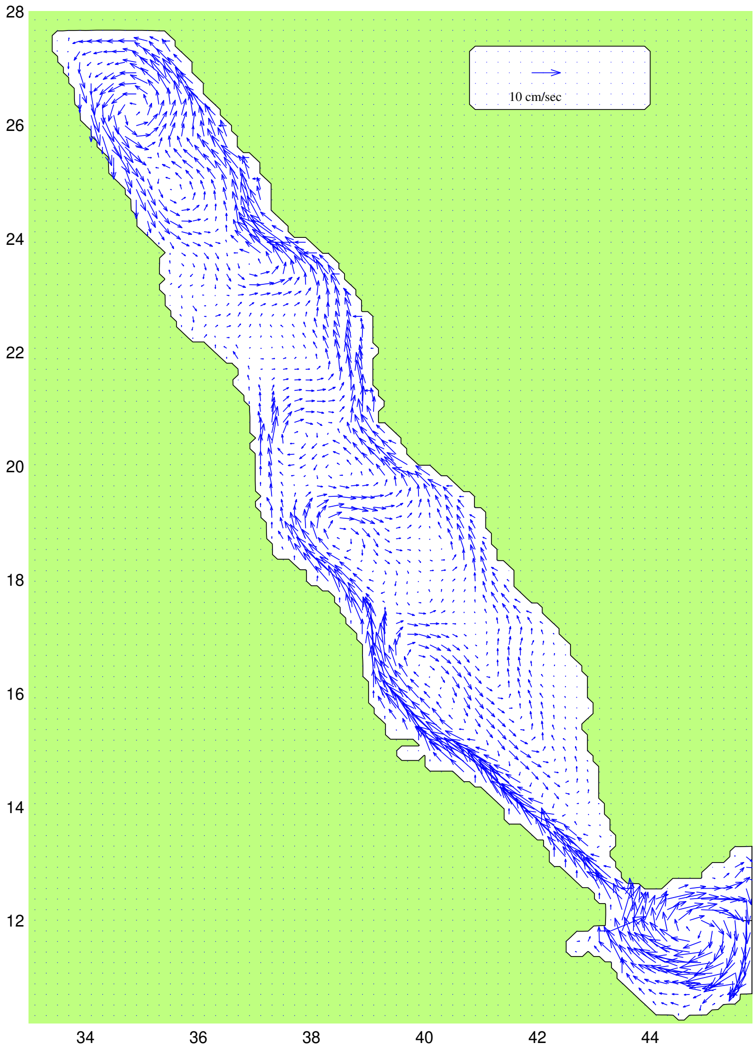

Figure 5.13: 9-year average sea surface velocity from the thermohaline-driven MICOM experiment (E2).

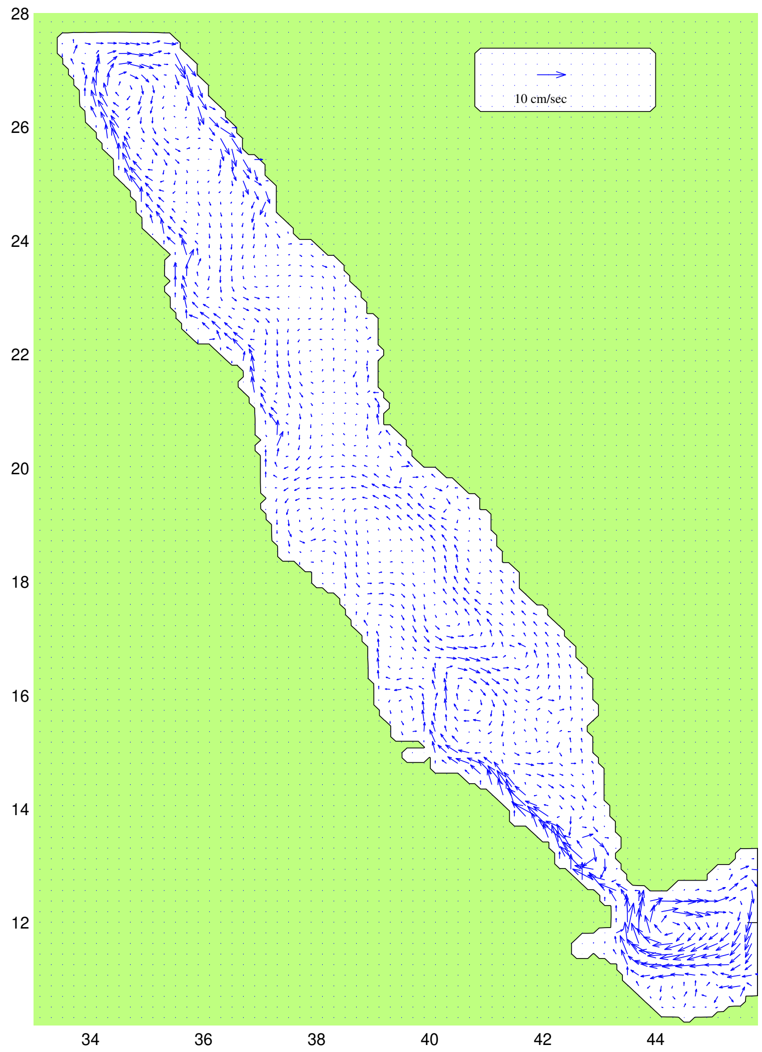

Figure 5.14: 9-year average sea surface velocity from the wind-driven MICOM experiment (E3).

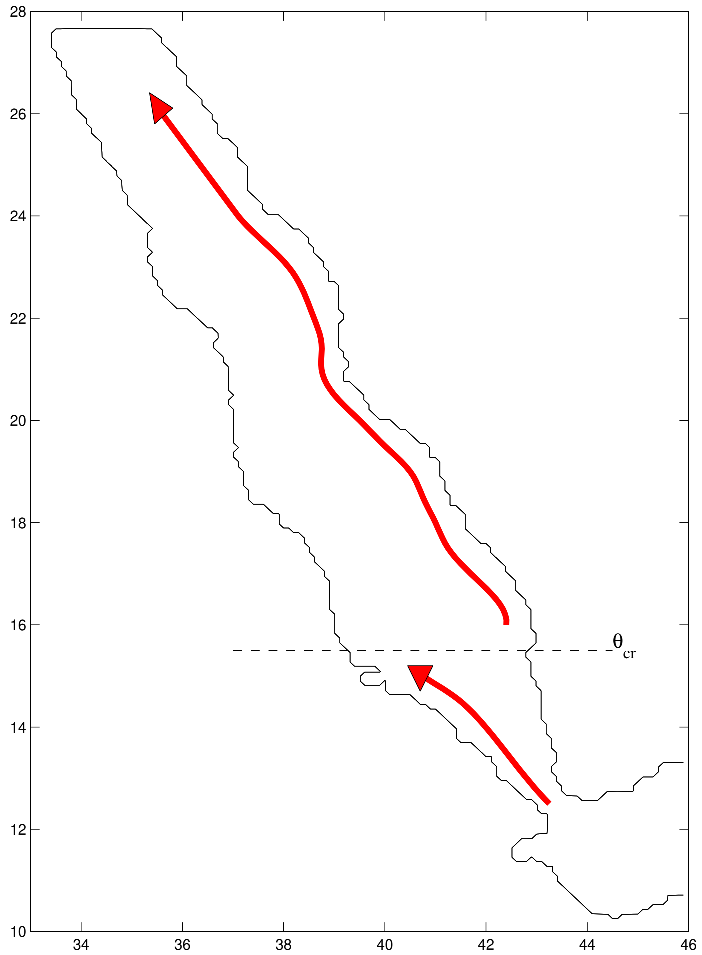

Figure 5.15: Schematic presentation of the flow intensification toward the coast.

Chapter 6

Intermediate water formation in the Red Sea

6.1 Introduction

One of the most distinctive water masses present in the Indian Ocean is the Red Sea Water (RSW). Its origin can be traced to the entrance of the Red Sea basin, the strait of Bab el Mandeb, where an annual mean transport of 0.36 Sv of hypersaline water outflows to the Gulf of Aden and further to the Indian Ocean (Chapter 2). Although the volume flux of the RSW is relatively small, its salinity is very high (39.7 psu at the outer part of the strait and about 36 psu after reaching the Arabian basin) and it can be identified far away from its source as a salinity maximum at intermediate depths (Rochford, 1964; Hamon, 1967; Grundlingh, 1985; Shapiro and Meschanov, 1991; Mantyla and Reid, 1995).

The location, time and mechanisms involved in the formation of the RSW inside the Red

Sea basin are not yet clear. Until recently the outflowing water mass was confused with the Red Sea Deep Water (RSDW), a very uniform type of water with extremely high salinity (about $40.6 psu$) which fills the the deeper parts of the basin from about $200 m$ depth to the bottom of the Red Sea (which reaches the 3000 m at some locations). Most investigators agree that the RSDW is formed during winter in the Gulf of Suez (Maillard, 1974; Wyrtki, 1974) where that water obtains extreme values of salinity and sinks to the bottom of the Red Sea basin entraining ambient water. The Gulf of Aqaba is thought to be a secondary source of RSDW (Wyrtki, 1974). Other modes of formation have been hypothesized, such as open ocean deep convection and formation on the continental shelf of the Red Sea, but there is no evidence to support them.

The idea that the outflow originates from intermediate depths was proposed by Neumann and McGill (1962). Analyzing tracer distributions (^{14}C and ^{3}He) from the GEOSECS Indian Ocean Expedition, Cember (1988) was the first to clearly identify a different water mass (here called RSW to distinguish it from the RSDW) comprising the core of the outflow. Further evidence that supports this distinction is the small rate of RSDW formation. The only direct observation of the transport at the mouth of the Gulf of Suez during the winter is that of Maillard (1974) during 1971-72 which gives an estimated deep water outflow of 0.082 Sv, or, assuming that this is representative of three winter months, an annual rate of approximately 0.02 Sv. Maillard (1974) assumed that this transport is doubled due to entrainment, so that the total RSDW production is $O(0.04\ Sv)$. This is a very small amount compared to the total outflow from the Red Sea which is 10 times larger. Recent observations in the Red Sea (Woelk and Quadfasel, 1996) of the oxygen distribution verify the distinction between deep and intermediate waters. An oxygen minimum at intermediate depths (about $300\,m$) separates a relatively new intermediate water mass (the RSW) from much older deep water (RSDW).

Cember (1988) proposed that this intermediate water mass is injected immediately beneath the pycnocline at a rate of $0.11 \pm 0.02\,Sv$ and located the place of formation at the extreme open northern Red Sea. Unfortunately, no direct observations are available to verify his theory and due to insufficient data very little can be said about the mechanisms involved in this formation process. Localized open ocean deep and intermediate convection is one of the most important mechanisms of water mass formation in the oceans and is present in many polar or low-latitude semi-enclosed basins such as the western Mediterranean (Swallow and Caston, 1972; Leaman and Schott, 1991) the eastern Mediterranean (Lascaratos, 1993), the Labrador Sea (Clarke and Cascard, 1983), the Greenland Sea (Schott et al., 1993; Visbeck et al., 1995) and Weddell Sea (Gordon, 1978; Muench, 1988; Alverson and Owens, 1996). The horizontal scales of of the observed convective structures are of order $50 - 200\,km$. Although localized buoyancy loss can be important in these features, the typical atmospheric scale of forcing is an order of magnitude larger than the observed structures. Furthermore, vertical stratification and the Coriolis force act together against convective motions. In order for deep or intermediate convection to take place two more conditions must also contribute, weak stratification and a "trapping mechanism" to keep the surface waters exposed to strong atmospheric forcing for enough time to acquire the proper temperature and salinity characteristics. These elements are known as the preconditioning phase (Swallow and Gaston, 1973; Hogg, 1973) which can result from a variety of mechanisms. In most of the known cases this preconditioning is associated with a cyclonic gyre where the stratification weakens due to upward tilt of the isopycnals and waters are exposed for a considerable time to intense buoyancy loss. In the eastern Mediterranean, where the atmospheric conditions resemble those of the northern Red Sea (i.e., extensive evaporation), the formation of the Levantine Intermediate Water is a localized winter process in the region of the Rhodes Gyre in the Levantine basin (Lascaratos et al., 1993).

The depth in which the convective plumes penetrate depends on the vertical stratification and the time and intensity of the buoyancy flux. The very dense (about $1028.6\,kgm^{-3}$) and uniform RSDW could act as a barrier to convection. Although open ocean deep convection is a possible additional source of deep water, in this paper we deal with the formation of intermediate waters (RSW) which lie between the pycnocline and the deep RSDW layer. Two models, a box model and the results from a Oceanic General Circulation Model (OGCM), will be used to investigate mechanisms involved in the RSW formation, possible locations and rates of production. Recent observations and climatological data are included in the configuration and validation of of the experiments.

6.2 A Box Model of RSW formation

The box model used here is based on the conservation of volume and salt in the Red Sea basin. All the calculations assume a steady state so that only the long term mean characteristics and fluxes will be considered. The approach presented here tries to incorporate the smallest number of possible parameters and preferably those that appear the most robust. Fortunately, recent observations at the strait of Bab el Mandeb (Murray and Johns, 1997) put reliable constraints on the volume and salt fluxes between the Red Sea and the Indian Ocean. According to these observations, for most of the year (October to May) a two-layer exchange is present with a relative fresh surface inflow and an outflow of the Red Sea Water (RSW), which is characterized by high salinity ($39.7\,psu$), at the bottom of the strait (with sill depth of about $160\,m$). This simple exchange is interrupted by a summer (June to September) three-layer exchange with a surface outflow, an intermediate intrusion of Gulf of Aden Water (GAW), and a much weaker RSW outflow. The annual mean $E-P$ rate estimated from these observations (Chapter 2) is $2.06\,m/year$.

The model is comprised of three boxes as can be seen in Figure **??**. The top one represents the surface layer, the next one represents the intermediate or RSW layer which

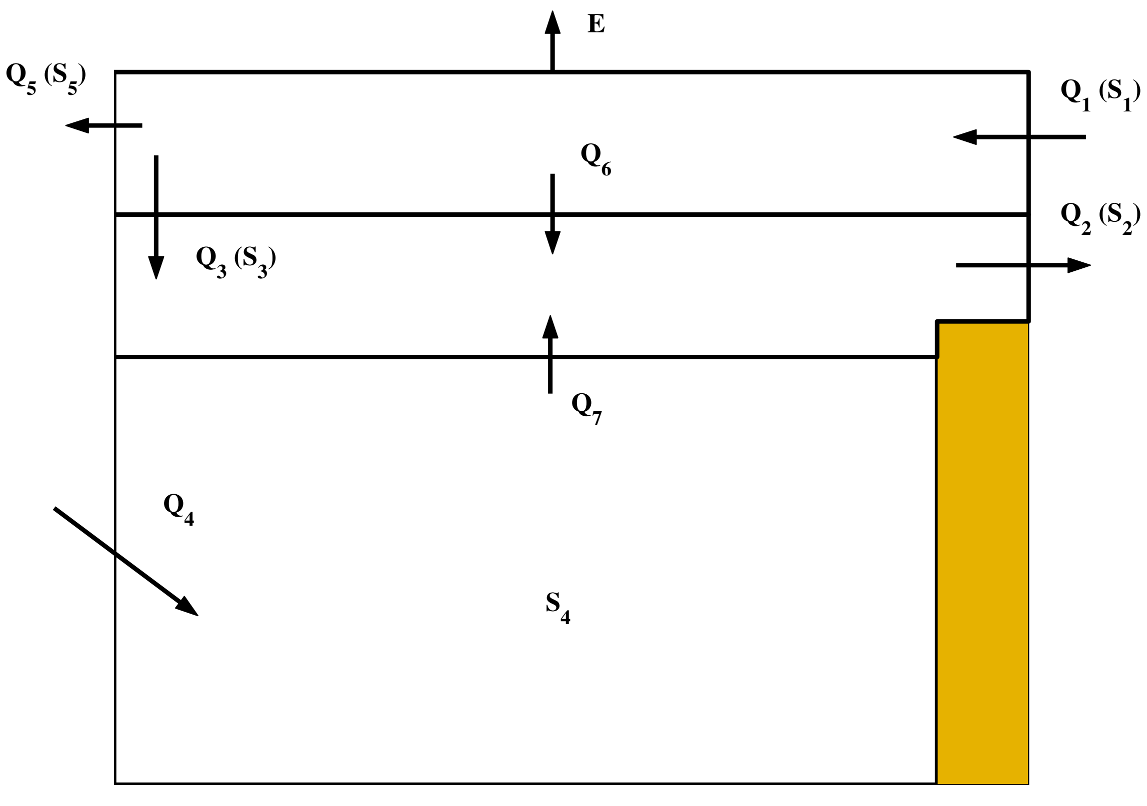

Figure 6.1: The box model. Arrows represent volume and salt fluxes.

at the strait corresponds to the RSW outflow, and the bottom one represents the RSDW which fills the deeper parts of the basin. The first two differ from the usual sense of boxes in most box models, since the characteristics (here the salinity) can change with latitude. For example, the salinity of the surface box changes from S_1 at the entrance of the Red Sea linearly to S_4 at the northern end of the basin (Table **??**). Apart from the volume and salt fluxes between the three boxes and the exchange at the strait, four more volume or salt fluxes are used in the configuration, the $E-P$, the production of RSDW (Q_4), the surface flow to the Gulf of Suez and to Gulf of Aqaba (Q_5,S_5) and a localized formation of intermediate water at the extreme northern Red Sea (Q_3,S_3). For a steady state the equations describing the box model can be summarized as

$$\sum_i Q_i = 0 \tag{6.1}$$

$$\sum_i Q_i S_i = 0 \tag{6.2}$$

where Q_i represent the the volume fluxes at the surfaces of each box and S_i are the associated salinities. The equations can be applied in each box and the domain as a whole. This yields a system of 8 equations from which 5 are independent (since the equations for the whole domain is just the sum of the equations for the boxes and the equations for the bottom box reduce to one equation). The system is solved by specifying the variables denoted in Tabel **??** and the values proposed are discussed below.

The National Oceanographic Data Center (NODC) data set was used for the salinity values of the surface and deep layer. As mentioned before, the salinity of the surface box varies with latitude, from 36.6 psu close to the strait to 40 psu at the northern end of the Red Sea. The salinity for the deep layer is 40.6 psu and the $E-P$ rate established by the

VARIABLE		DESCRIPTION	VALUE
Q_1	u	Inflow	0.393 Sv
Q_2	s	Outflow	0.36 Sv
Q_3	u	Loclized formation	0.23 Sv
Q_4	s	Deep water production	0.05 Sv
Q_5	u	Outflow to the Gulfs (and possible entrainment)	0.053 Sv
Q_6	u	Entraiment between surface and intermediate layer	0.09 Sv
Q_7	u	Entrainment between bottom and intermediate layer	0.05 Sv
S_1	s	Inflow salinity	36.8 psu
S_2	u	Outflow salinity	39.7 psu
S_3	s	Localized formation salinity	40.0 psu
S_4	s	Bottom layer salinity	40.6 psu
S_5	s	Salinity at the northern end of the Red Sea	40.0 psu
$E-P$	s	Evaporation minus precipitation	0.03 Sv

Table 6.1: Variables used or estimated by the box model, where 'u' defines the unknowns and 's' the specified variables.

fluxes at Bab el Mandeb is 2.06 $m/year$. For the RSDW formation rate a value of 0.05 Sv was chosen taking into account the available measurements of 0.04 Sv by Maillard (1974) and adding another 25% to include other possible sources of deep water (Gulf of Aqaba and deep convection). For the strait fluxes the recent observations provide quality data. But here there is a problem with the presence of the three-layer summer exchange which complicates the simple structure of the box model. There are two solutions: either include only the winter months in the computation or incorporate both the surface and intermediate summer fluxes in the surface layer box in the model. The second approach was chosen to avoid problems from the annual variability of parameters (such as the $E-P$ rate) and from storage terms in the basin that can be substantial. Nevertheless, both approaches give very similar results. The variables to be determined are the surface inflow (Q_1), the outflow salinity (S_2), the entrainment terms between the boxes (Q_6 and Q_7), the volume flux to the Gulf of Suez and Gulf of Aqaba (Q_5), and the localized formation rate (Q_3). Although Q_1

is measured, one of the strait fluxes (Q_1 or Q_2) must be left undetermined to let allow for an exact mass balance in the basin including the $E-P$. The outflow salinity (S_2) is also left as an additional unknown, so that by varying Q_3 we are seeking the value that matches S_2 with the observed salinity of the outflow. The variables of most interest are Q_3, Q_6 and Q_7, which differentiate a localized RSW formation process in the north ($Q_3 > Q_6 + Q_7$) from a more distributed formation process through the whole basin ($Q_3 \ll Q_6 + Q_7$). In Figure **??** S_2 is plotted as a function of the localized formation rate Q_3. The value of Q_3 which

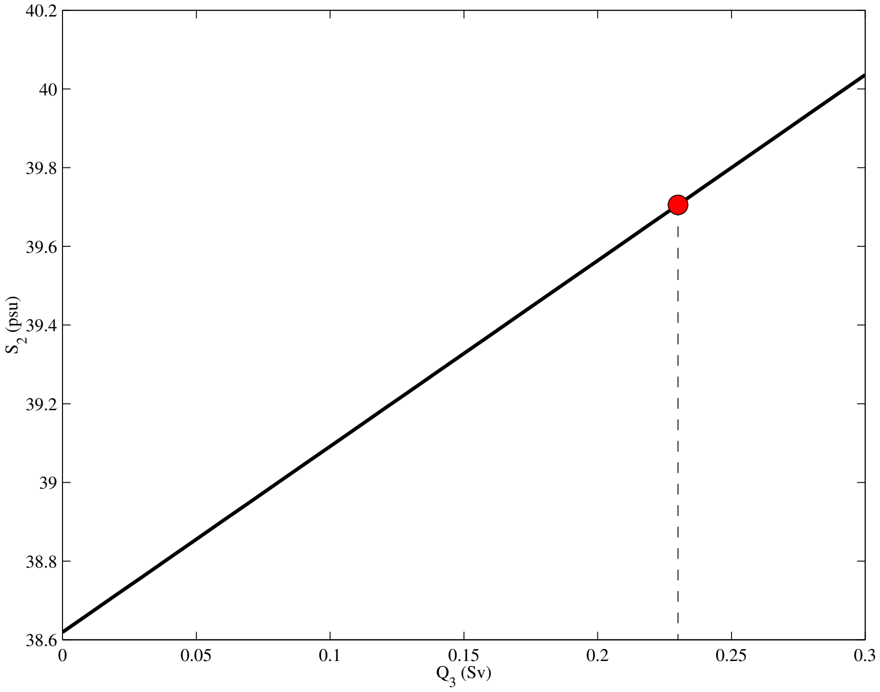

Figure 6.2: The outflow salinity as a function of the localized formation rate. The dot represents the values that match the observed salinity of the outflowing layer.

gives the observed outflow salinity (39.7 psu) is 0.23 Sv. This accounts for about 60% of the RSW outflow, showing that localized processes in the northern Red Sea are important for the formation of the hypersaline outflow from the basin.

The value of S_2 at $Q_3 = 0$ corresponds to a hypothetical “scenario” where the RSW outflow is formed by uniform mixing or convection from the surface layer over the whole basin. With this structure the predicted salinity of the outflow is 38.7 psu, which is far less than the observed outflow salinity (39.7 psu). Therefore, the final conclusion from this simple box model is that about 2/3 of the upper layer convection that forms the RSW must occur locally in the northern Red Sea, about 1/3 is contributed by widespread convection or mixing with the surface layer, and the rest 0.05 Sv is derived from mixing with the RSDW.

6.3 Results from a numerical simulation of the Red Sea

Although methods like the box model used in the previous section provide some ideas about the general budgets and the order of magnitude of processes contributing to the RSW formation they can say nothing about the actual mechanisms involved. These kinds of questions can be addressed only in three dimensional approaches using observations and OGCMs. Observations in the area of interest are very few and sparse in both space and time. In order to get ideas about the circulation in the northern Red Sea and the associated possible formation mechanisms, a numerical simulation was carried out for the whole basin and part of the adjacent Gulf of Aden. There are several reasons for including an extensive domain in the simulation instead of just the northern Red Sea where the formation is expected to occur. First, the strait of Bab el Mandeb at the southern end of the Red Sea is the only open boundary of the basin with the ocean where the fresh water and heat air-sea fluxes are compensated by advection. The dynamics of the region, including the water mass formation processes, are reflected in the exchange flow at the strait. Second, since the only recent and complete available data set comes from the area of the strait, it is the best point for validation of the results of the numerical simulation. The western Gulf of Aden is included in the domain because important water masses and features involved in the circulation can be located in the area outside the Red Sea basin (Patzert, 1974a).

The numerical experiments were carried out with the Miami Isopycnic Coordinate Ocean Model (MICOM) (Bleck et al., 1992; Bleck and Chassignet, 1994). In the experiment presented here a horizontal grid interval of 0.1^o (or about 10 km) was chosen in order to resolve the very narrow channel at Bab el Mandeb. Nevertheless, the two gulfs in northern end of the Red Sea (Suez and Aqaba) are very small and have very complicated topography and were not included in the present experiments. The domain is extended outside the Red Sea to incorporate part of the Gulf of Aden reaching 45^oE. The vertical density structure is defined by 6 isopycnic layers (with σ_θ $25.75, 26.25, 26.75, 27.25, 28.0$ and $28.6\,kgm^{-3}$) and a mixed layer (a thermodynamically active layer where density can vary in the horizontal), representing the basic water masses and density structure observed and involved in the Red Sea circulation. Bottom topography and coastlines are from a digital data set with $5'$ resolution (ETOPO5) by averaging the topographic data located in each grid box. A correction was applied in the area of the strait where ETOPO5 data had a maximum sill depth of about $100\,m$ which is $60\,m$ shallower than the $160\,m$ sill depth at the Hanish Sill. At the open end of the domain, in the Gulf of Aden, a 0.5^o wide buffer zone was fitted in which hydrography is relaxed towards monthly values derived from the Levitus (1982) climatology, with a relaxation time of 60 days.

Both mechanical and thermohaline forcing are used to drive the model. The momentum flux is given by the components of the wind stress. The thermodynamic forcing consists of the heat flux and the freshwater flux (which is imposed as a “virtual salt flux”, (Bleck et al., 1992)) and the mixed layer is stirred by turbulence generated by the oceanic friction velocity and the buoyancy flux. The atmospheric forcing functions applied to the model are derived from COADS (da Silva et al., 1994) but with two adjustments. An additional $0.5\, myear^{-1}$ $E-P$ and $60\, Wm^{-2}$ of heat loss to the atmosphere were added so that the annual mean of the air-sea fluxes matches the observed advective fluxes at the strait. These corrections were added uniformly in space and time, since the spatial distribution and the seasonal cycle of the atmospheric conditions involve great uncertainties. The model experiments were initialized using the NODC hydrographic data for the winter state. The simulation was integrated for 10 years. Although the simulation did not reach absolute equilibrium after this time, the circulation develops very fast (within a few months) and does not change perceptively after that. The results mentioned here are the average of the last 9 years of integration.

The simulation reproduces very well the observed seasonal variability as well as the strength of the exchange flow at Bab el Mandeb (Chapter 3). The predicted RSW outflow is 0.38 Sv which differs very little from the observed value (0.36 Sv). Although very few observations are available for the three-dimensional circulation in the Red Sea to verify the different features produced by the simulation, this good agreement increases our confidence in the model results. In Figure **??** the density and velocity of the surface layer is plotted for the mean state and in Figure **??** for different months representing the "preconditioning" and actual formation periods. The most important feature is a permanent cyclonic gyre centered at about 26^oN. Since this type of circulation is known to be a favorable environment for deep and intermediate water production we can hypothesize that it is the location of the RSW formation during the season of maximum buoyancy loss. Indeed, inside this gyre

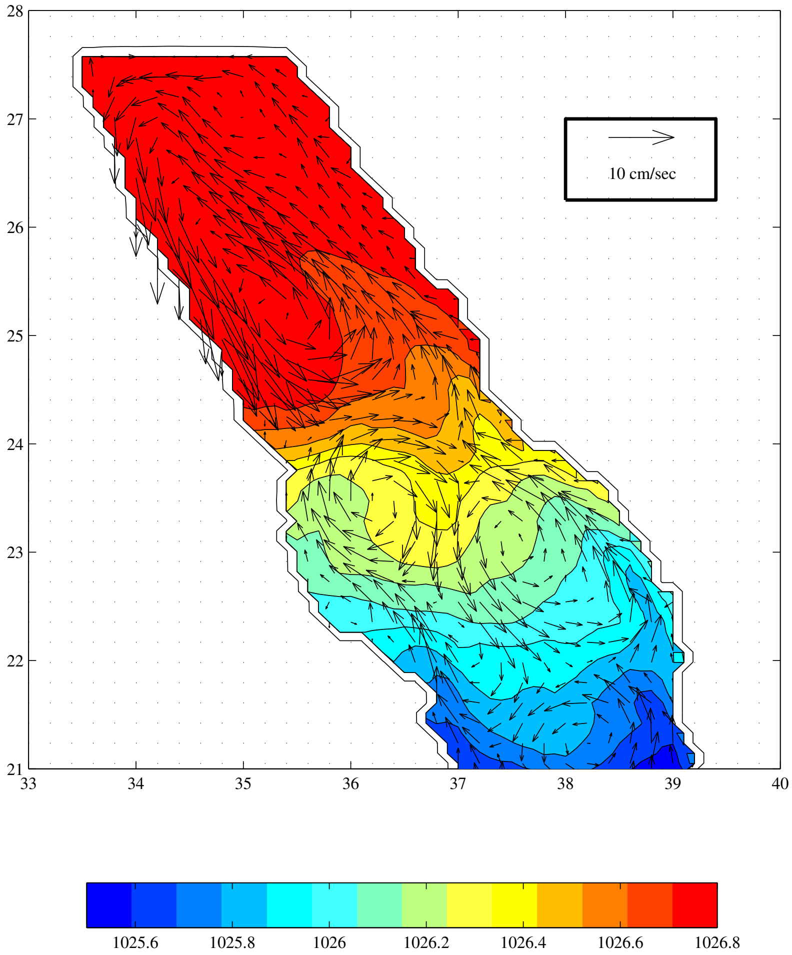

Figure 6.3: Mean surface velocity and density from the MICOM simulation at the northern Red Sea.

the mixed layer achieves high densities throughout the year and at the peak of the winter season the mixed layer has density close to the RSW layer. The "trapping ability" of this gyre is also evident from the density patterns.

In order to get a more quantitative estimation of the amount of RSW produced at the area of the cyclonic gyre, the mean overturning circulation on a σ_θ-latitude plane is plotted in Figure **??**. Since this is an average over all the months and the nine years of simulation it is a smooth representation of the mass fluxes inside the basin. The lowest latitude that the southern edge of the cyclonic gyre reaches during the year is 23.5^{o}N. The total formation

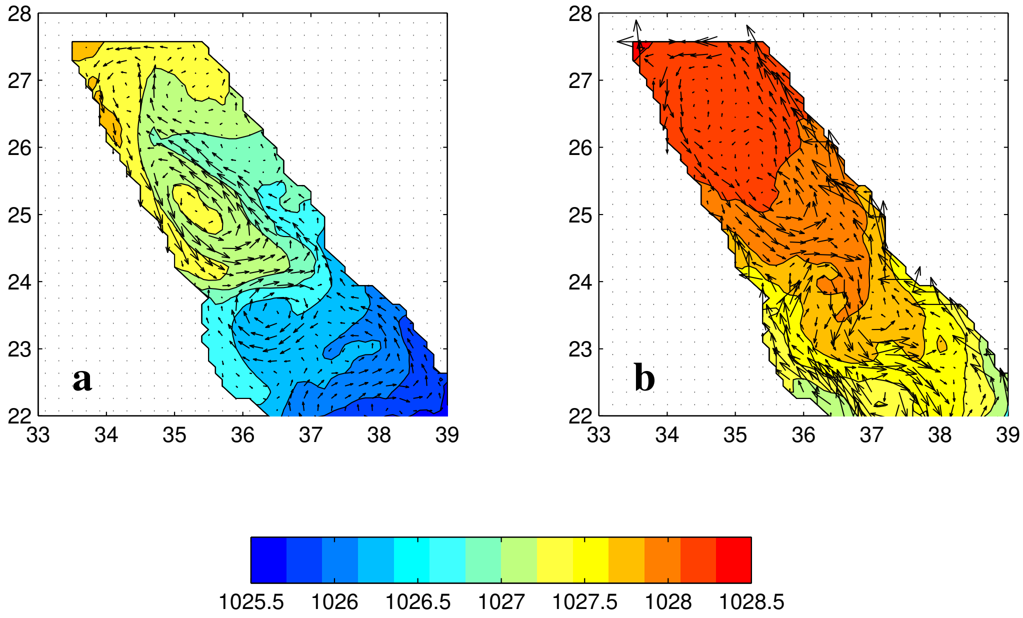

Figure 6.4: Mean surface velocity and density from the MICOM simulation at the northern Red Sea for (a) November and (b) February.

of RSW north of this latitude is about 0.25 Sv or about 65% of the RSW outflow. The remainder is formed north of 20^{o}N latitude.

6.4 Summary and Discussion

The only direct observations of the circulation in the area of the RSW formation shown by the model come from a series of drifter tracks (Clifford et al., 1997) during different seasons and years. All drifter tracks show a cyclonic rotation and, although the number is small (5), they support favorably the results presented here. So, the scenario proposed in this paper is that a large proportion (about 65%) of the hypersaline outflow exiting the strait of Bab el Mandeb is produced in a cyclonic gyre at the northern end of the Red

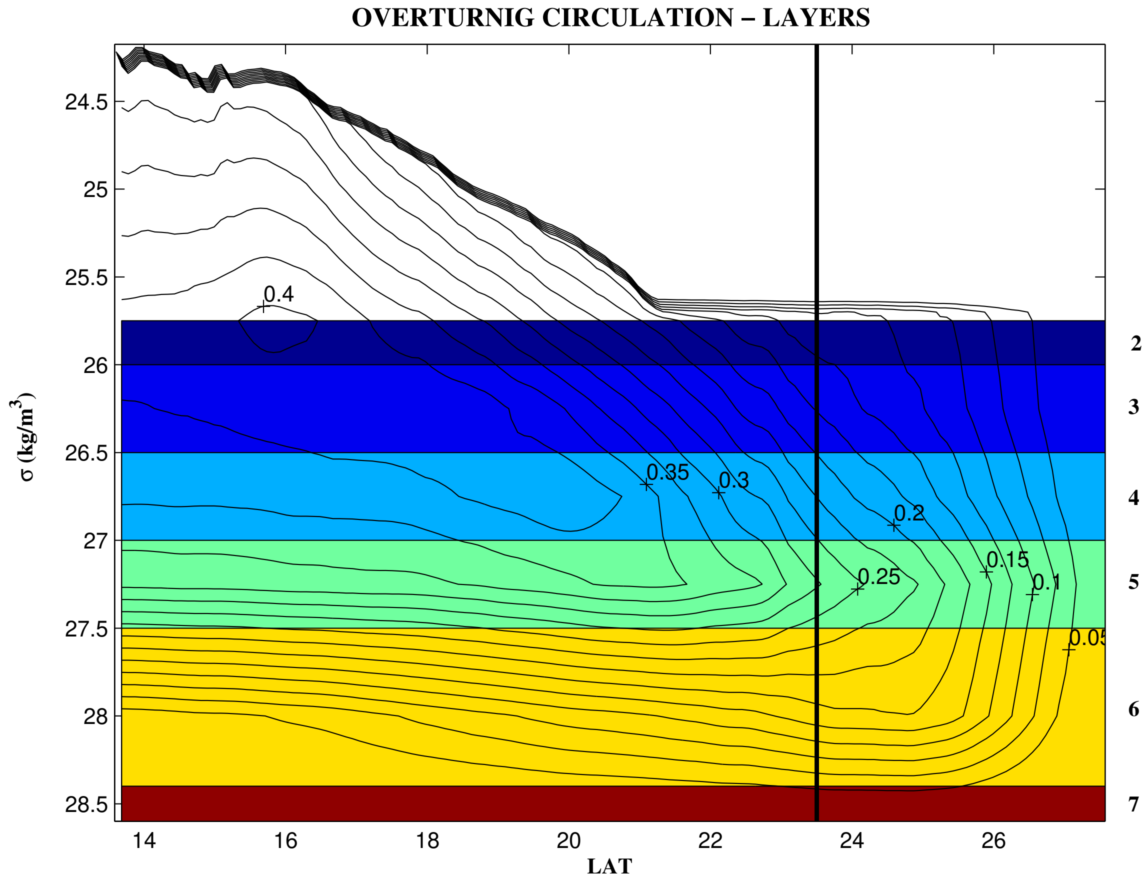

Figure 6.5: Mean overturning circulation from the MICOM simulation. The thick vertical line shows the southernmost annual limit of the northern cyclonic gyre where most of the RSW is formed.

Sea. This is twice the rate of RSW formation proposed by Cember. The remaining 40% is contributed by mixing with the surface and bottom layer.

The best known theoretical framework of the Red Sea circulation is the two-dimensional model by Phillips (1966). A two-layer flow is produced by turbulent convection driven by a constant buoyancy loss. This is sometimes described as a widespread formation of RSW all along the basin. But the vertical transport given by Phillips' similarity solutions have a latitudinal dependence of $x^{-2/3}$ (where x represents the latitude). Assuming a basin of length L the percentage of RSW formation at the 10% northernmost part of the basin (approximately 200 km) is given by

$$\alpha = \frac{\int_0^{\frac{L}{10}} A(z)x^{-2/3}dx}{\int_0^{L} A(z)x^{-2/3}dx} \tag{6.3}$$

where A is independent of latitude. About 46% of the intermediate water formation according to Phillips' solutions takes place in the northern 10% of the basin. Taking into account that this approach involves many simplifications (no rotation, constant width of the basin), and describes the steady state driven by a uniform thermohaline forcing all over the basin, this is a significant part of the total production.

Of course there is the possibility of direct outflow from the layer of RSDW. During summer the simulation presents a wind-driven cyclonic circulation north of the strait that can uplift the bottom layer and produce a pressure gradient to drive deep waters outside the basin. Indeed there is a small direct contribution of RSDW in the outflow during the summer season (June to August). Observations indicate that this contribution cannot be significant since the flow below the depth of the RSW is predominantly northward inside the Red Sea (Cember, 1988; Woelk and Quadfasel, 1997).

It is important to note that the results presented here are from a model which is forced by climatological (monthly mean) conditions of the Red Sea. In most of the explored cases of open ocean deep or intermediate water formation, the associated processes are taking place on shorter times scales, during events of especially strong atmospheric forcing (Leaman and Schott, 1991). The investigation of the effect of the variability of the atmospheric forcing at frequencies higher than the seasonal (synoptic time scales) is very important for our understanding of this kind of processes. Thus, a logical next step is to perform numerical experiments including synoptic atmospheric forcing.

Chapter 7

Atmospherically forced variability of the flow at Bab el Mandeb at synoptic time scales

7.1 Introduction

Straits and their influence on the oceanic flow always attracted the interest of the oceanographic community. This happens because there takes place a concentration of information but also because the local processes can play an important role in the dynamics of vast oceanic volumes. In the case of the semi-enclosed seas this role can be even more overwhelming, since it was shown that in some cases the topographic constriction can control the stratification and circulation of the whole basin (Stern, 1972; Whitehead et al., 1974; Gill, 1977; Garrett and Toulany, 1982; Bryden and Stommel, 1984; Pratt and Lundberg, 1991), and the local mixing can affect the characteristics of the water masses involved in the exchange flow between the semi-enclosed sea and the open ocean. The strait of Bab el Mandeb is located in the southern end of the Red Sea, connecting it with the Gulf of

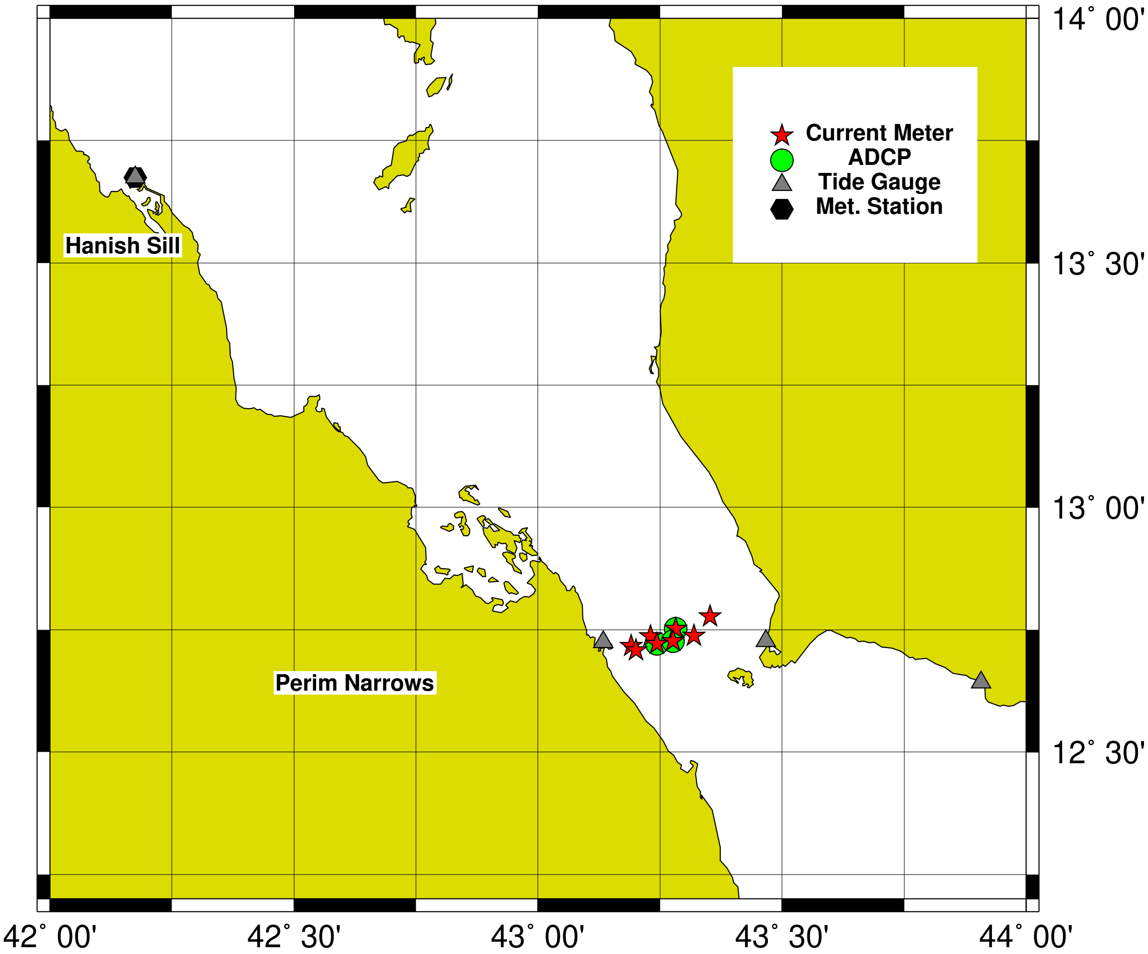

Figure 7.1: The strait of Bab el Mandeb and the location of the instruments, whose data will be used in this approach.

Aden and through this with the Indian Ocean. It is a narrow and shallow channel with the shallowest point located at the Hanish Sill (about 160 m deep) and the narrowest point at the Perim Narrows, where the width is approximately 25 km and the maximum depth about 220 m (Figure ??).

The Red Sea experiences strong forcing of both the wind and thermohaline kind. Due to the extensive evaporation (about $2\,m/year$) and negligible precipitation and river runoff, the basic form of exchange at the Bab el Mandeb is of the inverse estuarine type, with a fresh inflow to the sea on the top of an outflow of high salinity water ($39.7\,psu$ at the strait), the so called Red Sea Water (RSW). During summer (June to September), influenced by the wind and possibly by the annual cycle of the thermohaline forcing (Patzert, 1974a; Chapter 3; Chapter 4), the exchange takes place in a three layer pattern, with a shallow surface outflow, an intermediate inflow of the relatively fresh and cold Gulf of Aden Water (GAW) and a much weaker RSW outflow. Although this two-season pattern was known for a long time (Vercelli, 1931; Siedler, 1968; Maillard and Soliman, 1984), recent long term observations (Murray and Johns, 1997) of the currents and stratification in the strait revealed the complete annual cycle and strength of the exchange flow.

Beyond the seasonal variability the exchange experiences strong fluctuation at shorter time scales, tidal (tidal periods) and synoptic (from a few days to a few months). Although the effect of the tides can be important and complicated, since the strait connects two different regimes, the focus in this paper is on the variability at synoptic time scales. Lacombe and Richez (1982), investigating the variability of the flow and stratification in the strait of Gibraltar, proposed that the two mechanisms affecting the flow at these time scales are the local wind and the atmospheric pressure over the Mediterranean Sea which can change the sea level in the basin through the "inverted barometer" effect. Crepon (1965) found a considerable correlation between the atmospheric pressure in the western Mediterranean and the flow through Gibraltar, but unexpectedly they were out of phase in contradiction to mass conservation. Garrett (1983) and Garrett and Majaess (1984) trying to explain this paradox used a two-basin (eastern and western Mediterranean) model with geostrophic control (Garrett and Toulany, 1982) at the two straits (Gibraltar and Sicily) and forced by eastward propagating atmospheric pressure systems. They found that the phase difference between the flow through Gibraltar and the sea level in western Mediterranean (or negative atmospheric pressure) becomes small, but this is accompanied by a non-inverse barometer response of the sea level in the eastern Mediterranean.

Candela et al. (1989) used the same two-basin configuration but without the rotational effect and the forcing consists of the mean atmospheric pressure over the Mediterranean, which they found represents the most energetic mode of the atmospheric pressure fluctuations over the basin. Assuming a linear friction, of the form $\lambda \times u$, the model results agree quite good with the observations, explaining about 58% of the total variance at synoptic time scales. Two characteristic resonance frequencies, Helmholtz frequencies, are emerging from the model, depending on the size of the basins and the geometrical characteristics of the straits.

The effect of the local wind in these cases was ignored, although its importance is accepted widely, since the magnitude of the wind speed inside the straits is considerable due to orographic constraints. This effect in association with geostrophic control was investigated for the Bass Strait (Middleton and Viera, 1991; Hannah, 1992) and was found be important. The case of the Bass Strait is different from those described before, since it connects two open bodies of water, so that no conservation of mass constraint is imposed, and because of its small depth the flow is treated as barotropic.

In this paper we apply the model proposed by Candela et al. to the synoptic variability observed at the strait of Bab el Bandeb, extending it to include the local wind-stress action and allowing for a two-layer response of the strait. In the next Section the flow observation at the strait will be presented as well as the local wind field and the atmospheric pressure variability over the Red Sea. The model will be described in Section 3 and the comparison of its results with the observations will be presented in Section 4. Finally, Sections 5 and 6 include a discussion of the limitations of the model and the effects of remote forcing and stratification.

7.2 Data

The observations that will be used here include 18-month long velocity and stratification measurements from moorings at the two critical points of the strait (Hanish Sill and Perim Narrows), pressure gauges at several location around the strait and a meteorological station located at the region of the sill. The locations of the instruments can be seen in Figure **??** and are described in Murray and Johns (1997). Because the most complete coverage of the velocity field was achieved at a section in the narrows, the transport estimates that will be used here are derived from this mooring array (Chapter 2)'. To compensate for the fresh water loss to the atmosphere a net volume flux into the basin of about $0.03Sv$ is expected on the annual mean. Around this value a weak seasonal cycle is established related to fluctuation of the sea level inside the Red Sea. But this variability is at least one order of magnitude weaker than the high frequency one which can achieve amplitudes of more than one Sverdrup ($1\ Sv = 10^6\ m^3/sec$). If we use the mean RSW outflow as a measure of the strength of the exchange, which is about $0.36Sv$, the high frequency fluctuations can reach magnitudes of two to three times this value and alter significantly the exchange patterns. The time series of the net transport (mean, seasonal cycle and high frequency variability)

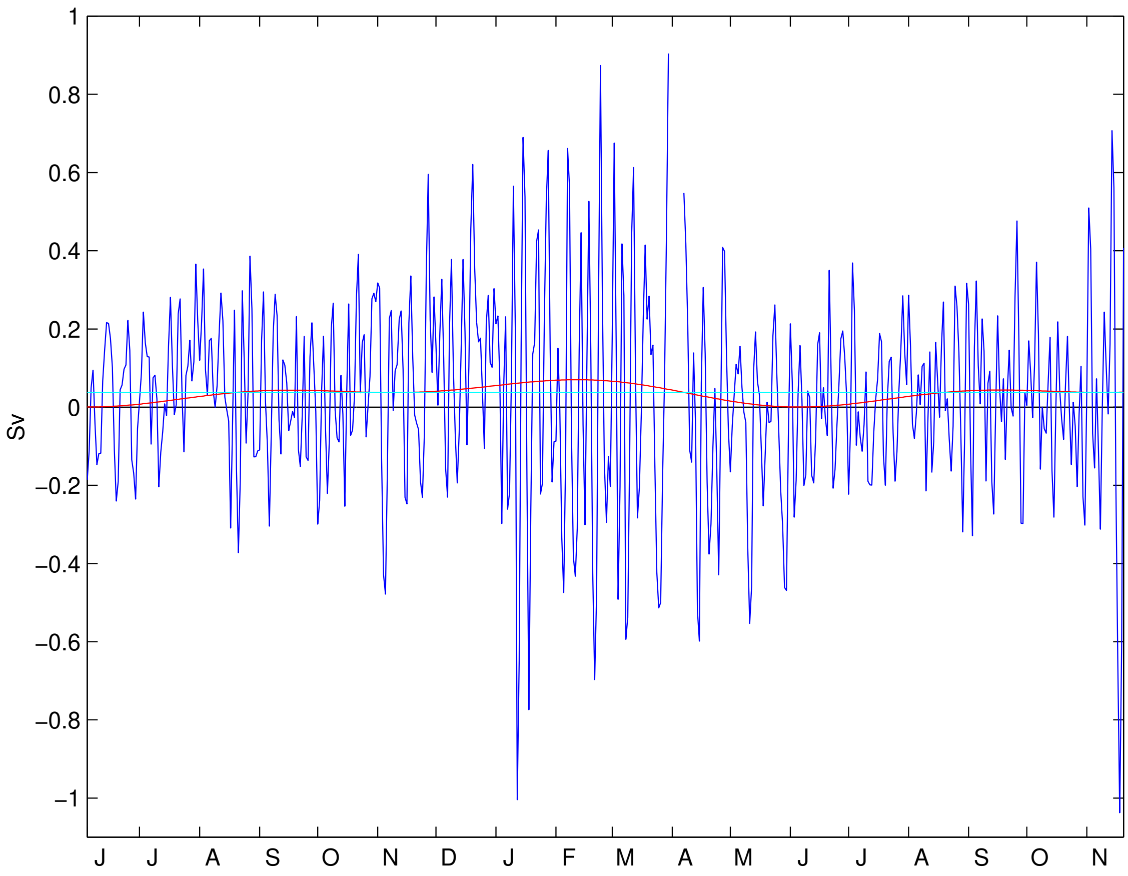

Figure 7.2: The net transport at the strait of Bab el Mandeb, mean (cyan), seasonal cycle (red) and synoptic variability (blue).

is plotted in Figure **??**, where positive values represent fluxes into the basin.

The transport profile at Perim (per unit depth in $m^2\ s^{-1}$) from June 1995 through November 1996 is presented in Figure **??**. Fluctuation with tidal periods are eliminated using a 40-hour Butterworth low-pass filter. In order to establish an idea of the modes of variability, a principal component analysis of the covariance matrix was used employing empirical orthogonal functions (EOFs). The first two EOFs explain 96.8% of the variance

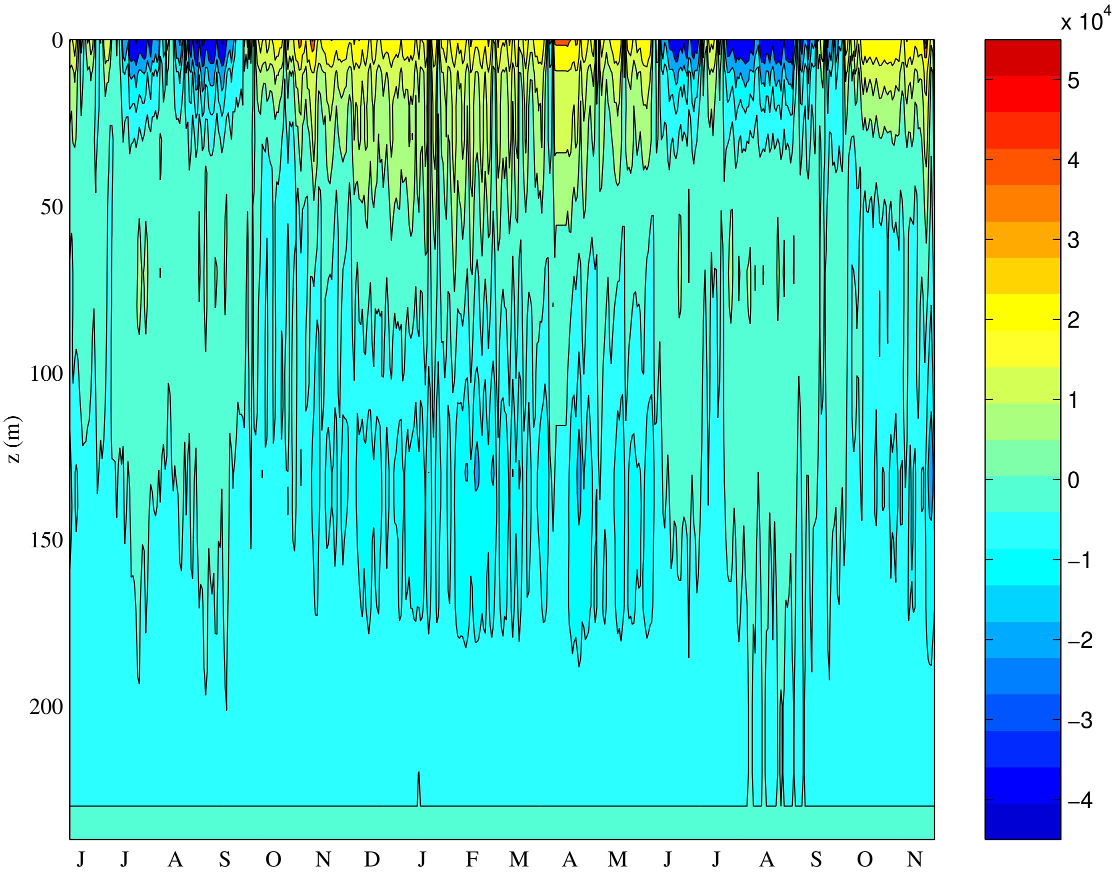

Figure 7.3: The transport per unit depth profile at Perim Narrows.

and their weights are plotted in Figure **??**. The transport profile time series was band-passed with a Butterworth band-pass filter, 2 to 60 days, to include variability only in the synoptic time scale. The EOFs of the band-passed time series were computed and the two most important are also plotted in Figure **??** (the thin line). The most important EOF (explaining more than 80% of the variance) presents a pattern of variability of the first baroclinic mode type with a zero crossing at about 70 m, so that fluctuations of a two-layer type are expected account for much of the variability observed at the strait. The second EOF explains 13.9% of the variance and is of a barotropic type with maximum weight at a depth of 130 m. But the response of the strait seems to be highly frequency

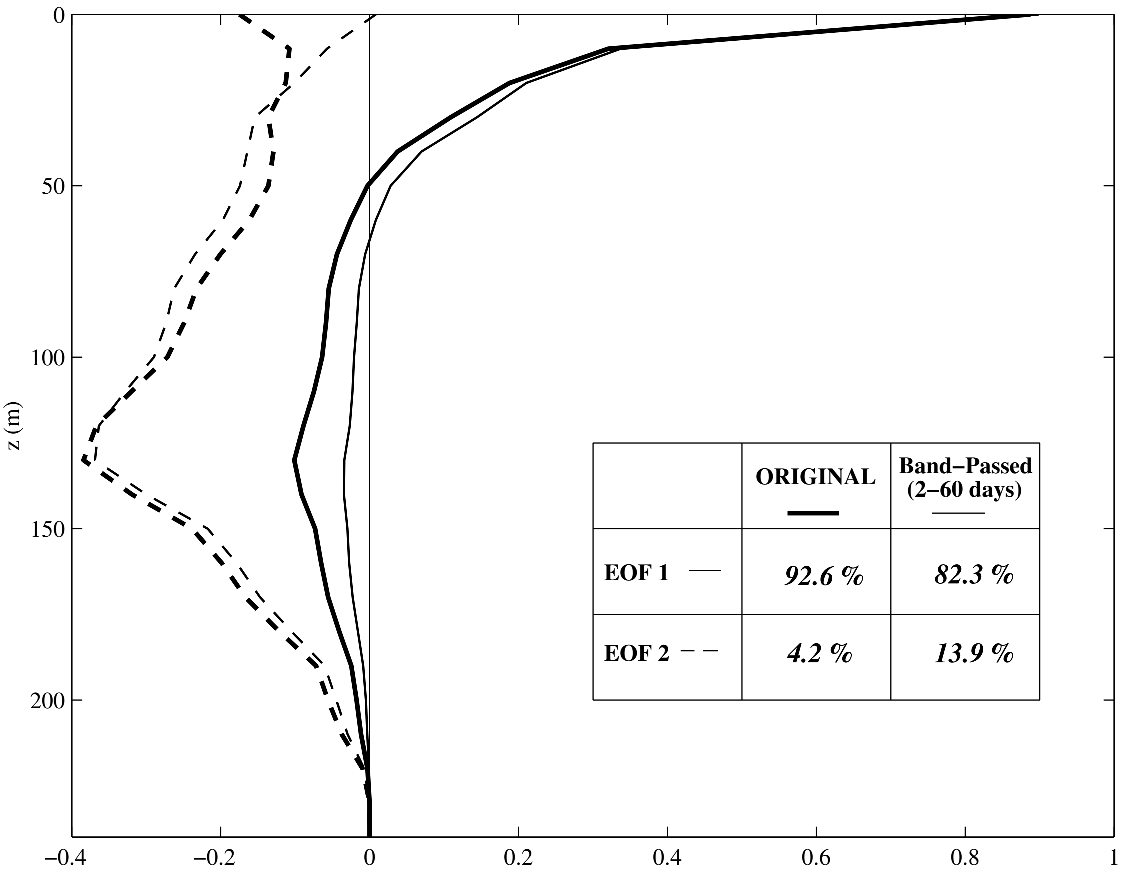

Figure 7.4: The first two EOFs of the transport at Perim, original time series (thick line), and band-passed (2-60 days) time series (thin line).

dependent. Figure ?? presents a part of the transport time series separated in two layers with the interface at 70 m and the wind speed from the meteorological station at the same period. Two pieces of this series are enlarged in Figure ??c and d. During wind events of large period the transport in the two layer is out of phase, while during higher frequency events the two layers respond in phase. The dependence of the flow on the frequency of the atmospheric forcing will be investigated in the next Section.

Atmospheric pressure data for the period when the observations at Bab el Mandeb took place, come from six coastal meteorological stations spread around the Red Sea basin (Figure ??) and obtained from the National Climatic Data Center (NCDC). The patterns

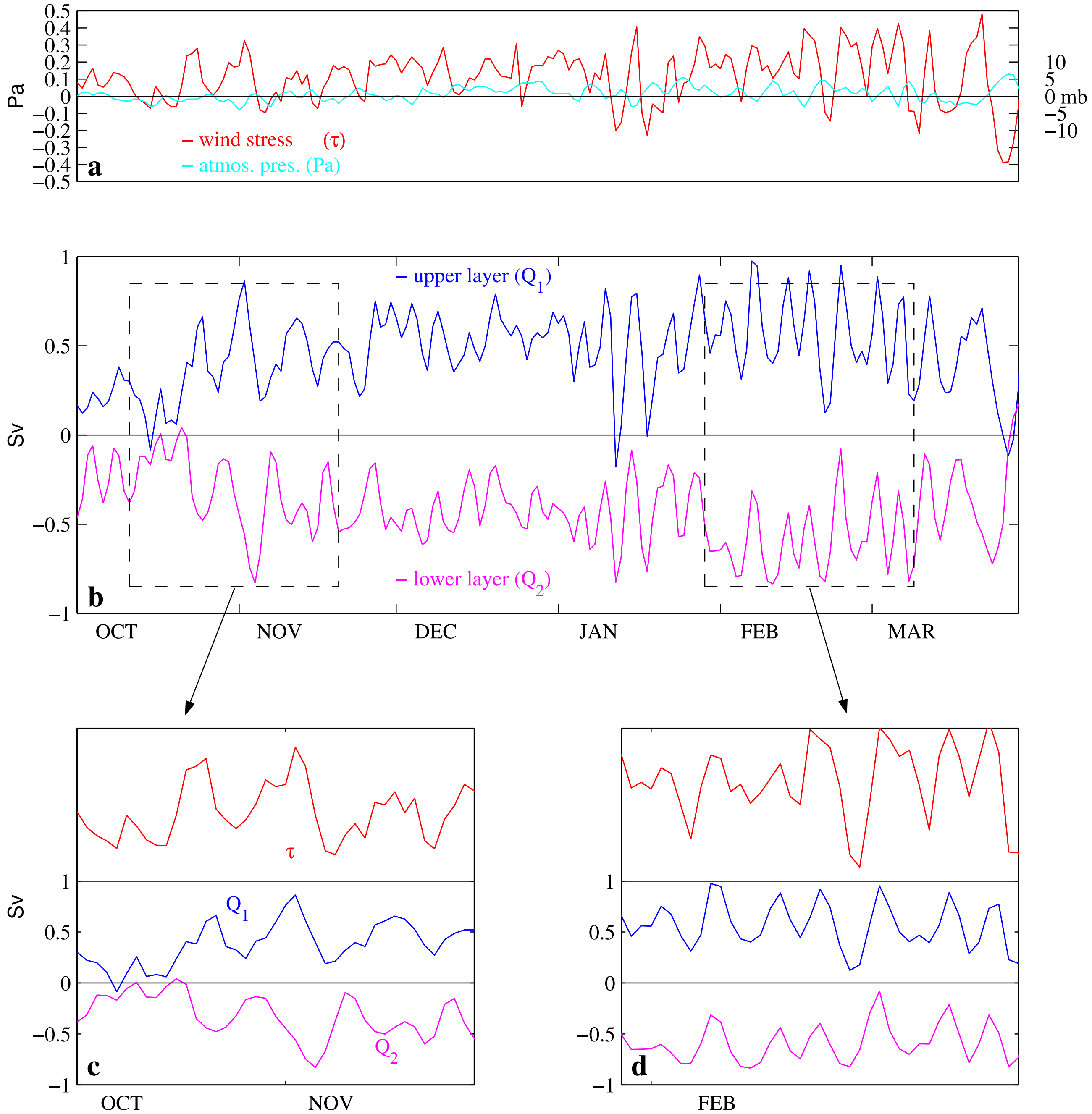

Figure 7.5: Wind-stress (a) and the two-layer response (b). In (c) and (d) events of different frequency are enlarged.

of atmospheric pressure fluctuations were examined using the same principal component analysis method. The first EOF mode represents the covarying pattern (the atmospheric pressure from all stations is in phase) and explains 83.4% of the variance. The second most significant EOF (explaining 10.4% of the variance) has a zero node at 26^oN close to the northern end of the basin. The spatial weights of the two EOFs are plotted in Figure **??**. Since the dominant fluctuations of the atmospheric pressure are of the covarying type, the mean atmospheric pressure over the Red Sea was computed, using the station measurements weighted by the area of the basin which each one represents. This time series is plotted in Figure **??** and will be used as one of the forcing functions investigated in the following sections.

The other important mechanism for forcing the synoptic time scale variability of the flow in Bab el Mandeb, mentioned in the Introduction, is the local wind field. Due to the presence of mountains on the two sides of the strait the low level winds are orographically steered along the axis of the strait and the across axis component of the wind is typically one order of magnitude weaker. The local wind is obtained from an anemometer station installed on a isolated islet at the west side of the Hanish Sill during the period of the oceanographic observations. The component parallel to the main axis of the strait is plotted in Figure **??**. A strong annual cycle is present with SSE winds during winter and NNW wind during summer. The winter wind field is stronger than the summer one with typical values of $8\,m/sec$ and $4\,m/sec$, respectively. Around this seasonal pattern strong variability is present with typical time scales from a few days two a few weeks. The amplitude of this variability is about 5 to $10\,m/sec$ but can reach the $20\,m/sec$. The strongest fluctuations on synoptic time scales take place during winter with the exception of a few very strong

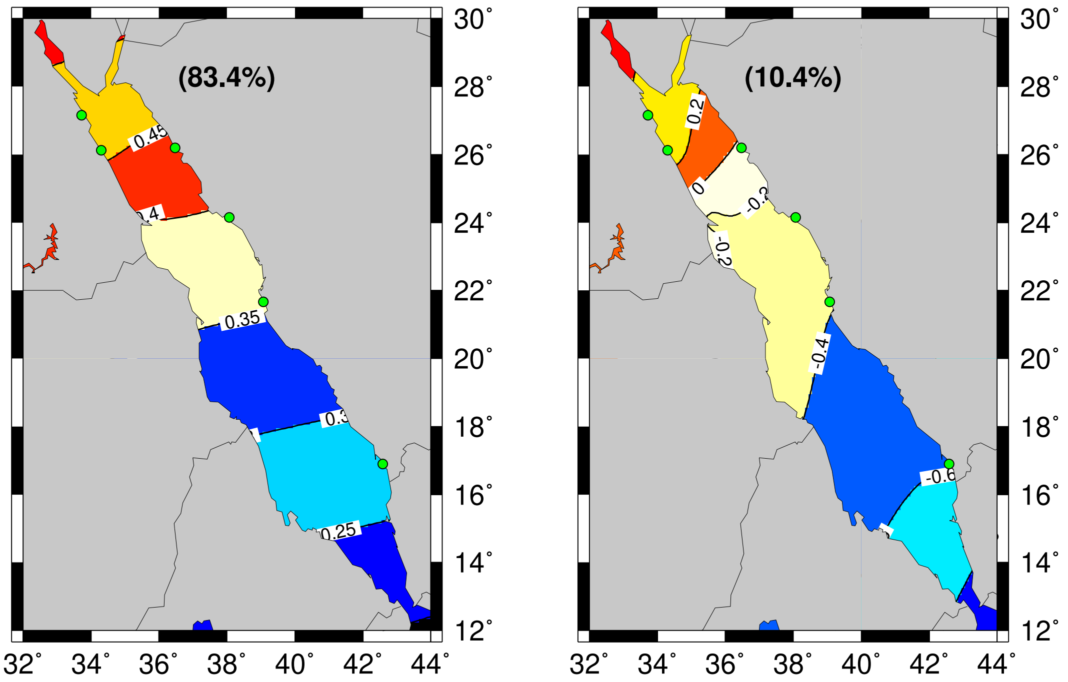

Figure 7.6: Meteorological stations whose atm. pressure data are used here and the spatial weights of the two first EOFs.

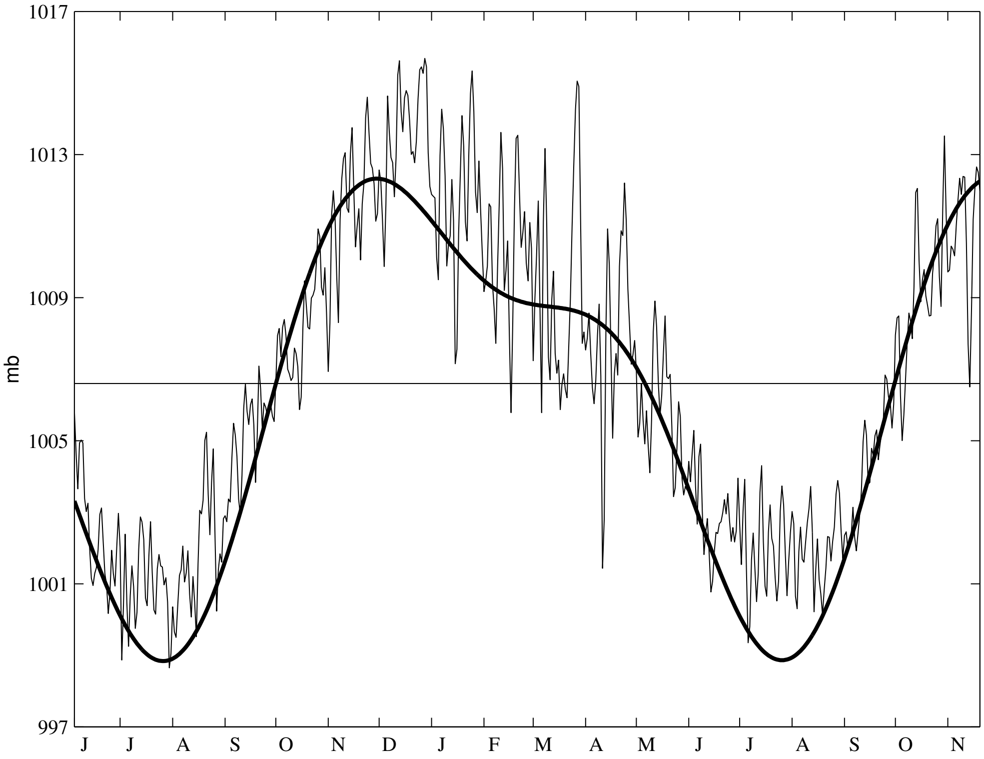

Figure 7.7: Time series of the mean atm. pressure over the Red Sea.

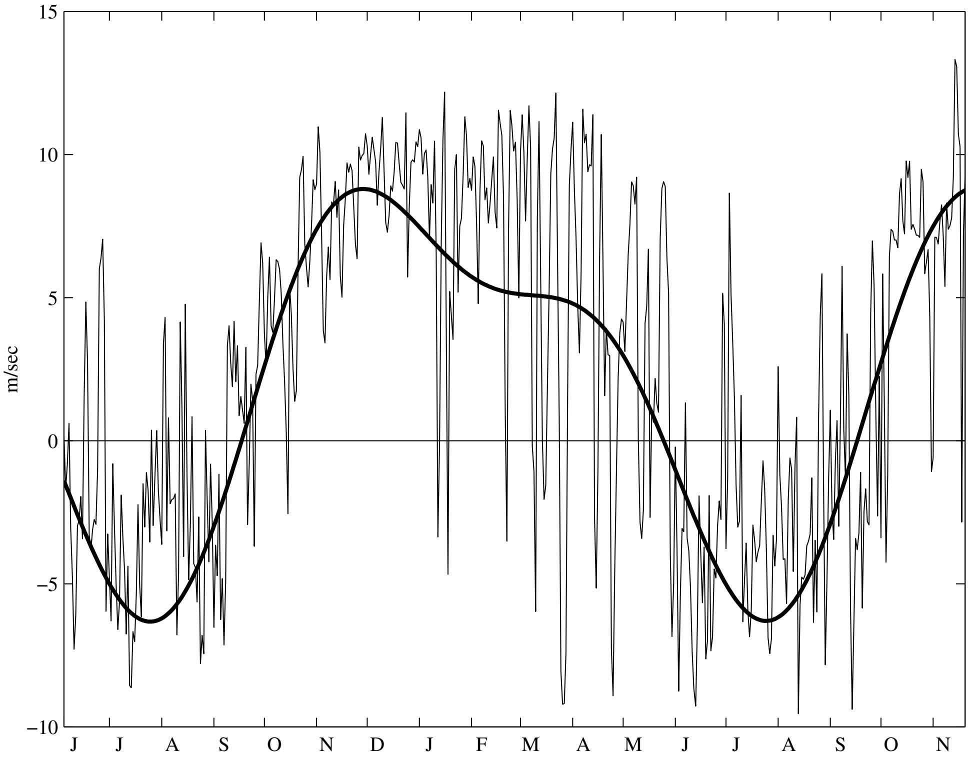

Figure 7.8: Time series of the wind field along the axis of the strait.

summer events when reversal of the wind field takes place.

7.3 Model

In order to explain some of the variability observed at the strait, a simple, linear model of the response of the strait to the local wind and changes of the atmospheric pressure over the Red Sea is developed here. The basic variables and constants used are shown in the schematic of Figure **??** and their values are presented in Table **??**. Several assumptions and simplifications are used in the basic equations describing the model. The present approach

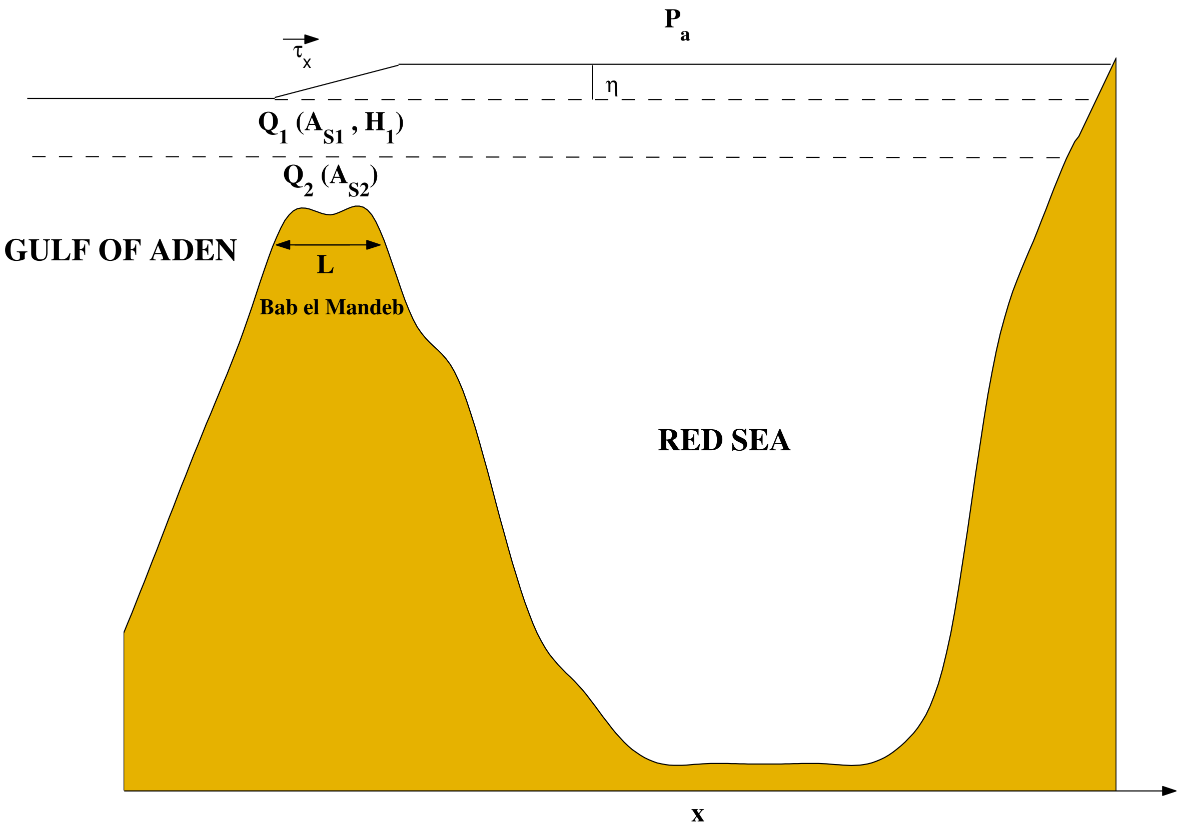

Figure 7.9: Schech of configuration used in the model.

is two-dimensional, so that the rotational effect is neglected and no geostrophic control is

CONSTANT	DESCRIPTION	VALUE
A_{RS}	surface area of the Red Sea	$4.5 \times 10^{11}\, m^2$
A_S	cross-sectional area of Bab el Mandeb	$2.4 \times 10^6\, m^2$
A_{S_1}	cross-sectional area of the upper layer	$1.2 \times 10^6\, m^2$
A_{S_2}	cross-sectional area of the lower layer	$1.2 \times 10^6\, m^2$
L_S	length of the strait	$270\, km$
H_1	depth of upper layer	$70\, m$
ρ	mean density of seawater	$1027\, kg\, m^{-3}$

Table 7.1: Numerical values and description of the constants used in the model.

implied. This is not an unreasonable approximation, since the external Rossby Radius of Deformation (RRD) is $O(1300\, km)$ and the internal RRD is $O(35\, km)$ which close to the average width of the strait.

The sea level inside the basin is taken to be uniform. Long gravity waves are much faster than the atmospheric fluctuations and can smooth the sea level at synoptic time scales. Outside the basin the sea surface is assumed to respond isostatically to the atmospheric pressure forcing, so that a constant sea level is present at the entrance of the strait (here taken as zero for simplicity). Changes of the sea level outside the strait induced by the wind field at the Gulf of Aden can play a role [Garrett (1983) suggests that this effect is less important than atmospheric pressure in inducing flows through the strait] especially since they are correlated with the wind field inside the strait and possibly with changes in the atmospheric pressure over the basin. Here this effect will be neglected and we will revisit this problem in a later section.

An important difference of this model with previous approaches is not only the introduction of the local winds but also the assumption that the effect of the wind is "felt" only in an upper layer of thickness H_1, which be taken as $70\, m$, the depth of the zero crossing of the most energetic EOF. This layer does not necessarily coincide with surface layer of the inverse estuarine exchange. In order to simplify the solution forms, density differences will be not taken into account and a average density (ρ_0) will be used in the equations. A more complete baroclinic response of the strait employing two layers with distinct density and an interface that can oscillate with the forcing are examined in Section 5.

Under these assumptions the governing equations are

$$\frac{\partial Q_1}{\partial t} = -\frac{A_{S_1}}{\rho_0}\frac{\partial P}{\partial x} + \frac{A_{S_1}\tau_x}{H_1\rho_0} - \lambda_1 Q_1 \tag{7.1}$$

$$\frac{\partial Q_2}{\partial t} = -\frac{A_{S_2}}{\rho_0}\frac{\partial P}{\partial x} - \lambda_2 Q_2 \tag{7.2}$$

$$\frac{\partial \eta}{\partial t} = \frac{Q_1 + Q_2}{A_{RS}} \tag{7.3}$$

$$P = P_a + g\,\rho_0\,\eta \tag{7.4}$$

where A_{S_1} and A_{S_2} are the cross-sectional areas of the two layers and they sum to the cross-sectional area of the strait ($A_{S_1} + A_{S_2} = A_S$) taken as the average value somewhere in the middle of the channel. Q_1 and Q_2 represent the transport at the surface and lower layer, respectively. A_{RS} is the surface area of the Red Sea and η the sea level in the basin. The friction is represented by the linear forms $\lambda_1 Q_1$ and $\lambda_2 Q_2$, following Candela et al. (1989) and Middleton and Viera (1991), although the values they use differ by almost an order of magnitude. In general $\lambda_1 \neq \lambda_2$ and friction at the lower layer is expected to be larger than that of the surface one. In the set of solutions presented here and the comparison of the results with the observations a unique value ($\lambda_1 = \lambda_2 = \lambda$) is used in order to reduce the number of parameters involved in the discussion.

P_a and τ_x are the forcing functions of the atmospheric pressure fluctuations and the wind-stress parallel to axis of the strait, respectively. Taking both to behave as $e^{i\omega t}$ and seeking solutions of Q_1, Q_2 and η of the same form we get

$$Q_1 = \frac{A_{S_1}}{\rho_0 H_1}\left\{\frac{\lambda(\Pi_1^2+\Pi_2^2)-\omega_{01}^2(\lambda\Pi_1-\omega\Pi_2)+i[\omega_{01}^2\lambda\Pi_2+\omega_{01}^2\omega\Pi_1-\omega(\Pi_1^2+\Pi_2^2)]}{(\Pi_1^2+\Pi_2^2)(\lambda^2+\omega^2)}\right\}\tau_x - \frac{A_{S_1}\omega}{\rho_0 L_S}\left\{\frac{\Pi_2+i\,\Pi_1}{\Pi_1^2+\Pi_2^2}\right\}P_a \tag{7.5}$$

$$Q_2 = \frac{A_{S_2}\omega_{01}^2}{\rho_0 H_1}\left\{\frac{\omega\Pi_2-\lambda\Pi_1+i(\lambda\Pi_2+\omega\Pi_1)}{(\Pi_1^2+\Pi_2^2)(\lambda^2+\omega^2)}\right\}\tau_x + \frac{A_{S_2}\omega}{\rho_0 L_S}\left\{\frac{\Pi_2+i\,\Pi_1)}{\Pi_1^2+\Pi_2^2}\right\}P_a \tag{7.6}$$

$$\eta = \left\{\frac{A_{S_1}(\Pi_1-i\,\Pi_2)}{\rho_0 H_1 A_{RS}(\Pi_1^2+\Pi_2^2)}\right\}\tau_x - \left\{\frac{\omega_0^2(\Pi_1-i\,\Pi_2)}{\rho_0 g(\Pi_1^2+\Pi_2^2)}\right\}P_a \tag{7.7}$$

where

$$\Pi_1 = \omega_0^2 - \omega^2 \qquad \Pi_2 = \lambda\omega \tag{7.8}$$

and

$$\omega_0 = \sqrt{\frac{gA_S}{A_{RS}L_S}} \quad \omega_{01} = \sqrt{\frac{gA_{S_1}}{A_{RS}L_S}} \quad \omega_{02} = \sqrt{\frac{gA_{S_2}}{A_{RS}L_S}} \tag{7.9}$$

In the absence of friction the basin and the strait resonate at the ω_0, which is the Helmholtz resonance frequency for the geometrical characteristics of the Red Sea and Bab el Mandeb system. The most uncertain parameter included in ω_0 is the length of the strait (L_S) which is not necessarily the distance between the sill and the narrows, but extends north and south of this point to include the whole shallow channel. Taking into consideration the transport and sea level behavior from the available observations, the optimum value for L_S is around 270 km (or extending 100 km beyond the two critical points). Using the values of Table **??** ω_0 is estimated at about 5 days. Friction can limit the strength of the flow through the strait but can also influence the frequency of maximum response. Since the solutions are a linear addition of the effect of the wind and the atmospheric forcing, we can examine the influence of each forcing mechanism separately. The solutions for the upper layer transport (Q_1), the lower layer transport (Q_2), net transport (Q_n) and the sea level (η)inside the basin are plotted in the frequency domain (gain and phase) and presented in Figures **??**, **??**, **??** and **??**, respectively, for different λs (the different axes in the phase plots were chosen so that there are not "jumps" in the solution representations). At the inviscid limit all of the responses present an abrupt change in phase at the Helmholtz frequency.

At low frequencies the P_a leads transport by 90^o and is out of phase with the sea level anomaly in the basin as is expected for a response of the inverse barometer kind. At frequencies greater than the resonance one, the response is changed and the atmospheric pressure forcing lags the transport by 90^o and it is in phase with η. The response of the sea level and transport to the local wind-stress is far more complicated as expected by the

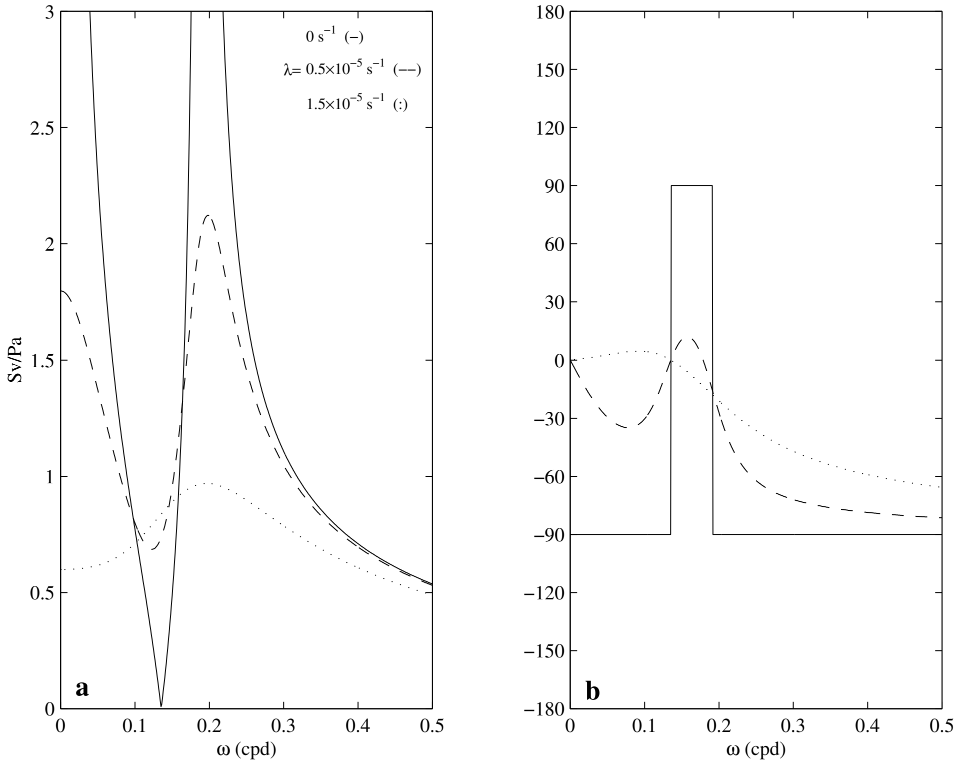

Figure 7.10: The solution for the surface layer transport forced by the local winds in the frequency domain: (a) gain and (b) phase, for the inviscid case and two different frictional parameters.

two-layer response since the upper layer "feels" both the wind-stress and the changes of the sea level inside the basin, but the lower layer "feels" only the gradient in η. At low frequencies , τ_x and η are in phase tending to force the two layers in opposite directions. At frequencies higher than the Helmholtz resonance frequency they are out of phase and work together to force a barotropic type of response. The most complicated phase pattern is the one relating the wind-stress and the upper layer transport. There are two frequencies of changing phase, associated with change of sign in the solutions, ω_0 and ω_{02}, related to the ability of the lower layer to drain water from the basin. Between these two frequencies η dominates and opposes τ_x diminishing the flow of the upper layer. The introduction of friction smooths all these phase patterns.

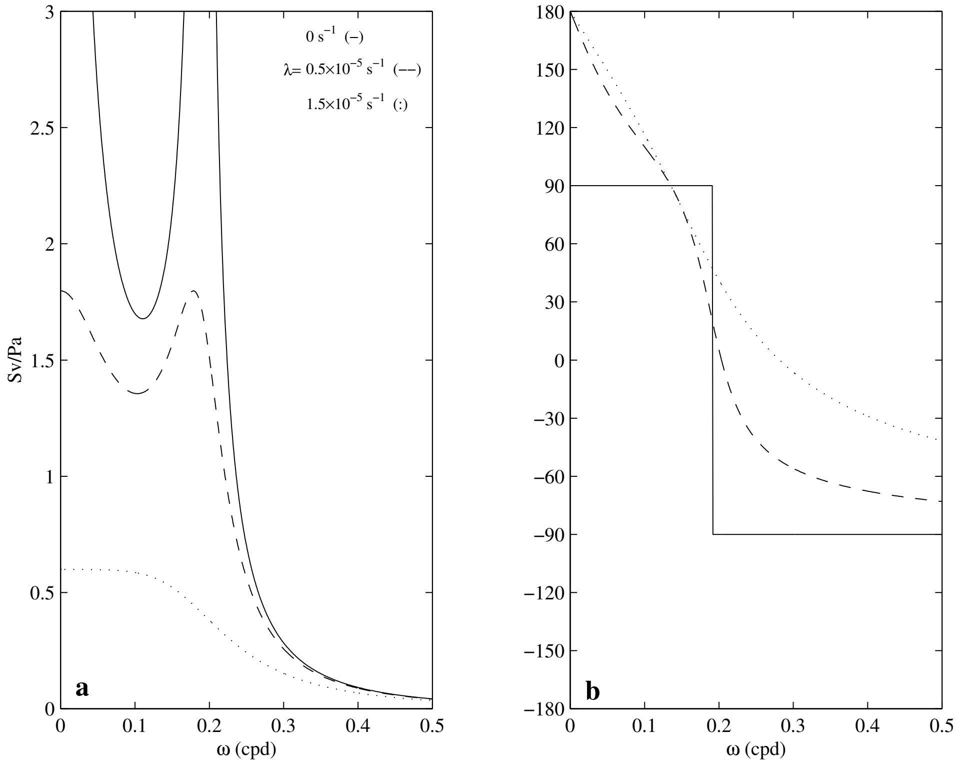

Figure 7.11: The solution for the lower layer transport forced by the local winds in the frequency domain: (a) gain and (b) phase, for the inviscid case and two different frictional parameters.

All the gain functions present a peak at the Helmholtz resonance frequency (ω_0). The upper and lower layer transport have a second peak at $\omega = 0$ but since they are out of phase they do not contribute to a net transport ($Q_n = Q_1 + Q_2$). The effect of friction is to decrease the response of the system but it can also change the value of the resonance frequency (or the frequency of maximum response). At the limit where the resonance frequency becomes equal to ω_{02} there is no shift in the phase relation of the surface layer with the wind-stress and a single resonance peak is present in both transports.

7.4 Comparison with the observations

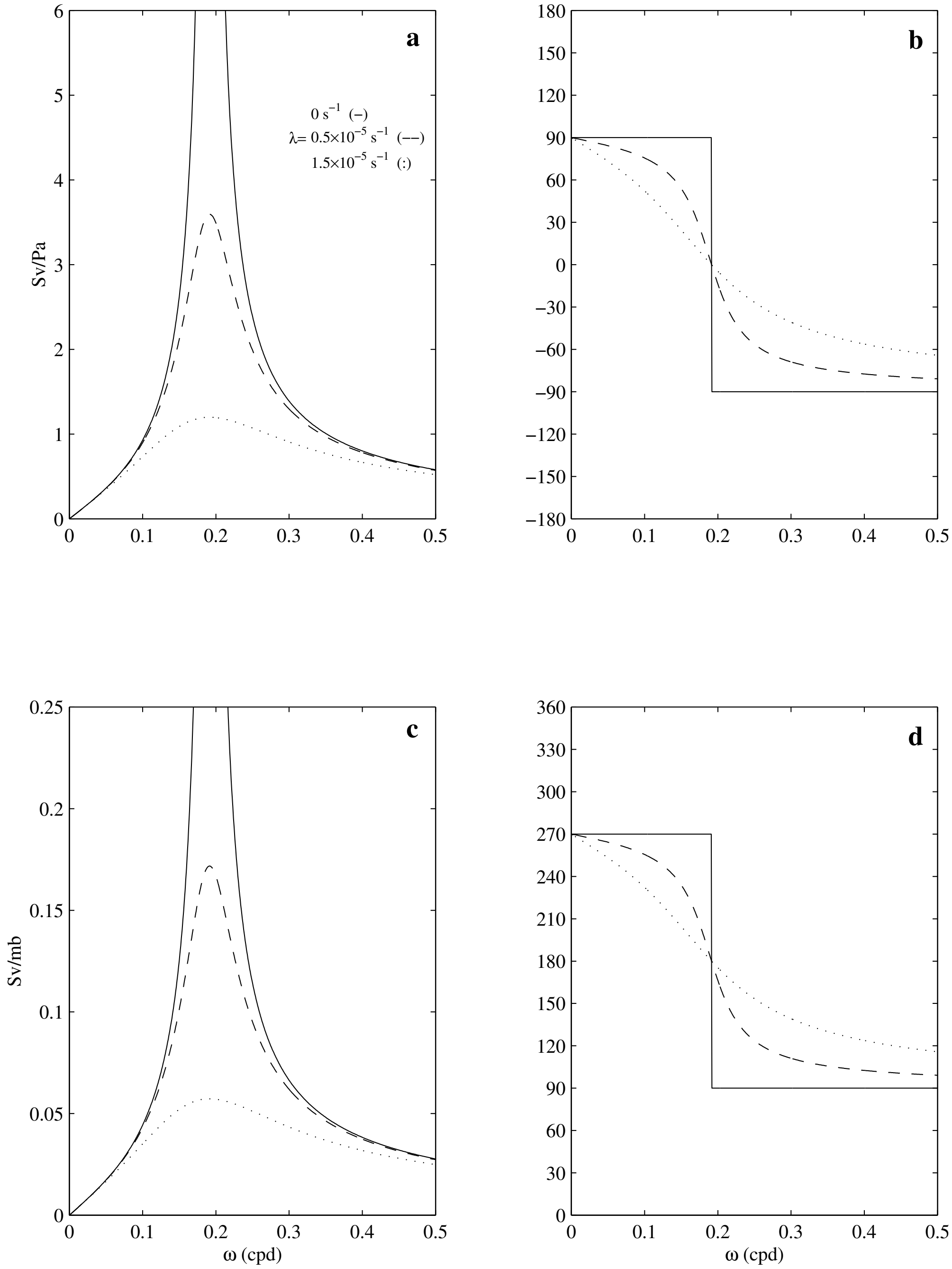

Figure 7.12: The solution for the net transport forced by the local winds ((a) and (b)) and the atmospheric pressure over the Red Sea ((c) and (d)), for the inviscid case and two different frictional parameters.

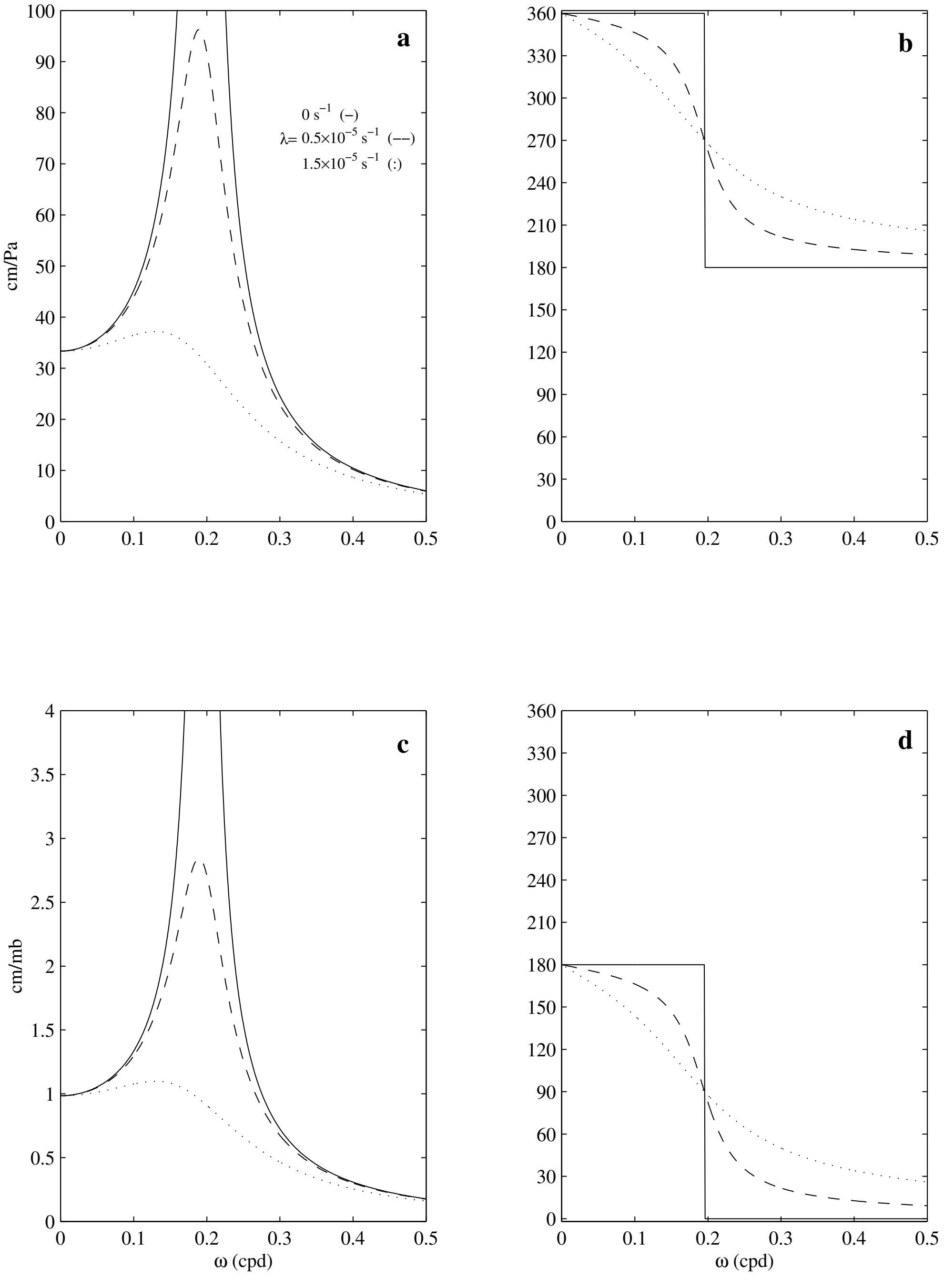

Figure 7.13: The solution for the sea level forced by the local winds ((a) and (b)) and the atmospheric pressure over the Red Sea ((c) and (d)), for the inviscid case and two different frictional parameters.

The solutions presented above in the frequency domain can be compared with the corresponding gain and phase relations of the observations. The two-layer transport relation to the wind stress is plotted in Figure **??** and compared with the solutions for three frictional parameters ($\lambda = 0.25 \times 10^{-5}$, $\lambda = 0.5 \times 10^{-5} sec^{-1}$ $\lambda = 1.25 \times 10^{-5} sec^{-1}$) which seem to be the most appropriate values according to the observations. Following Candela et al. (1989), a reasonable value for λ can be obtain by $\lambda = C_D U/H$, where C_D is the drag coefficient, U is the characteristic flow velocity and H is the the hydraulic depth (cross sectional area over width). With $C_D = 2.5 \times 10^{-3}$, $U = 0.5 m\, sec^{-1}$ and $H = 120 m$ we get $\lambda = 1.0 \times 10^{-5} sec^{-1}$.

The wind stress and the atmospheric pressure over the Red Sea are loosely correlated (the correlation coefficient is -0.18) and the available data can be examined separately. In Figure **??** the solutions for the net transport response to the wind-stress and the atmospheric presure forcing fields is compared with the observations. The most obvious result is that the wind-driven solution fits much better to the observations. Furthermore, the effect of the wind is more important. Taking into account the magnitude of the fluctuations and the gain response of the transport at intermediate frequencies the wind-induced response is three to four times larger than that of the atmospheric pressure. At very high and low frequencies observations and solutions do not match very well, but this expected since other effects come to play (like the low frequency variability of the thermohaline circulation) and some of the assumptions are questionable (like the uniform sea level response inside the basin).

Finally, the comparison between observations and model solutions for the sea level response is plotted in Figure **??**. For the sea surface elevation in the Red Sea the data from the pressure gauge located at the west side of the Hanish Sill were used. The data from all

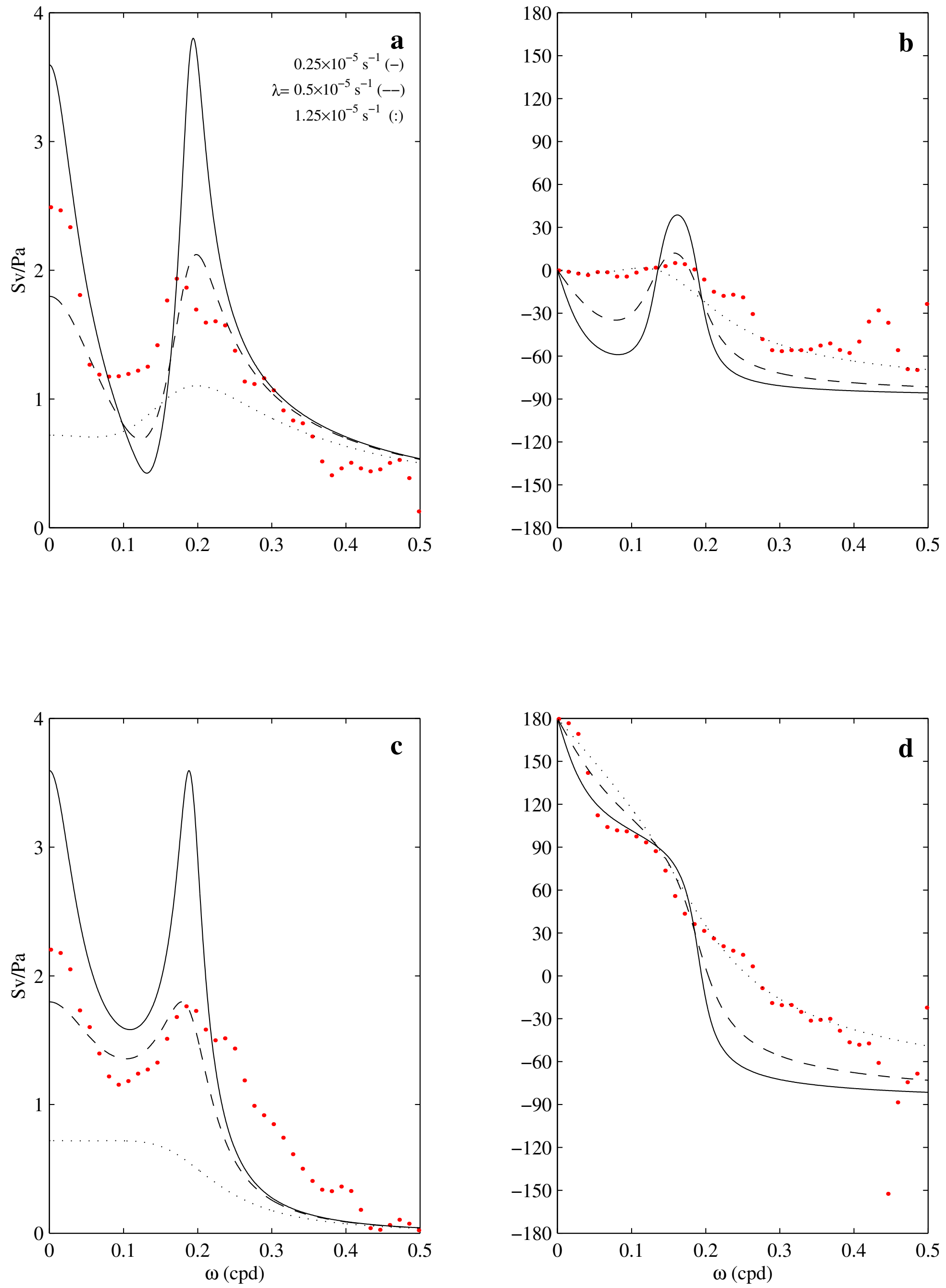

Figure 7.14: Comparison between observation and model (three frictional parameters) results for the transport in the two layers.

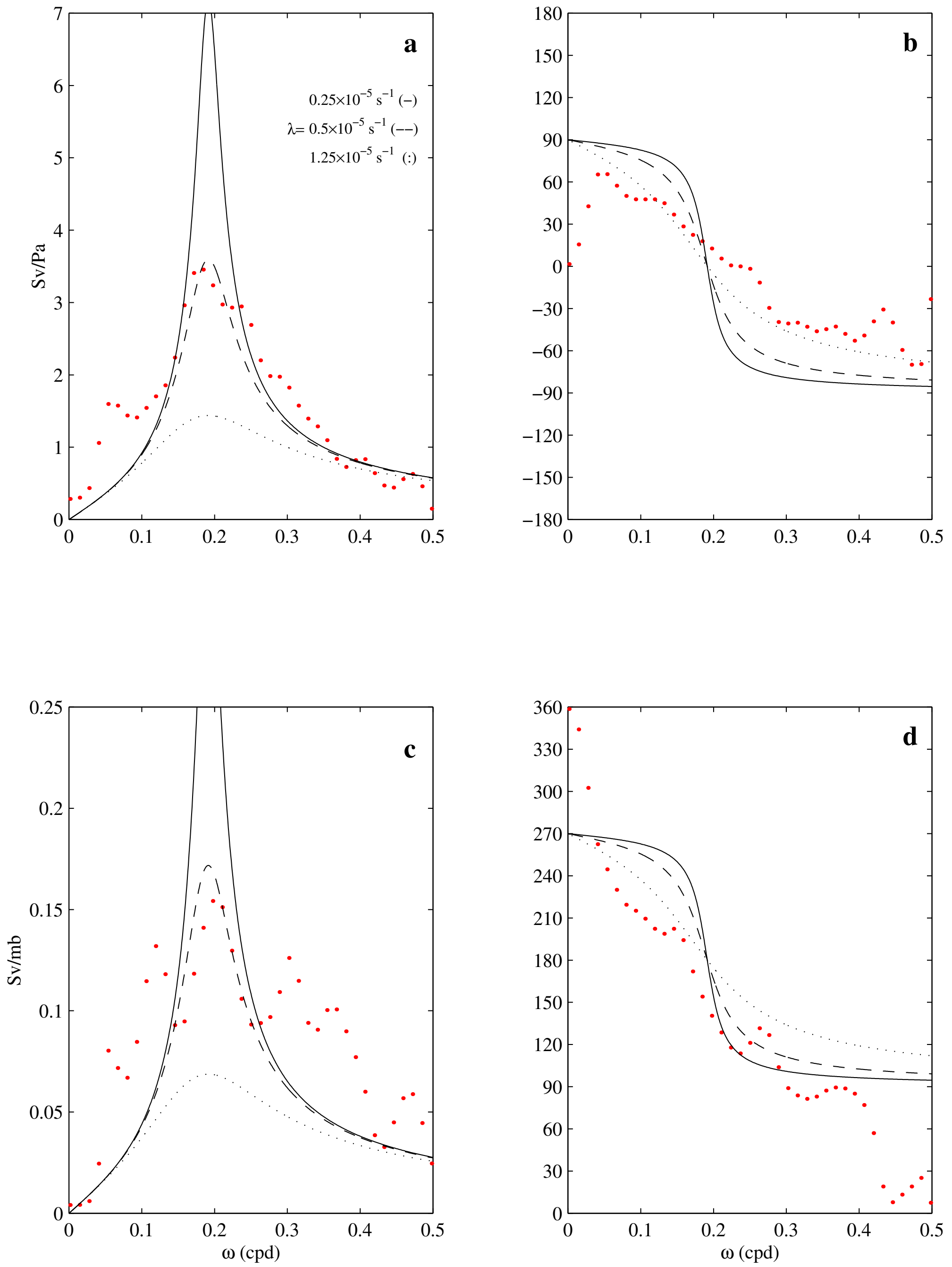

Figure 7.15: Comparison between observation and model (three frictional parameters) results for the net transport forced by the winds ((a) and (b)) and the atmospheric pressure over the Red Sea ((c) and (d)).

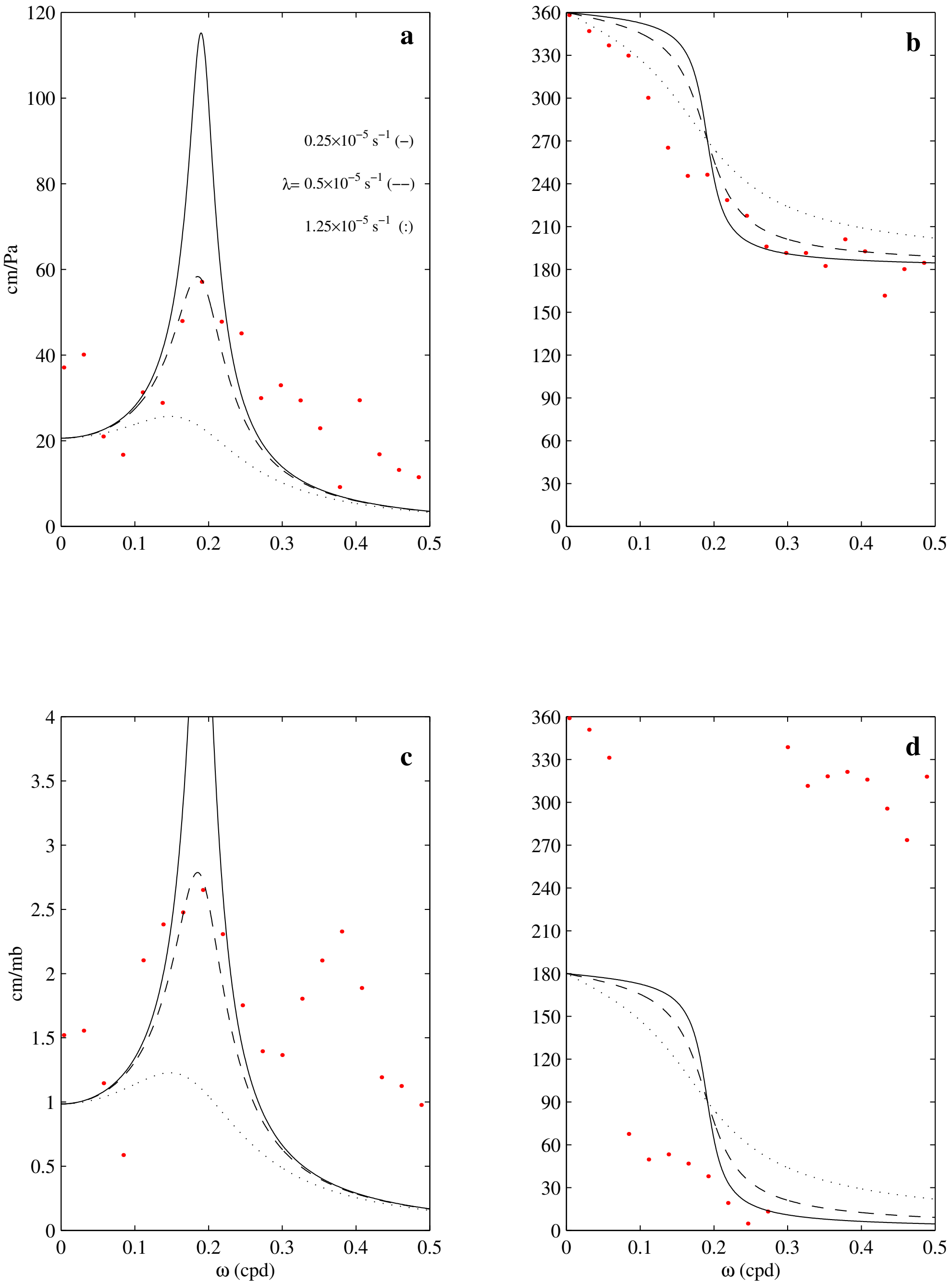

Figure 7.16: Comparison between observation and model (three frictional parameters) results for the sea leval of the Red Sea, forced by the winds ((a) and (b)) and the atmospheric pressure ((c) and (d)).

the pressure gauges inside the strait are in phase, but the response increases to the north, related to the oscillation of the sea level with the atmospheric forcing. Although there is a good agreement between observations and model for the wind-driven solution, the corresponding solution for the atmospheric pressure does not seem to describe the observations. Several explanations can be found for this discrepancy, such as the quality of the data from the meteorological stations and the location that the observations took place, which is in the area of the direct influence of the local wind field and most probably can not represent the sea level anomaly of the whole basin. Unfortunately there are no available data for the sea level variability inside the basin during the period of observations at Bab el Mandeb and a more accurate comparison is impossible.

Using the parameters discussed before and the local wind and atmospheric pressure as forcing we can produce a model in the time domain and compare with the observations. The results of this model (or "predictions") for the net transport (red line) and the observed transport blue line are plotted in Figure **??** using a value of $\lambda = 1.0 \times 10^{-5} sec^{-1}$. There is a very good agreement and the correlation coefficient between prediction and observed transport is 0.84 (or the model explains 70% of the observed variance). Other mechanisms that can affect the exchange at Bab el Mandeb at synoptic time scales will be discussed in the next section.

7.5 The baroclinic response and the remote forcing

Until now we assumed a homogeneous ocean, where the penetration of the wind is confined in a surface layer. If we want to include two distinct layers of different densities

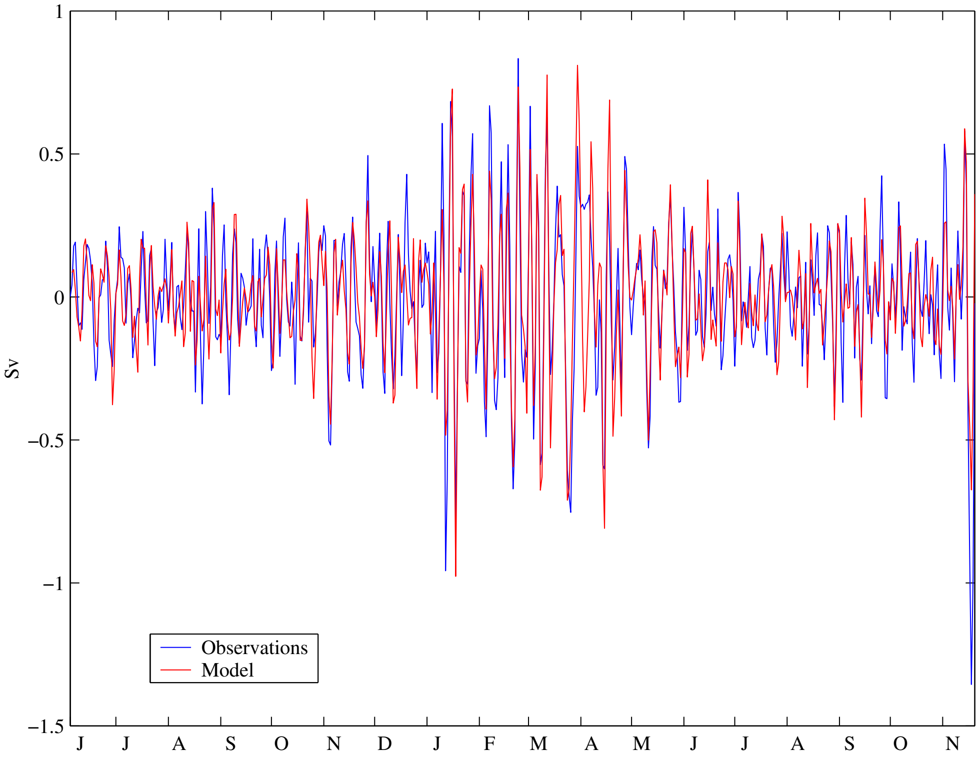

Figure 7.17: Comparison between observation and model results in the time domain.

(ρ_1 and ρ_2), which is a more accurate representation for the case of the Red Sea or other concentration basins in general, the response can be different. The interface separating the two layers can oscillate too and a baroclinic response is expected. Most of the assumptions discussed before are still valid, but the internal gravity waves that can smooth the interface to render it uniform during variations of synoptic time scales, are much slower than the long surface gravity waves. So, the behavior of the system at high frequencies is far more complicated. Nevertheless, assuming that the sea level and the interface between the layers inside the basin respond uniformly and ignoring the effect of atmospheric pressure, we can write a new set of equations that instead of a total conservation of mass inside the basin they assume a conservation of mass in each layer

$$\frac{\partial Q_1}{\partial t} = -gA_{S_1}\frac{\partial \eta}{\partial x} + \frac{A_{S_1}\tau_x}{H_1\rho_1} - \lambda_1 Q_1 \tag{7.10}$$

$$\frac{\partial Q_2}{\partial t} = -\frac{A_{S_2}\rho_1}{\rho_2}\frac{\partial \eta}{\partial x} - g'\frac{\partial \eta_i}{\partial x} - \lambda_2 Q_2 \tag{7.11}$$

$$\frac{\partial \eta}{\partial t} - \frac{\partial \eta_i}{\partial t} = \frac{Q_1}{A_{RS}} \tag{7.12}$$

$$\frac{\partial \eta_i}{\partial t} = \frac{Q_2}{A_{RS}} \tag{7.13}$$

where η_i is the interface perturbation, $g' = g(\rho_2 - \rho_1)/\rho_2$ and the surface and interface areas were taken as equal. The solutions are now very complicated but some preliminary conclusions can be driven from the simpler inviscid limit. The relation between η_i and η is

$$\eta_i = \frac{\omega_{02}^2}{\omega^2 - \omega_0'^2 2}\, \eta \qquad \left(\omega_0' 2 = \sqrt{\frac{g' A_{S_2}}{A_{RS} L_S}}\right) \tag{7.14}$$

so that fror frequencies greater than $\omega_0' 2$ the two levels are in phase and both layers "feel" primarily the effects of the sea level perturbation, as in the case described in the previous sections. During events of very low frequencies they are out of phase. Also at frequencies around $\omega_0' 2$ the fluctuations of the interface become much greater than those of the sea level. However, at this limit we are not dealing any more with synoptic time scales, since this band of periods corresponds to time scales equal or greater than the seasonal. At the frequency band that we examine here, which is associated with meteorological forcing, the solutions discussed in previous sections seem an appropriate approximation of the respond of the strait.

The remote forcing that can affect the flow at Bab el Mandeb can have several forms, like the remote wind effect or incident waves traveling in the region from remote areas. The most interesting and easy to treat is the effect of the wind outside the strait, at the western Gulf of Aden. This can be supposed to be in phase with the wind field inside the strait and will change the sea level at the entrance of the channel, "piling" water when the wind is positive (towards the basin) and lowering the sea level during periods that the wind blows towards the exit of the Red Sea. This effect will decrease the pressure gradient between the two ends of the strait and enable stronger flows at periods when the sea level inside the basin and the wind-stress compete each other. The simpler approximation of this effect is the addition of a term of the form $\alpha\tau_x/\rho_0 H_1$ in the momentum equations. If α is $O(1)$ the effect of the remote winds can be enormous and for example, the fluctuations of η inside the basin will increase by a factor of $1 + 2\,\alpha$. But because the winds are much weaker away from the strait (Cromwell and Smeed, 1998) the effect is going to be much smaller than the influence of the local winds ($\alpha \ll 1$). Furthermore, as we go away from the strait the width of the sea upon which the wind is acting become bigger and rotational effects become important. The only data of sea level outside of the strait but close enough to affect the exchange flow is located in Aden (12.64^oN and 43.91^oE or $35\,km$ from the Perim Narrows). The correlation between the strait winds and the sea level from this pressure gauge is very poor at synoptic time scales (correlation coefficient 0.35) showing that different considerations must be taken into account.

7.6 Summary and Discussion

Although it is simple, the model can reproduce the basic response of Bab el Mandeb to local meteorological forcing and the atmospheric pressure variability inside the Red Sea. It can explain 70% of the observed variance and if we consider only the winter season (October to May) when the atmospheric forcing is much stronger this value mounts up to almost 80%. The wind seems to be more important in the case of Bab el Mandeb and the correlation between observations and model wind-driven solutions is much better. This can be attributed to the strength of the fluctuations and the orographic effect in combination with the small width of the channel.

The flow variability at synoptic time scales can be important for the dynamics of the Bab el Mandeb-Red Sea system. It can modify the mixing in the strait and affect parameters involved in controlling mechanisms. This becomes more obvious in the case where the surface and lower layer are accelerating in different directions. Pratt et al. (1999) found that during periods of the year the flow is close to criticality with respect to hydraulic control. Atmospheric fluctuations of the type described here can make this kind of control intermittent.

More elaborate models can investigate the influence of parameters neglected in the model described here, like the rotation effect when layers of different density are allowed and the internal RRD becomes critically close to the width of the strait. The choice of a constant λ can simplify our derivations but the investigation of other forms of friction may improve the performance of similar models. Furthermore, the role of the different forms of remote forcing that can influence the variability in the strait should be investigated. Future numerical models incorporating synoptic meteorological forcing can produced a more detailed picture and improve our understanding of the dynamics governing the region.

Chapter 8

Conclusions

The objective of the study presented here has been the investigation of the mechanisms controlling the circulation and water mass formation in the Red Sea, and how these are reflected in the exchange flow between the Red Sea and the Indian Ocean. The questions associated with this objective were addressed using a variety of methods, including an OGCM (MICOM), and involve different time scales (synoptic, seasonal and the annual mean state). The results were summarized and discussed in each chapter where they were presented. In this concluding section the basic findings of this study are reviewed, and some remarks associated with the open questions and the future work in the region are discussed.

The need for accurate data sets of the atmospheric forcing over the Red Sea describing the temporal and spatial variability of the air-sea fluxes is crucial for our understanding of the dynamical balances in the region. The numerical experiments presented in Chapter 2 showed that the annual cycle of the forcing mechanisms is not only important for the seasonal variability of the circulation but is closely connected with the total amount of Red Sea Water (RSW) that is formed inside the basin. Without the seasonal variability of the thermohaline forcing the RSW outflow rate is reduced by 40% and the circulation pattern is significantly weakened. Thus, the variability of the forcing affects not only the variability of the circulation but is a crucial factor controlling the mean state of the basin. The annual mean budget estimates from the advective fluxes at the strait (Chapter 2) do not give information about the seasonal cycle of the air-sea fluxes or the their distribution inside the basin but can be used to constrain the present and future estimates of the atmospheric forcing in the region.

One of the main questions addressed throughout this study is the relative importance of the atmospheric forcing mechanisms, wind-stress and thermohaline air-sea fluxes, and the role of each one in the observed variability. The modified Phillips' model presented in Chapter 3 reproduces basic characteristics of the seasonal flow observed at Bab el Mandeb, supporting the idea that the seasonally variable buoyancy flux plays an important role in the circulation of the region. The MICOM experiments carried out with different forcing fields (full forcing, wind-stress, or buoyancy flux through the surface of the sea) showed that the circulation produced by the thermohaline forcing is overall stronger and dominates the wind-driven part of the circulation. The main circulation pattern is related to the seasonal buoyancy flux (mostly due to the fresh water fluxes) which increases the density to the north and produces a northward pressure gradient associated with the sloping of the sea surface. The response of the eastern boundary to a mean cross-basin geostrophic current depends on the stratification and β-effect. In the northern part of the basin this results to an eastward intensification but in the south the traditional westward intensification takes place.

In the southern part of the basin and the strait of Bab el Mandeb the circulation presents higher seasonal variability. It is in this region that the winds, influenced by the Indian Monsoon, reverse seasonally. The combination of the seasonal winds and the seasonal thermohaline forcing produce the circulation in the area and the observed exchange flow at the strait. Their combination is not a simple linear addition but they interact to produce the final circulation pattern. The MICOM experiments verified the presence of another mechanism influencing the exchange flow at Bab el Mandeb, proposed by Patzert (1974a), in which wind-induced upwelling in the northwestern Gulf of Aden produces opposite surface and subsurface pressure gradients through the strait, driving the surface layer out and the intermediate Gulf of Aden Water into the basin. The effect of this mechanism is comparable in strength to the direct wind-stress effect on the surface layer.

The rate of RSW formation, as was mentioned before, depends on the seasonal buoyancy flux. It is during winter and in the northern part of the basin that the largest amount of this water mass (about 2/3 of the final outflowing layer) is formed. Two different methods, a simple box model of volume and salt conservation and a three-dimensional model (MICOM), verify this result. The simulations indicate also that the permanent cyclonic gyre in the northern end of the basin is the most probable location for the formation to take place. Inside this feature the stratification becomes weaker due to doming of the isopycnals. This and the ability of the gyre to trap surface waters and expose them to the winter intense buoyancy loss are characteristics that make the region preferable location for water mass formation, as is the case in other seas where intermediate or deep water formation takes place. Further analysis of the RSW formation should include observation and modelling efforts at synoptic time scales and higher resolution, since the available examples from other basins (Mediterranean, Labrador Sea etc.) show that convective processes of this type are extremely variable at these scales.

The variability of the exchange flow at Bab el Mandeb at synoptic time scales was presented in the last chapter, and a simple, linear, two-dimensional model was employed to explain the main mechanisms involved. Interestingly, the local wind-stress seems to be the most important forcing mechanism, which combined with changes of the atmospheric pressure inside the Red Sea basin at synoptic time scales can explain 70% of the observed variance. The extension of these ideas in the three-dimensional framework of a numerical model may improve our understanding of the high frequency variability in the region including more realistic and complete dynamics.

In closing, I would like to emphasize the invaluable contribution of the recent observations at Bab el Mandeb (Murray and Johns, 1997) in this work. Almost all the ideas and methods described here had as starting point and basis this data set. This is another indication of the importance of the observational efforts in all the aspects and approaches used in physical oceanography. Further oceanographic exploration of the Red Sea basin will be crucial in order to advance our understanding of the dynamics governing the region in a more advanced level.

Bibliography

Ahmad, F., and S. A. R. Sultan, 1987, On the heat terms in the central region of the Red Sea, *Deep-Sea Res.*, 34, 1757-1760.

Ahmad, F., and S. A. R. Sultan, 1989, Surface heat fluxes and their comparison with the oceanic heat flow in the Red Sea, *Oceanol. Acta*, 12, 33-36.

Alverson, K., and W. B. Owens, 1996, Topographic preconditioning of open-ocean deep convection, *J. Phys. Oceanogr.*, 26, 2196-2213.

Bethoux, J. P., 1979, Budgets of the Mediterranean Sea. Their depndence on the local climate and the characteristics of the Atlantic waters, *Oceanol. Acta*, 2, 157-163.

Bethoux, J. P., 1987, Variabilite climatique des echanges entre la Mer Rouge et l'Ocean Indien, *Oceanol. Acta*, 10, 285-291.

Bleck, R., C. Rooth, D. Hu, and L. T. Smith, 1992, Salinity-driven thermocline transients in wind- and thermohaline-forced isopycnic coordinate model of the North Atlantic, *J. Phys. Oceanogr.*, 22, 1486-1505.

Bleck, R., and E. P. Chassignet, 1994, Simulating the oceanic circulation with isopycnic-coordinate models, in: *The Oceans: Physical-chemical dynamics and human impact*, S. K. Majumar, E. W. Miller, G. S. Forbes, R. F. Schmalz, and A. A. Panah eds., The Pennsylvania Academy of Science, Pennsylvania, 17-39.

Bogdanova, A. K., 1974, Indirect estimation of the seasonal variation of the water exchange through Bab el Mandeb, in: *L'oceanographie physique de la Mer Rouge*, CNEXO, Paris, 253-265.

Bryden, H. L., and H. M. Stommel, 1984, Limiting processes that determine basic features of the circulation in the Mediterranean Sea, *Oceanol. Acta*, 7, 289-296.

Budyko, M. I., 1963, Atlas of the heat balance of the earth, Glabnaia Geofiz. Obsev.

Bunker, A. F., 1976, Computations of surface energy flux and annual air-sea interaction cycles of the North Atlantic Ocean, *Mon. Wea. Rev.*, 104, 1122-1140.

Bunker, A. F., H. Charnock, and R. A. Goldsmith, 1982, A note on the heat balance of the

Mediterranean and Red seas, *J. Mar. res.*, 40, 73-84.

Candela, J., C. D. Winant, and H. L. Bryden, 1989, Meteorologically forced subinertial flows through the Strait of Gibraltar, *J. Geophys. Res.*, 94, 12667-12679.

Cember, R. P., 1988, On the sources, formation, and circulation of Red Sea Deep Water, *J. Geophys. Res.*, 93, 8175-8191.

Clarke, R. A., and J. C. Gascard, 1983, The formation of Labrador Sea Water, Part I: Large-scale processes, *J. Phys. Oceanogr.*, 13, 1764-1778.

Clifford, M., C. Horton, J. Schmitz and L. H. Kantha, 1997, An oceanographic nowcast/forecast system for the Red Sea, *J. Geophys. Res.*, 102, 25101-25122.

Crepon, M., 1965, Influence de la pression atmospherique sur le niveau moyen de la Mediterranee Occidentale et sur le flux a travers le detroitde Gibraltar, *Cah. Oceanogr.*, 1, 15-32.

Cromwell, D., and D. A. Smeed, 1998, Altimetric observations of sea level near the strait of Bab al Mandab, *Int. J. Remote Sensing*, 19, 1561-1578.

da Silva, A. M., C. C. Young, and S. Levitus, 1994, Atlas of surface marine data 1994. Volume 1: Algorithms and procedures. NOAA Atlas NESDIS 8, U. S. Department of Commerce, NOAA, NESDIS, 83 pp.

Eshel, G., and N. H. Naik, 1997, Climatological coastal jet collision, intermediate water formation, and the general circulation of the Red Sea, *J. Phys. Oceanogr.*, 27, 1233-1257.

Garrett, C., and B. Toulany, 1982, Sea level variability due to meteorological orcing in the Northeast Gulf of St. Lawrence, *J. Geophys. Res.*, 87, 1968- 1978.

Garrett, C., 1983, Variable sea level and strait flows in the editerranean: a theoretical study of the response to meteorological forcing, *Oceanol. Acta*, 6, 79-87.

Garrett, C., and F. Majaess, 1984, Nonisostatic response of sea level to atmospheric pressure in the Eastern Mediterranean, *J. Phys. Oceanogr.*, 14, 656-665.

Garrett, C., K. Speer, and E. Tragou, 1995, The relationship between water mass formation and the surface buoyancy flux, with application to Phillips' Red Sea model, *J. Phys. Oceanogr.*, 25, 1696-1705.

Gaspar, P., 1988, Modeling the seasonal cycle of the upper ocean, *J.Phys. Oceanogr.*, 18, 161-180.

Gill, A. E., 1977, The hydraulics of rotating-channel flow, *J. Fluid Mech.*, 80, 641-671.

Goldsbrough, G., 1933, Ocean currents produced by evaporation and precipitation, *Proc. Roy. Soc. London*, A141, 512-517.

Gordon, A. L., 1978, Deep Antarctic convection west of Maud Rise, *J. Phys. Oceanogr.*, 8, 600-612.

Grundlingh, M. L., 1985, Occurrence of Red Sea Water in the Southwestern Indian Ocean, 1981, *J.Phys. Oceanogr.*, 15, 207-212.

Hamon, B. V., 1967, Medium-scale temperature and salinity structure in the upper 1500 m in the Indian Ocean, *Deep-Sea Res.*, 14, 169-181.

Hannah, G. C., 1992, Geostrophic control with wind forcing: Application to Bass Strait, *J. Phys. Oceanogr.*, 22, 1596-1599.

Hastenrath, S., and P. J. Lamb, 1979, Climatic Atlas of the Indian Ocean, Univ. Wisconsin Press, Madison.

Hogg, N. G., 1973, The prconditioning phase of Medoc 1969 - II. Topographic effects, *Deep-Sea Res.*, 20, 449-459.

Husar, R. B., J. M. Prospero, and L. L. Stowe, 1997, Characterization of tropospheric aerosols over the oceans with the NOAA advanced high resolution radiometer optical thickness operational product, *J. Geophys. Res.*, 102, 16889-16909.

Koninklijk Nederlands Meteorologisch Instituut, 1949, Red Sea and Gulf of Aden oceangraphic and meteorological data, Publication 129, 26 pp.

Kraus, E. B., and J. S. Turner, 1967, A one-dimensional model of the seasonal thermocline. II. The genaral theory and its consequences, *Tellus*, 19, 98-105.

Krümmel, O., 1911, *Handbuch der Ozeanographie*, 2, Stuttgard.

Lacomb, H., and C. Richez, 1982, The regime of the Strait of Gibraltar, in: *Hydrodynamics of Semi-Enclosed Seas*, J. C. J. Nihoul, Ed., Elsevier, 13-72.

Lascaratos, A., R. G. Williams, and E. Tragou,1993, A mixed-layer study of the formation of Levantine Intermediate Water, *J. Geophys. Res.*, 98, 14739-14749.

Lascaratos, A., 993, Estimation of deep and intermediate water mass formation rates in the Mediterranean Sea, *Deep-sea Res.*, 40, 1327-1332.

Leaman, K. D., and F. A. Schott, 1991, Hydrographic structure of the convection regime in the Gulf of Lions: Winter 1987, *J. Phys. Oceanogr.*, 21, 575-598.

Levitus, S., 1982, Climatological atlas of the world ocean, NOAA Prof. Paper No 13, U. S. Govt. Printing Office, 173 pp.

Luksch, 1901, Expedition S. M. POLA in das Rota Meer, nordliche Halfte (October 1895 - Mai 1896). Wissenschaftliche Ergebnisse, physikalische Untersuchungen, Denkschrift d. kaiserl. Akad. Wissensch. in Wien, 69, 337pp.

Maillard, C., 1974, Eaux intermediaires et formation d'eau profonde en Mer Rouge, in: *L'oceanographie physique de la Mer Rouge*, CNEXO, Paris, 105- 133.

Maillard, C., and G. Soliman, 1986, Hydrography of the Red Sea and exchanges with the Indian Ocean in summer, *Oceanol. Acta*, 9, 249-269.

Mantyla, A. W., and J. L. Reid, 1995, On the origins of deep and bottom waters of the Indian Ocean, *J. Geophys. Res.*, 100, 2417-2439.

Maury, M. F., 1855, The physical geography of the sea and its meteorology, The Harvard Library, Cambridge, Mass, 432 pp.

Maxworthy, T., 1997, A frictionally and hydraulically constrained model of the convectively driven mean flow in partially enclosed seas, *Deep Sea Res*, 44, 1339-1354.

McCreary, J. P., S. R. Shetye, and P. K. Kundu, 1986, Thermohaline forcing of eastern boundary currents: With application to the circulation off the west coast of Australia, *J. Mar. Res.*, 44, 71-92.

Middleton, J. F., and F. Viera, 1991, The forcing of low frequency motions within Bass Strait, *J. Phys. Oceanogr.*, 21, 695-708.

Morcos, S. A., 1970, Physical and chemical oceanography of the Red Sea, *Oceanogr. Mar. Biol. Ann. Rev.*, 8, 73-202.

Morcos, S., and G. F. Soliman, 1974, Circulation and deep water formation in the Northern Red Sea in winter (based on R/V Mabahiss sections, January- February, 1935), in: *L'oceanographie physique de la Mer Rouge*, CNEXO, Paris, 91-103.

Muench, R. D., 1988, Relict convective features in the Weddell Sea, in: *Deep Convection and Deep water Formation in the Oceans*, P. C. Chu and J. C. Gascard, Eds., Elsevier, 53-67.

Murray, S. P., and W. Johns, 1997, Direct observations of seasonal exchange through the Bab el Mandeb strait, *Geophys. Res. Let.*, 24, 2557-2560.

Neumann, J., 1952, Evaporation from the Red Sea, *Israel Explor. J.*, 2, 153-162.

Neumann, A. C., and D. A. McGill, 1962, Circulation of the Red Sea in early summer, *Deep-Sea Res.*, 8, 223-235.

Osman, M. M., 1985, Evaporation from coastal water off Port-Sudan, emphJournal of the Faculty of Marine Science, 4, 29-37.

Patzert, W. C., 1974, Wind-induced reversal in Red Sea circulation, *Deep-Sea Res.*, 21, 109-121.

Patzert, W. C., 1974, Seasonal reversal in the Red Sea circulation, in: *L'oceanographie physique de la Mer Rouge*, CNEXO, Paris, 55-89.

Patzert, W. C., 1974, Volume and heat transports between the Red Sea and Gulf of Aden, notes on the Red Sea heat budget, in: *L'oceanographie physique de la Mer Rouge*, CNEXO, Paris, 191-201.

Pedgley, D. E., 1974, An outline of the weather and climate of the Red Sea, in: *L'oceanographie physique de la Mer Rouge*, CNEXO, Paris, 9-27.

Phillips, O. M., 1966, On turbulent convection currents and the circulation of the Red Sea, *Deep-Sea Res.*, 13, 1149-1160.

Pratt, L. J., and P. A. Lundberg, 1991, Hydraulics of rotating strait and sill flow, *Ann. Rev. Fluid Mech.*, 23, 81-106.

Pratt, L. J., W. Johns, S. P. Murray and K. Katsumata, 1999, Hydraulic interpretation of direct velocity measurements in the Bab al Mandab, *J. Phys. Oceanogr.*, 29, 2769-2784.

Privett, D. W., 1959, Monthly charts of evaporation from the Indian Ocean (including the Red Sea and the Persian Gulf), *Q. Jl. R. Met. Soc.*, 85, 424-428.

Privett, D. W., 1960, The exchange of energy between the atmosphere and the oceans of the southern hemisphere, *Geophys. Mem. Met. Office*, 13, No 104, 61 pp.

Quadfasel, D., and H. Baunder, 1993, Gyre-scale circulation cells in the Red Sea, *Oceanol. Acta*, 16, 221-229.

Robinson, M. K., 1974, Atlas of monthly mean sea surface and subsurface temperature and the depth of the thermocline, in: *L'oceanographie physique de la Mer Rouge*, CNEXO, Paris, 29-54.

Rochford, D. J., 1964, Salinity maxima in the upper 1000 meters of the North Indian Ocean, *Aust. J. Mar. Freshw. Res.*, 15, 1-24.

Schott, F., M. Visbeck, and J. Fischer, 1993, Observations of vertical currents and convection in the central Greenland Sea during the winter of 1988-89, *J. Geophys. Res.*, 98, 14401-14421.

Schott, G., 1929, Uber die Wasserbewegungen im Bab el Mandeb, *Ann. d. Hydrog.*, 62, 10-14.

Sewell, R. B. S., 1934, The John Murray Expedition to the Arabian Sea, *Nature*, 133, 86-89.

Shapiro, G. I., and S. L. Meschanov, 1991, Distribution and spreading of the Red Sea Water and salt lens formation in the northwest Indian Ocean, *Deep-Sea Res.*, 38, 21-34.

Sharaf el-Din, S. H., and E. E. Mohamed, 1984, The circulation pattern and hydrographic structure of the southern Red Sea and Gulf of Aden, in: *Proc. Symp. Coral Reef Environment of the Red Sea*, Jeddah, 14-18 January 1984, 60-101.

Siedler, G., 1968, Schichtungs- und Bewegungsverhaltnisse am Sudausgang des Roten Meeres, *"Meteor" Forschungsergebn*, A(4), 1-76.

Siedler, G., 1969, General circulation of the water masses in the Red Sea, in: *Hot brines and recent heavy metal deposits in the Red Sea*, E. T. Degens and D. A. Ross eds., New York, 131-137.

Smeed, D., 1997, Seasonal variation of the flow in the strait of Bab el Mandeb, *Oceanol. Acta*, 20, 773-781.

Stern, M. E., 1972, Hydraulically critical rotating flow, *Phys. Fluids*, 15, 2062-2064.

Stommel, H.,1957, A survey of ocean current theory, *Deep-Sea Res.*, 4, 149-184.

Stommel, H.,1984 The delicate interplay between wind-stress and buoyancy nput in ocean circulation: the Goldsbrough variations, *Tellus*, 36, 111-119.

Sverdrup, H. U., M. W. Johnson, and R. H. Fleming, 1942, The oceans, their physics chemistry and general biology, Prentice-Hall, New York, 1087 pp.

Swallow, J. C., and G. F. Caston, 1973, The preconditioning phase of MEDOC 1969 - I. Observations, *Deep-Sea Res.*, 20, 429-448.

Thompson, E. F., 1939a, Chemical and physical investigations. The general hydrography of the Red Sea, *John Murray Expedition 1933-34*, Scienific Reports, 2, 83.

Thompson, E. F., 1939b, Chemical and physical investigations. The exchange of water between the Red Sea and the Gulf of Aden over the "Sill", *John Murray Expedition 1933-34*, Scienific Reports, 2, 105.

Tragou, E., and C. Garrett, 1997, The shallow thermohaline circulation of the Red Sea, *Deep-Sea Res.*, 44, 1355-1376.

Tragou, E., R. Outerbridge, C. Garrett, and C. Gilman, 1998, The heat and freshwater budgets of the Red Sea, *Submitted - J. Phys. Oceanogr.*.

Vercelli, E., 1925, Richerche di oceanografia fisica eseguite della R. N. AMMIRAGLIO MAGNAGHI (1923-24), Part I. Correnti e maree, *Annali Idrografici*, 11, 1-188.

Vercelli, E., 1927, Richerche di oceanografia fisica eseguite della R. N. AMMIRAGLIO MAGNAGHI (1923-24), Part IV. La temperatura e la salinita, *Annali Idrografici*, 11, 1-66.

Vercelli, E., 1931, Nuove richerche sulli correnti marine nel Mar Rosso, *Annali Idrografici*, 12, 1-74.

Vercelli, E., 1931, Le esplorazioni talassografiche nel Mar Rosso, *Atti del Primo Congresso di Studi Coloniali*, Firenze, 23pp.

Visbeck, M., J. Fischer, and F, Schott, 1995, Preconditioning the Greenland Sea for deep convection: Ice formation and ice drift, *J. Geophys. Res.*, 100, 18489-18502.

Whitehead, J. A., A. Leetmaa, and R. A. Knox, 1974, Rotating hydraulics of strait and sill flows, *Geophys. Fluid Dyn.*, 6, 101-125.

Woelk, S., and D. Quadfasel, 1996, Renewal of deep water in the Red Sea during 1982-1987, *J. Geophys. Res.*, 101, 18155-18165.

Wust, G., 1954, Gesetzmäbige Wechselbeziehungen zwischen Ozean und Atmosphäre in der zonalen Verteilung von Oberflächensalzgehalt, Verdunstung und Niederschlag, *Atch. Met. Geophys. Bioklim.*, A(7), 305-328.

Wyrtki, K., 1974, On the deep circulation of the Red Sea, in: *L'oceanographie physique de la Mer Rouge*, CNEXO, Paris, 135-163.

Yegorov, N. I., 1950, Calculation of the heat balance of the Red Sea, *Meteorologia igidrologia*, 3, 49-56.